THESIS

CONTRIBUTION OF BIOMASS BURNING TO CARBONACEOUS AEROSOLS IN MEXICO CITY DURING MAY 2013

Submitted by

Zitely Asafay Tzompa Sosa

Department of Atmospheric Science

In partial fulfillment of the requirements

For the Degree of Master of Science

Colorado State University

Fort Collins, Colorado

Summer 2014

Masterôs Committee:

Advisor: Sonia M. Kreidenweis

Emily Fischer
Amy Sullivan
John Volckens

ABSTRACT

CONTRIBUTION OF BIOMASS BURNING TO

CARBONACEOUS AEROSOLS IN MEXICO CITY DURING MAY 2013

The Mexico City Metropolitan Area (MCMA) is one of the largest megacities in the world with a population of 20 million people. Anthropogenic emissions have been controlled in past decades; however, emissions transported from outside the basin, such as wildfires and agricultural burning, represent a potentially large contribution to air quality degradation.

This study analyzed PM_{10} filter samples from six different stations located across the MCMA from May, 2013, which represented the month with the most reported fire counts in the region over the last 11 years (2002-2013). Two meteorological regimes were established considering the number of satellite derived fire counts, changes in predominant wind direction, ambient concentrations of CO, PM_{10} and $PM_{2.5}$, and precipitation patterns inside MCMA. The filter samples were analyzed for biomass burning tracers including levoglucosan (LEV), water-soluble potassium (WSK^+); and water-soluble organic carbon (WSOC). Results of these analyses show that LEV concentrations correlated positively with ambient concentrations of $PM_{2.5}$ and PM_{10} (R^2=0.61 and R^2=0.46, respectively). Strong correlations were also found between WSOC and LEV (R^2=0.94) and between WSK^+ and LEV (R^2=0.75). An average LEV/WSOC ratio of 0.0147 was estimated for Regime 1 and 0.0062 for Regime 2. Our LEV concentrations and LEV/WSOC ratios are consistent with results found during the MILAGRO campaign (March, 2006). To the best of our knowledge, only total potassium concentrations have been measured in

aerosol samples from MCMA. Therefore, this is the first study in MCMA to measure ambient concentrations of WSK^+.

Analysis of gravimetric mass concentrations showed that $PM_{2.5}$ accounted for 60% of the PM_{10} mass concentration with an estimated $PM_{10}/PM_{2.5}$ ratio of 1.68. Estimates from our laboratory filter sample characterization indicated that we measured 37% of the total PM_{10} mass concentration. The missing mass is most likely crustal material (soil or dust) and carbonaceous aerosols that were not segregated into WSOC fraction.

Assuming that LEV is inert in the atmosphere, the estimated biomass burning contributions to WSOC ranged from 7-23%. When assuming a LEV lifetime of 1.1 to 5 days, the estimated contributions increased on average 80%. Thus, we conclude that biomass burning sources had a large impact on WSOC and $PM_{2.5}$ during May 2013, potentially explaining up to half of the measured WSOC.

Our results indicate that primary emissions from biomass burning sources represent significant contributions to ambient PM. Future studies are needed to improve the emission inventories that are commonly used by decision makers in the MCMA to design air quality policies and emission source controls.

ACKNOWLEDGEMENTS

I want to thank my advisor Sonia Kredenweis for all her support and guidance throughout my master studies. She made this dream come true three years ago, when she offered me the opportunity to come to CSU and work in her research group. I have learned so much from her strong scientific ethics and honesty.

I would like to thank Amy Sullivan for her patience and willingness to help me in every step of my research work. Thanks to the rest of my committee members, Emily Fischer and John Volckens, for their time and great input to my work.

Also, I would like to thank Jeff Collett for all his support, Jamie Schmidt for her never ending kindness and willingness to help, and Annareli Morales for her friendship and constant help throughout my masters.

From Mexico, I want to give special thanks to Armando Retama for helping me design a project aimed at better understanding an important air quality problem impacting my beloved hometown (Mexico City). From Mario Molina Center, special thanks to Rodolfo Lacy, who I admire for being a great boss and humble person, and whom always encouraged me to pursue my graduate studies in this field. Also, thanks to Oscar Peralta, Juan Carlos Belausteguigoitia, Carlos Mena and Mario Molina for their unconditional support.

This research was supported by the Consejo Nacional de Ciencia y Tecnología (CONACyT) fellowship.

DEDICATION

TO MY FAMILYé and by family I mean by blood and by choice. You are my strength and a very important part of my happiness.

TABLE OF CONTENTS

LIST OF TABLES

LIST OF FIGURES

LIST OF ACRONYMS

CI	confidence interval
CO	carbon monoxide
CONACyT	Consejo Nacional de Ciencia y Tecnología
CSU	Colorado State University
D_{gn}	mean diameter for number distributions
D_{gv}	mean diameter for volume size distributions
EC	elemental carbon
FINN	Fire Inventory from NCAR
FLAME	Fire Laboratory at Missoula Experiments
HC	hydrocarbons
HPAEC-PAD	high-performance anion-exchange chromatography with pulsed amperometric detection
HYSPLIT	Hybrid Single Particle Lagrangian Integrated Trajectory Model
LAC	light absorbing carbon
LEV	levoglucosan
LOD	limit of detection
LPR	La Presa sampling station
MASL	meters above sea level
MCMA	Mexico City Metropolitan Area
MER	Merced sampling station
MILAGRO	Megacity Initiative: Local and Global Research Observations
NAAPS	Navy Aerosol Analysis and Prediction System
NAM	North American Mesoscale
NASA	National Aeronautics and Space Administration
NCAR	National Center for Atmospheric Research
NEZ	Nezahualcóyotl sampling station
NOAA	National Oceanic and Atmospheric Administration
NO_X	nitrogen oxides
O_3	ozone
OA	organic aerosol
OC	organic carbon
OC_{BB}	organic carbon from biomass burning sources
OH	hydroxyl radical

PM_{10}	particulate matter less than 10 micrometers in diameter
$PM_{2.5}$	particulate matter less than 2.5 micrometers in diameter
POM	particulate organic material
SACMEX	Sistema de Aguas de la Ciudad de México (Mexico City's Water System)
SIMAT	Sistema de Monitoreo Atmosférico (Atmospheric Monitoring Network)
SO_2	sulfur dioxide
SOA	secondary organic aerosol
TLA	Tlalnepantla sampling station
TC	total carbon
UAM	UAM-Iztapalapa sampling station
USA	United Stated of America
VOC	volatile organic compound
WSOC	water-soluble organic carbon
$WSOC_{BB}$	water-soluble organic carbon from biomass burning sources
$WSOK^{+}$	water-soluble potassium
XAL	Xalostoc sampling station

1. MOTIVATION

Mexico City Metropolitan Area (MCMA) is one of the most populated megacities in the Northern Hemisphere. Within the air basin surrounded by mountains where MCMA is located, 20 million people live and 3.5 million vehicles circulate (INEGI, 2012). Due to its geographical location that creates favorable conditions for photochemical reactions and its unique topography where thermal inversions are common, the air quality within the air basin has been a focal point since the 1950ôs when high concentrations of particles frequently reduced the visual range to 2 km. Some particle measurements were done in 1967, but it was not until 1984 that an automatic monitoring network was installed within MCMA and its first results led to several air quality policies aimed at reducing particles, lead, hydrocarbons (HC), carbon monoxide (CO), nitrogen oxides (NO_X), and ozone (O_3) concentrations. The air quality policies implemented in subsequent decades focused mainly on the reduction of vehicle emissions, gasoline reformulation and management, as well as the closure of a refinery inside the city and new guidelines for industries (Fenn et al., 2002).

As explained above, Mexico City has complex air quality conditions that interest scientists all over the world. During the spring seasons of 2003 and 2006, two large-scale field campaigns took palace in Mexico City: MCMA-2003 (Mexico City Metropolitan Area - 2003) and the MILAGRO (Megacity Initiative: Local and Global Research Observations) Campaign. Both field campaigns helped improve understanding of the air quality problem in megacities, as well as exposing new sources that have not been well described. In particular, wildfires were revealed as a potentially important source of pollutants to MCMA (Aiken et al., 2010, Aiken et al., 2009, Crounse et al., 2009, Stone et al., 2008, Yokelson et al., 2011, Yokelson et al., 2007).

The impacts of biomass burning and its contribution to air quality degradation in Mexico Cityôs air basin were taken seriously only after the results of the MCMA-2003 and MILAGRO campaigns were published. Both campaigns took place during the wildfire season (warm-dry season), and especially the MILAGRO campaign occurred in a very active fire period (Aiken et al., 2010). However, a clear biomass burning contribution was difficult to determine due to considerable variations in wildfire contribution estimates among several studies (Aiken et al., 2010, Querol et al., 2008, Yokelson et al., 2007).

The present study is aimed at contributing to an improved understanding of the influence of biomass burning on carbonaceous aerosol concentrations in Mexico City. We analyzed PM_{10} samples of ambient aerosol obtained in MCMA during May 2013, which represented the month from the period 2002-2013 with the maximum satellite derived fire counts. We expected PM_{10} to be influenced by local sources of primary particle emissions, such as dust from paved and unpaved roads, and biomass burning primary emissions to contribute mostly to the $PM_{2.5}$ fraction. Also, we expected to find high concentrations of organic and inorganic biomass burning markers in the air samples collected that were correlated to ambient concentrations of CO, PM_{10} and $PM_{2.5}$ in MCMA. Finally, our main goals were to use this initial dataset to estimate the contribution of biomass burning to water-soluble organic carbon (WSOC) concentrations, demonstrating a strategy for development of quantitative understanding of the importance of biomass burning sources to MCMA air quality degradation during active fire periods.

2. INTRODUCTION

In order to understand the relevance and importance of the contribution of biomass burning to air quality degradation in Mexico City, a description of the demographic, geographic and air quality characteristics and challenges is necessary. This chapter will provide a conceptual framework not only to understand the challenges, but also the current available capabilities and information resources to assess them.

2.1 AIR QUALITY IN MEGACITIES

In the last century, migration from rural to urban areas as well as other demographic characteristics have led some cities with high growth rates to become megacities. A megacity is defined as a city with population over 10 million people. In 2012, there were 23 megacities around the world and by 2025, this number is expected to increase to 37 (Zhu et al., 2012).

The intense economic activities and the growing levels of industrialization within megacities generate a series of environment-related problems, including degraded air quality, an important environmental and health problem. The anthropogenic emissions released to the atmosphere in megacities can have effects on local and regional scales and are primarily associated with fossil fuel burning that is related to high energy consumption (e.g. cooling, heating, illumination, transportation and industries). However, air quality degradation is also affected by different factors which include geographic location, topography, meteorology, and the level and rate of industrialization and socio-economic development (WHO/UNEP, 1992).

In urban environments the most common air pollutants include carbon monoxide (CO), nitrogen oxides (NO_X), sulfur dioxide (SO_2), particles, hydrocarbons (HC), and ozone (O_3).

Regulating and quantifying these emissions as well as monitoring their concentrations have been priorities in some urban areas.

Mexico City is an example of a megacity that has suffered air pollution problems since the 1950ôs and is determined to improve air quality by building on the experiences of other cities such as Los Angeles, USA. The air quality policies and air quality controls implemented for major pollution sources in Mexico City have led to a gradual decrease in air pollution levels. However, the contributions of minor sources and transport of emissions from other regions have not yet been well defined and controlled. To understand Mexico Cityôs air quality problem, the next sections will discuss briefly its history, demographics, geography and physical characteristics.

2.2 MEXICO CITY METROPOLITAN AREA

2.2.1 BRIEF HISTORY AND DEMOGRAPHICS

Mexico City was founded in 1325 and is the oldest city still inhabited in the Americas. When the Spaniards conquered the city 200 years later (1521), it had an estimated population of 100,000 people (Figure 2.1). The Spaniards, using ancient techniques, continued to build a European-style city over the surrounding lake.

In the 20th century, a demographic explosion occurred in the whole country (especially from the 60's to the 80's), generating a high migration to cities where there was an increase in demand for food, services, and jobs. In 1950, Mexico City had 3 million people and by 1970 its population had more than doubled (6.8 million) (INEGI, 2012). Despite the strict population control policy implemented by the national government during the following decades, the city continued growing and joining with surrounding cities and MCMA was created. Most of the

growth occurred towards the north and industry which originally was located outside the city, in just two decades, became part of the urban landscape. Massive transportation systems were created to meet the large demand for mobility; however vehicles for private use still dominate car statistics. MCMAôs vehicle fleet currently amounts to 3.5 million and represents one ninth of the total vehicles that circulate in the country. Also, the 20 million people that live in MCMA represent one fifth of the total population of the country, making it one of the most inhabited megacities in the Northern Hemisphere (INEGI, 2012).

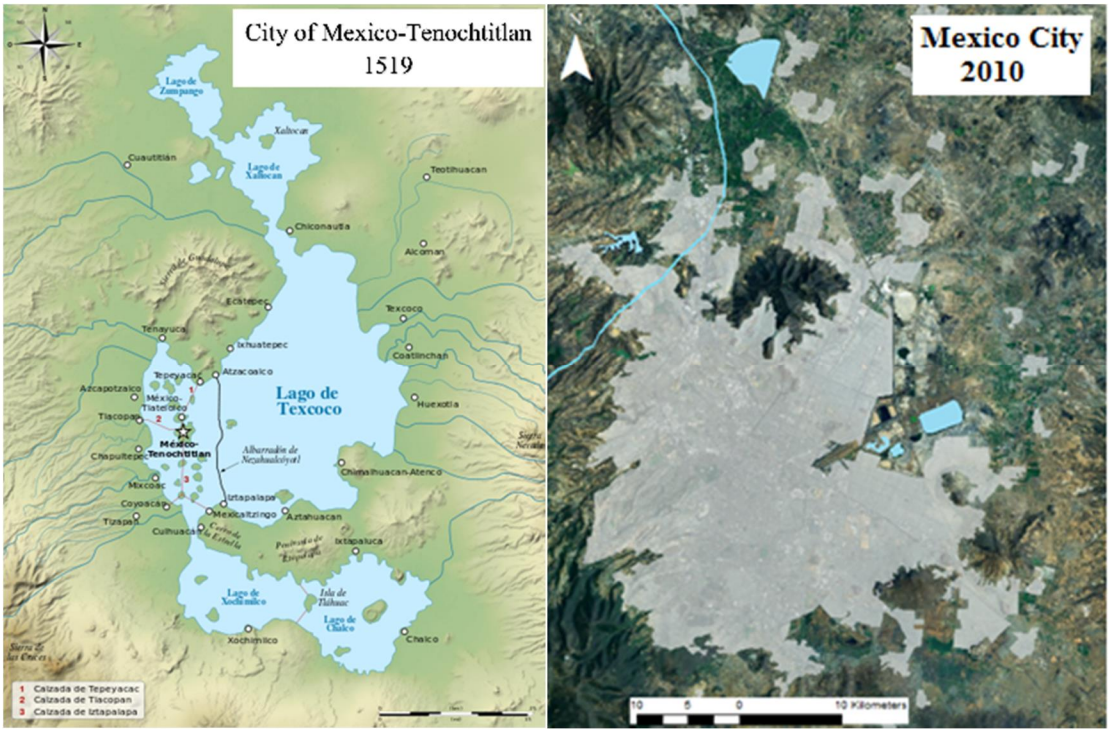

Figure 2.1 Transformation of the Valley of Mexico City from 1519 to 2010. The left figure shows the lakes and extent of Mexico City in 1519, before the Spaniards conquered Mexico (from Centro de Estudios Mexicanos y Centroamericanos). The right figure shows MCMA in 2010, in approximately the same land extension. The lakes that covered a large section of the basin have almost disappeared. Map created using ArcMap (ESRI, 2012).

2.2.2 GEOGRAPHY

The MCMA has a total area of 7,866 km^2 and is the only megacity in the country. The city is located within a basin at 2,240 meters above sea level (latitude 19°26ô N and longitude 99°02ô W), where approximately 60% of it is surrounded by mountains. Two volcanoes (Popocatepetl and Iztaccihuatl) are located in the southeast of the basin with a maximum height of 5,500 MASL (see Figure 2.2); one is currently active and some of the ash expelled often reaches the MCMA. Like other megacities, the MCMA encompasses more than one urban center and it is mainly comprised of two States: Distrito Federal and Estado de Mexico.

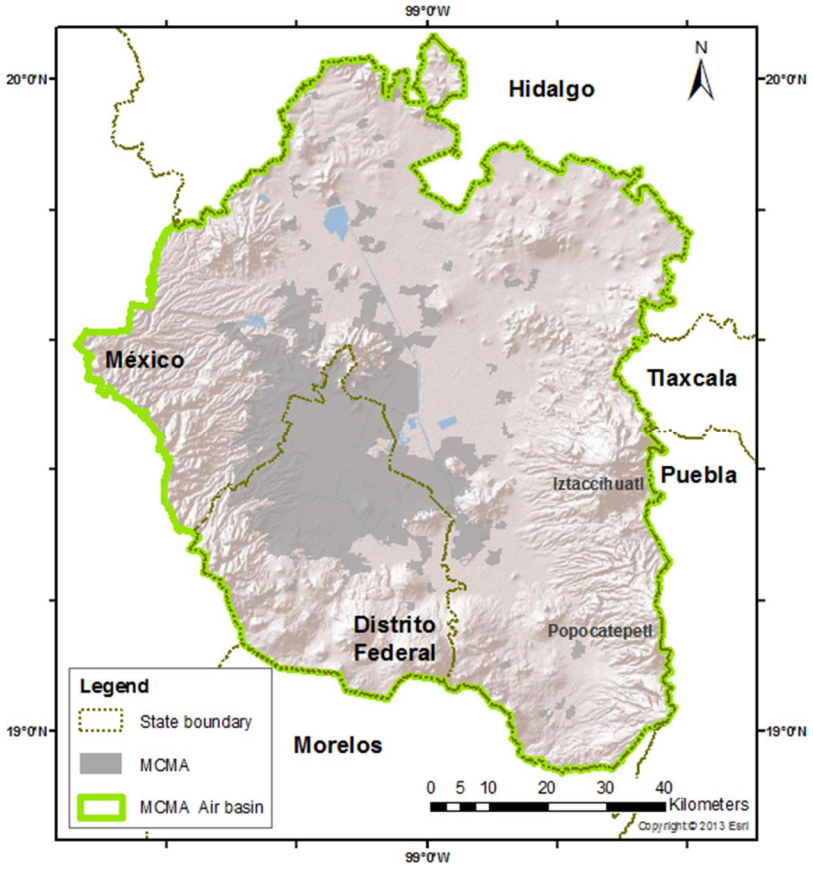

Figure 2.2 Mexico City Metropolitan Area (MCMA).
The MCMA air basin is highlighted in green. The Popocatepetl and Iztaccihuatl volcanoes are high elevations located at the Southeast side of the air basin.
Map created using ArcMap (ESRI, 2012).

2.3 METEOROLOGY

2.3.1 WET AND DRY SEASONS

The MCMA has three seasons: the cold-dry season, the warm-dry season and the wet season. The cold-dry season starts in November and finishes in February. During this season, cold fronts coming from North America usually reach the basin causing a drop in temperature, sparse rain and occasionally snow over the mountain ranges to the south and east. After these fronts pass, anticyclonic weather systems with clear skies and calm winds prevail, favoring the development of strong surface inversions that enable high concentrations of pollutants inside the basin (Fenn et al., 2002). The warm-dry season goes from March through May and has warmer temperatures than the cold-dry season (SEDEMA, 2012a). Turbulent winds are common generating convective activity near the surface, associated with frequent severe dust storms (Fenn et al., 2002). Finally, the wet season covers the months from June to October and reports the highest precipitation rates and temperatures of the year (Figure 2.3 and Figure 2.4) (SEDEMA, 2012a).

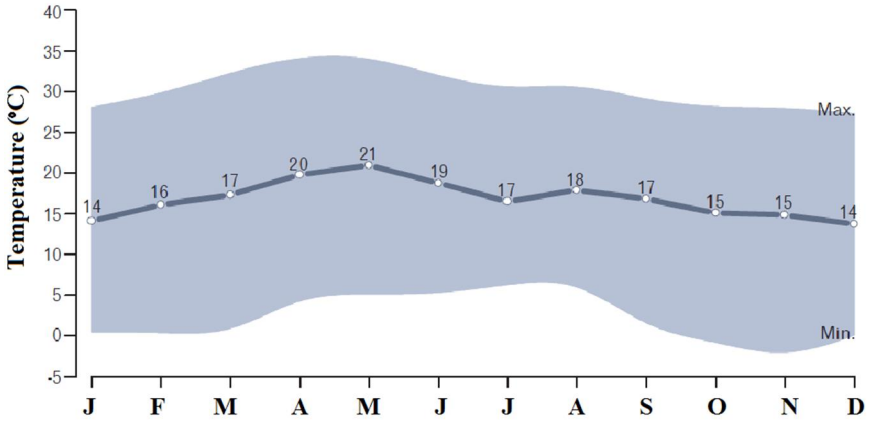

Figure 2.3 Monthly temperatures (°C) in the MCMA during 2011. The solid line represents the monthly average. The shaded area encompasses the maximum and minimum temperature values. From SEDEMA (2012a).

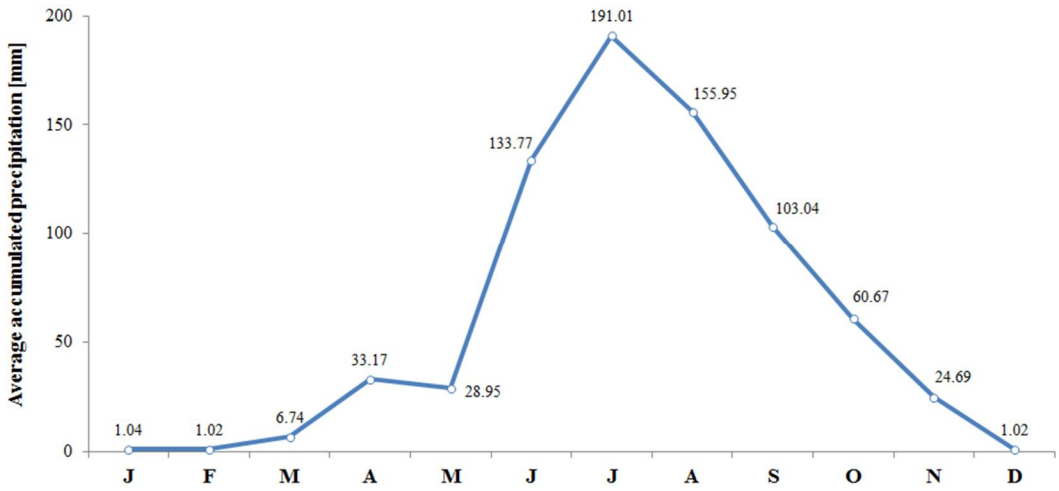

Figure 2.4 Monthly average accumulated precipitation (mm) in the MCMA during 2011.
Data obtained from SACMEX (2013).

2.3.2 SEASONAL WIND PATTERNS

The morning wind patterns during the dry season of 2011, had predominant winds coming from the north west, while during the wet season, the predominant winds came from the north east and east. These wind patterns transported the air pollutants towards the south of the air basin, where they escaped through the lower mountains at the south of the MCMA basin (Figure 2.5). At night, the winds change directions especially during the dry season, when the downslope winds converge in the center of the basin, creating a stable layer that contribute to the formation of thermal inversions mainly during the winter (SEDEMA, 2012a).

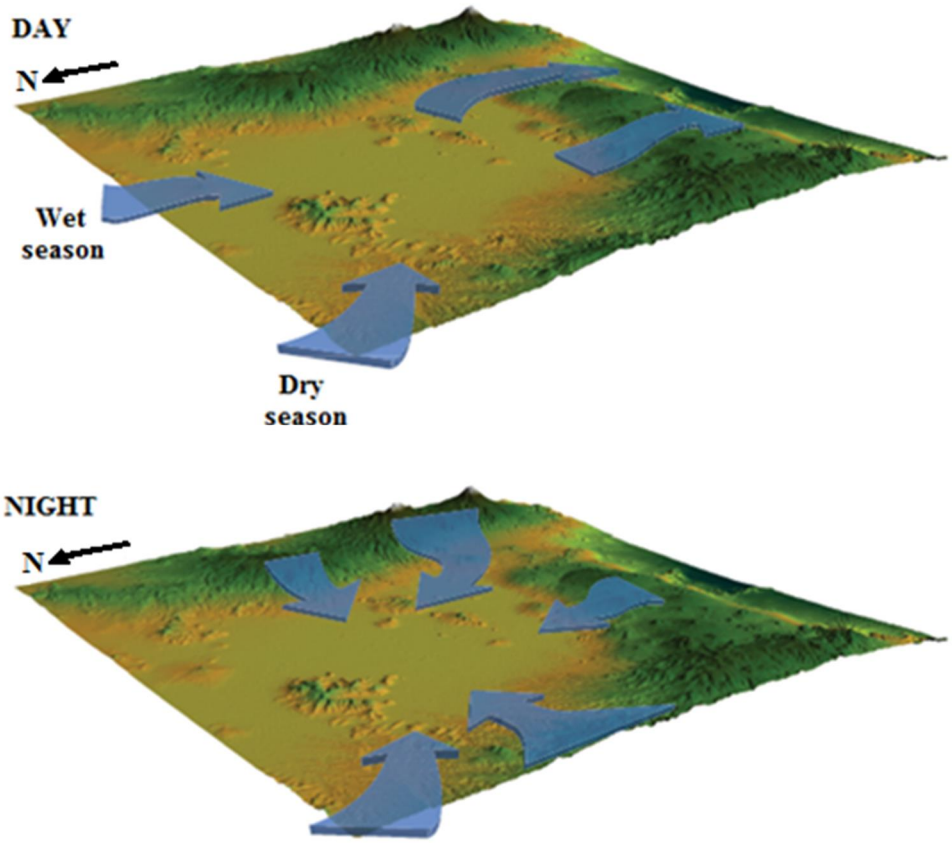

Figure 2.5 Diurnal and nocturnal wind patterns in the MCMA basin. From SEDEMA (2012a).

2.3.3 THERMAL INVERSIONS

In the troposphere, generally the temperature decreases with height at an average lapse rate of 6.5 °C/km. Thermal inversions occur when there are layers within the troposphere where temperature increases with height. The warm air mass above a colder air mass inhibits vertical mixing (Wallace and Hobbs, 2006). Thermal inversions occurring over urban regions can strongly degrade air quality by trapping pollutants near the surface. The combination of a thermal inversion with dry air conditions, light winds and clear sky nights can increase the severity of air pollution episodes.

Due to the geographical location of the MCMA, thermal inversions are frequent inside the basin. The most common thermal inversions over the MCMA are: radiation inversions, advection inversions and subsidence inversions (SEDEMA, 2006). Radiation inversions are produced during the night when no shortwave radiation from the Sun heats the ground. Since the ground cools off faster than the air above it, a layer where temperature increases with height forms near the ground. Advection inversions occur when downslope air flows from the mountains to the basin, as seen in Figure 2.6-a. The air warms by compression as it descends over the basin at a dry adiabatic rate of 10 °C/km. The colder air near the surface gets trapped by the sinking air, generating a thermal inversion that lasts until the Sun heats the ground and the atmospheric layer above it enough to break the stable conditions that inhibit vertical mixing (Figure 2.6-b). Lastly, subsidence inversions in the MCMA develop when large high-pressure centers sit over the basin. The downward moving air masses from the anticyclonic high pressure center warms adiabatically by compression. As a result, the sinking warm air diverges horizontally over a colder layer near the surface (Figure 2.7) (Markowski, 2010, Turco, 2002).

Generally thermal inversions in the MCMA break up before noon (SEDEMA, 2006). During 2011, 93 thermal inversions occurred and almost 90% of them (83) took place during the dry season (cold-dry and warm-dry seasons). December and January (during cold-dry season) reported the highest monthly number of thermal inversions that broke on average at 11:00 am. In contrast, from March through May (entire warm-dry season) the breaking hour of thermal inversions was between 9:00 and 10:00 am. Throughout June, July and August no thermal inversions were registered (Figure 2.8) (SEDEMA, 2012a).

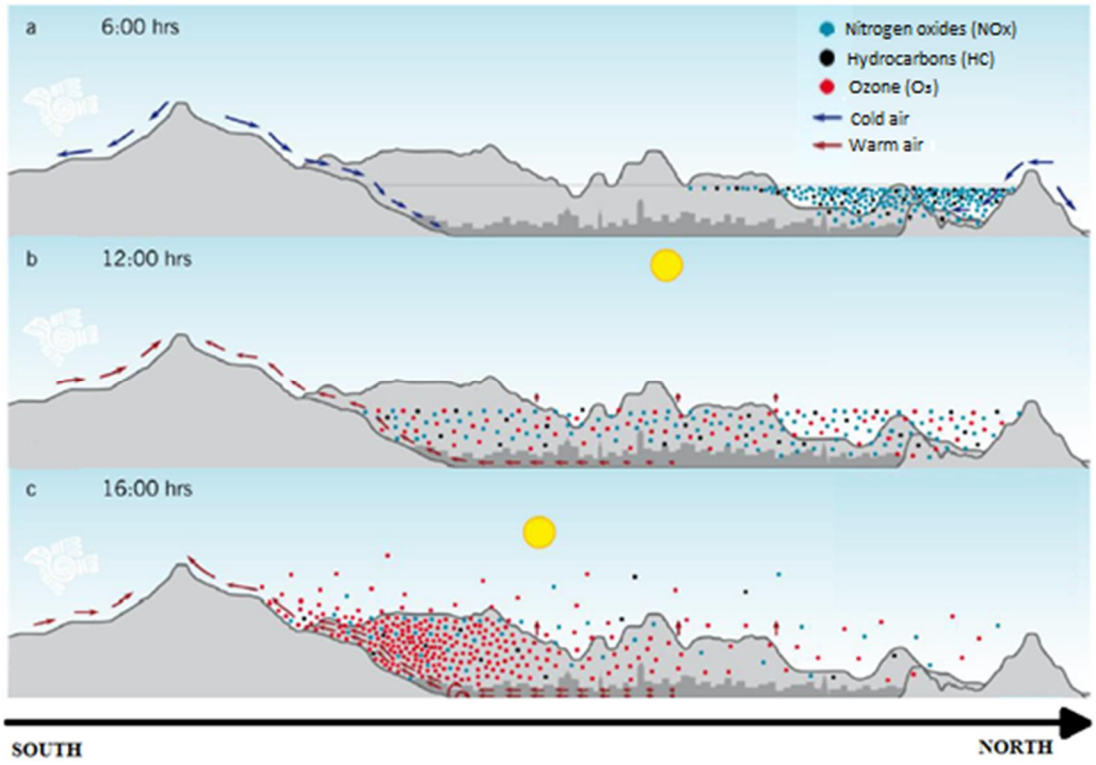

Figure 2.6 Schematic of an advection thermal inversion over MCMA. During the early mornings, cold air trapped near the surface builds up pollutant concentrations. Before noon the thermal inversion breaks allowing vertical mixing. Convection allows dispersion of pollutants during the afternoon.
From SEDEMA (2011).

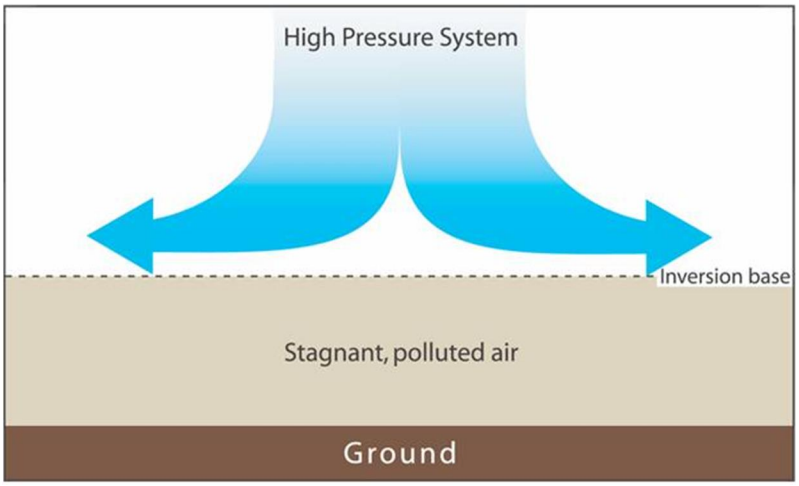

Figure 2.7 Schematic of a subsidence inversion.
From Turco (2002).

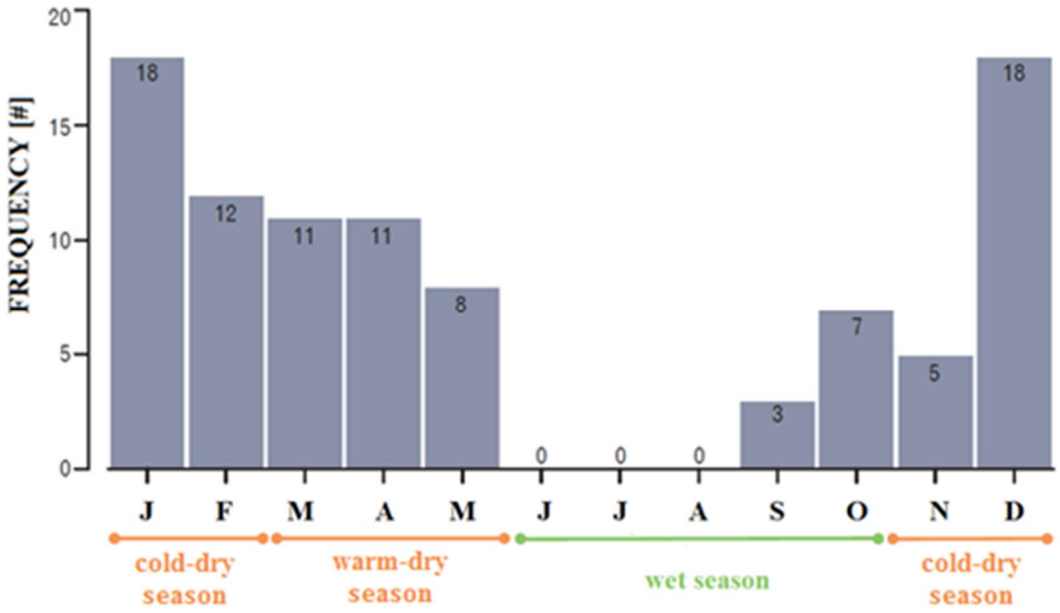

Figure 2.8 Frequency of thermal inversions in MCMA during 2011. From SEDEMA (2012a).

2.4 BIOMASS BURNING

Biomass burning is an important primary source of organic aerosols in the atmosphere (Simoneit and Elias, 2001). It has a significant impact on $PM_{2.5}$ concentrations (Costa et al., 2012, Hosseini et al., 2013, Levin, 2013, Levin et al., 2010, McMeeking, 2004), and is one of the major local and global sources of particulate-phase organic carbon (OC) (Sheesley et al., 2007) and volatile organic compound gases (VOC), some of which are precursors for secondary organic aerosols (Grieshop et al., 2009). Although biomass burning includes a wide range of sources, they can be grouped into six main categories that include wildfires, prescribed burns and agricultural burning (Figure 2.9). In general, depending on the time of year, vegetation, local economic activities, and other characteristics, the local and regional impacts of each source may vary.

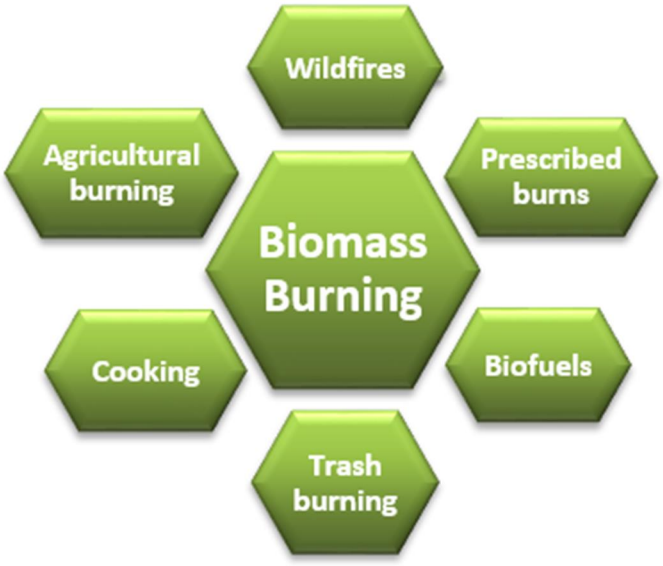

Figure 2.9 Main biomass burning sources.

2.4.1 PARTICLE SIZE DISTRIBUTIONS

Fine mode particles ($PM_{2.5}$) dominate biomass burning emissions (Costa et al., 2012, Levin, 2013, McMeeking, 2004). Laboratory measurements conducted by Hosseini et al. (2013) showed that the major mode of biomass burning particle size distributions by number was in the diameter range of 0.029 to 0.052 μm (Figure 2.10-a), and that most of the mass could be found in particles less than 0.3 μm (Figure 2.10-b). Mack et al. (2010) and Levin et al. (2010) reported data from the Fire Laboratory at Missoula Experiments (FLAME) 2 study conducted in 2007 at the Fire Sciences Laboratory in Missoula, MT, where 21 chamber burns were performed using 18 fuels that are common to the western and southeastern U.S.A. Volume distributions for different fuels measured by Mack et al. (2010) are presented in Figure 2.11. Levin et al. (2010) calculated geometric mean diameters for both the number distributions (D_{gn}) and volume size distributions (D_{gv}) every 10 min over a time period of an hour. The initial geometric mean diameters ranged from 0.05 to 0.14 μm and generally moved toward larger numbers during the

experiment, while the initial D_{gv} ranged from 0.20 to 0.61 μm and decreased over time for most of the experiments. Thus we conclude that most of the number and mass concentrations of particle emissions from biomass burning will be contained in the fine aerosol mode ($PM_{2.5}$).

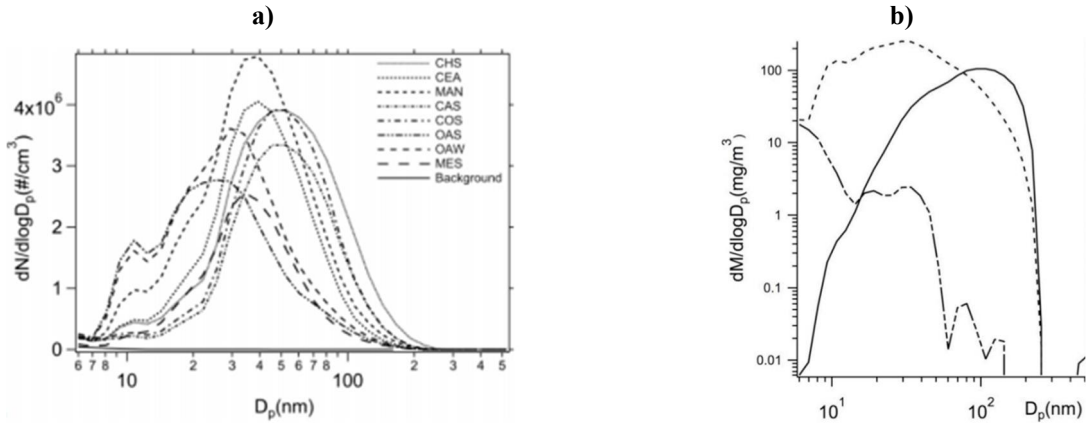

Figure 2.10 Particle size and mass distributions from biomass combustion. a) Particle size distribution for the whole burn of different fuels and bed properties, b) Mass size distribution corresponding to a typical burn. Solid line refers to PM mass, dashed line to particle number concentration and dashed-dotted line to background concentration. From Hosseini et al. (2013).

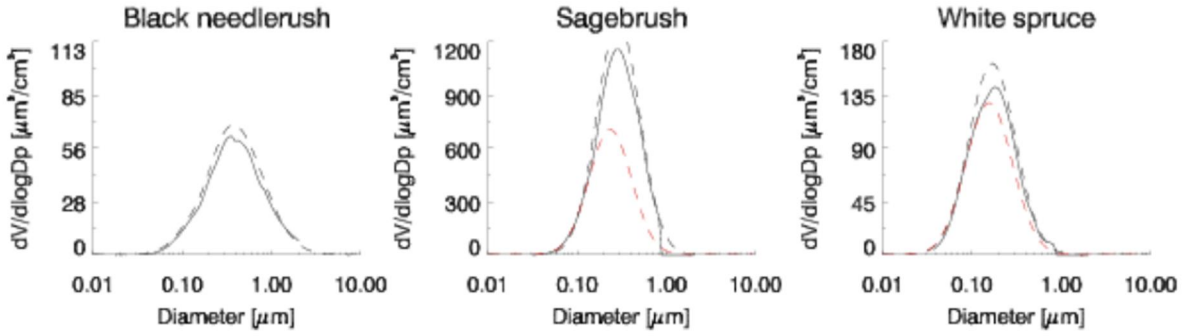

Figure 2.11 Aerosol volume distributions for three different fuels. From Mack et al. (2010).

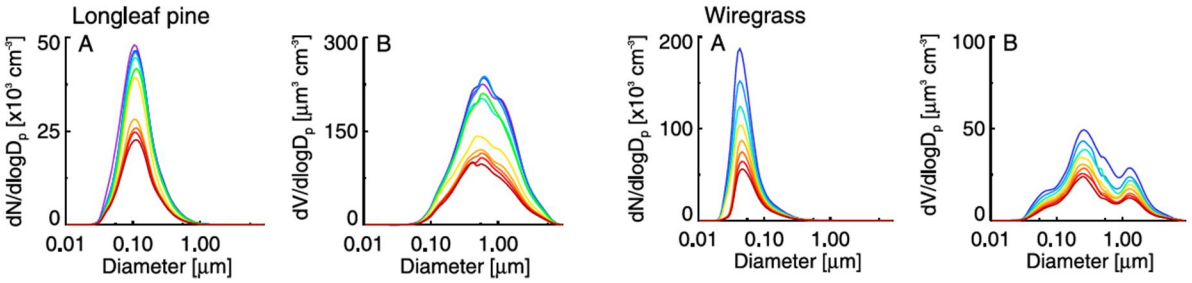

Figure 2.12 Number and volume distributions for Longleaf pine and wiregrass fuels.
Time progresses from purple to red with each distribution 10 minutes apart. From Levin et al. (2010).

2.4.2 BIOMASS BURNING MARKERS

Particulate matter in the atmosphere can be analyzed for organic tracers from biomass burning emissions (Simoneit and Elias, 2001). The heat intensity, aeration, and duration of smoldering and þaming conditions determine the distributions and ratios of tracer compounds in smoke (Simoneit et al., 1999).

2.4.2.1 LEVOGLUCOSAN AND POLYSACCHARIDES

An organic compound often used as a smoke marker to estimate the contribution of biomass burning is levoglucosan ($C_6H_{10}O_5$, 1,6 anhydro-ɓ-D-glucopyranose; LEV). This sugar anhydride is the main pyrolysis product from cellulose and hemicellulose during the flaming combustion process (at temperatures above 300°C) (Simoneit et al., 1999).

LEV has been widely used in numerous aerosol studies as a biomass tracer (Mkoma et al., 2012, Mochida et al., 2010, Urban et al., 2012). LEV concentrations found in remote marine areas (Mochida et al., 2010) and polar regions (Kehrwald et al., 2012) suggest a long-range transport capability and allows its usage as a proxy of past fire activity in snow pits and ice cores.

LEV represents an important fraction of water-soluble organic carbon (WSOC) in carbonaceous aerosols impacted by residential wood burning and wildfires. The mass ratio of LEV to OC and LEV to WSOC determined from source samples can be used to determine the contribution of primary biomass smoke to the total OC or WSOC concentrations in ambient samples (Sullivan et al., 2008). According to Sullivan et al. (2014), the LEV/WSOC ratio is thought to depend on the type of fuel being burned and not to depend on the age of the smoke plume or fire dynamics. In this study they presented LEV/WSOC ratios (µgC/µgC) for four different types of fuel (Table 2.1), which will be used in this study to estimate the biomass burning contribution to WSOC.

Table 2.1 LEV/WSOC ratios (µgC/µgC) from controlled laboratory burns from the Fire Lab at Missoula Experiments (FLAME). From Sullivan et al. (2014).

FUEL TYPE	LEV/WSOC (µgC/µgC)
Grasses	0.149 ± 0.012
Leaves	0.095 ± 0.006
Needles	0.064 ± 0.008
Marsh grasses	0.017 ± 0.014

Other anhydromonosaccharides from combustion of hemicellulose such as glucose, xylose and arabinose, are also emitted from biomass burning but in lower concentrations than LEV (Simoneit et al., 1999). Galactosan (1,6-anhydro-ϐ-D-galactopyranose) and mannosan (1,6-anhydro-ϐ-D-mannopyranose) are not formed by hydrolysis or microbial alteration of carbohydrates, thus they are specific for burning (Simoneit and Elias, 2001).

Levoglucosan stability in the atmosphere

Formerly, LEV was considered as an inert molecule in the atmosphere. Locker (1988) spiked filters with known LEV concentrations and exposed them to sunlight under ambient conditions, finding no degradation of LEV within 8 hours and concluding that LEV was stable enough in the atmosphere to be used as a biomass burning marker. Likewise, acid-catalyzed hydrolysis of LEV under atmospheric conditions was studied by Fraser and Lakshmanan (2000). They analyzed PM_{10} samples collected in Texas that were impacted by biomass burning from Mexico and Central America. Their results showed no degradation of LEV within 10 days under acidic conditions. However, other studies have demonstrated the oxidation of LEV in an aqueous media by hydroxyl radicals (OH), resulting in the formation of higher molecular weight compounds and loss of LEV in ambient samples (Holmes and Petrucci, 2007, Holmes and Petrucci, 2006). Moreover, Hoffmann et al. (2009) studied the reactivity of LEV with OH in aqueous solutions to investigate the degradation fluxes of LEV in cloud droplets and in deliquescent particles (Figure 2.13). They modeled aqueous-phase LEV concentrations for six idealized scenarios: summer and winter clouds (for two cases, low and high relative humidity between cloud cycles), and summer and winter non-cloud conditions. Their results suggested that aqueous phase oxidation can substantially degrade the observed LEV concentrations in the atmosphere; however the presence of other species that compete for free radicals will increase the lifetime of LEV. They estimated the time until the initial LEV concentration was reduced by half ($\tau_{1/2}$) for four scenarios: summer cloud ($\tau_{1/2}$ = 12.7 hours), summer non-cloud ($\tau_{1/2}$ = 33.1 hours), winter cloud ($\tau_{1/2}$ = 72.8 hours), and winter non-cloud ($\tau_{1/2}$ = 83.2 hours). Results showed that the highest degradation of LEV occurs during humid, summer, daytime conditions and the minimum during arid, winter, nighttime conditions.

Another recent laboratory study by Hennigan et al. (2010) examined the reactivity of LEV to gas-phase OH in three aerosol systems: pure LEV particles, wood smoke extract particles, and particles emitted from wood combustion. They found a range of lifetimes from 0.7 to 2.2 days, meaning that 30-75% of the levoglucosan will react within one day at typical summertime atmospheric OH concentrations. Thus estimated lifetimes of LEV are expected to be sensitive to the photochemical environment and to the presence of clouds, with literature estimates ranging from less than one day (0.7) up to 5 days, whereas observations of LEV in remote regions suggest stability in the atmosphere for 4 days and much longer after deposition to snow and ice (Kehrwald et al., 2012). Future studies are needed to better simulate LEV degradation rates under different environments.

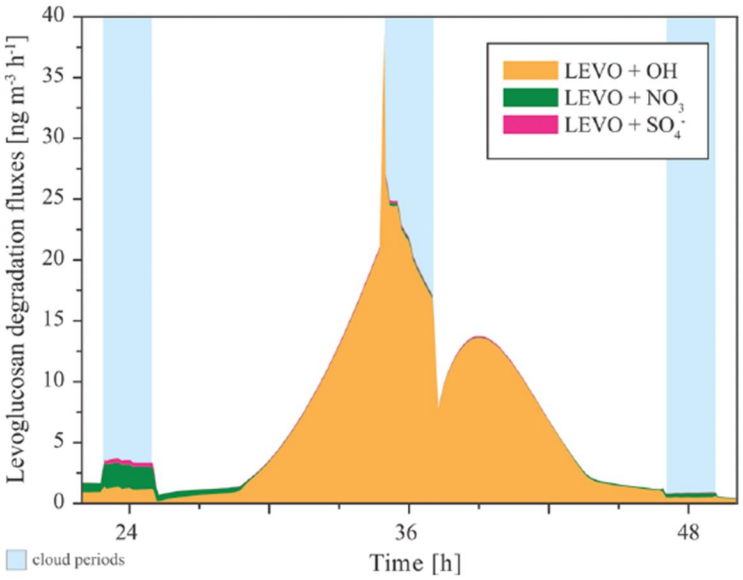

Figure 2.13 Modeled aqueous-phase chemical degradation mass fluxes. Chemical sinks by different radical oxidants of LEV (ng/m^3h) (second day of the model simulation for the Summer Cloud case) are shown. From Hoffmann et al. (2009).

2.4.2.2 WATER-SOLUBLE POTASSIUM

Another commonly used elemental tracer to estimate the contribution of biomass burning to ambient aerosols is water-soluble potassium (WSK^+) (Sullivan et al., 2008, Urban et al., 2012). This element is one of the soluble ions emitted in largest concentrations during biomass burning combustion (Levine, 1991). The usage of WSK^+ instead of elemental potassium is to exclude water-insoluble forms of potassium present in mineral aerosols (Munchak et al., 2011). However, this inorganic indicator is less specific since potassium has complex sources that include, besides biomass burning, sea salt and crustal material (Cheng et al., 2013); furthermore, the large emission variability of potassium and low emission factor may lead to uncertain estimates (Khalil and Rasmussen, 2003). Finally, Lee et al. (2010), who studied smoke markers emitted during flaming and smoldering phases from open burning of numerous wildland fuel types, concluded that mass fraction emissions of WSK^+ are higher during flaming phase. Thus WSK^+ is not a robust tracer for biomass burning.

2.4.2.3 WATER-SOLUBLE ORGANIC CARBON

Water-soluble organic carbon (WSOC) compounds have multiple sources from both primary emissions and secondary products from biogenic and anthropogenic sources (Sullivan et al., 2006). In a non-biomass burning environment, the formation of secondary organic aerosol (SOA) is one of the major sources of WSOC. WSOC is produced by the condensation of low volatility products that are generated by the oxidation of carbonaceous gases (Sullivan et al., 2004, Sullivan et al., 2006).

WSOC species are a major component of emitted biomass burning primary organic aerosols and are also produced as SOA in gas and aqueous-phase reactions (Sullivan et al., 2006, Wonaschütz et al., 2011). According to Gao et al. (2003), WSOC is mainly produced during the

smoldering phase of a fire. Due to its high emission rates, WSOC emissions in biomass burning have been characterized and used to assign a portion of the observed ambient WSOC to a biomass burning source (Hu et al., 2013, Mayol-Bracero et al., 2002, Psichoudaki and Pandis, 2013, Sullivan et al., 2006, Wonaschütz et al., 2011).

As explained in section 2.4.2.1, the LEV/WSOC ratio in smoke source samples is used to determine the contribution of biomass burning direct particulate matter emissions to total observed WSOC in ambient samples. This ratio has been compiled from a number of emissions studies (Cheng et al., 2013, Sullivan et al., 2014, Urban et al., 2012).

2.4.3 BIOMASS BURNING IN MCMA

In MCMA during the dry season, numerous studies conducted as part of the MILAGRO campaign (Molina et al., 2010) suggested that in March 2006, wildfires were the main biomass burning source and contributed significantly to $PM_{2.5}$ concentrations and air quality degradation. MILAGRO-2006 was held during a high fire period, since fire counts in a 120 km radius around MCMA were approximately twice the average of previous years (Aiken et al., 2010). However, there were considerable variations on the contribution estimates among several studies, due to different techniques and apportionment methods in quantifying biomass burning emissions.

Yokelson et al. (2007) concluded that 50±30% of the aged fine particle mass in MCMA outflow could come from forest fires. Another study by Crounse et al. (2009) (Figure 2.14) estimated a fire contribution of approximately one third of the observed CO, benzene and odd nitrogen (NOy) concentrations (31±3%, 36±3% and 34±7%, respectively) and more than half of the organic aerosol (OA) mass and submicron aerosol scattering coefficient (which affects visibility).

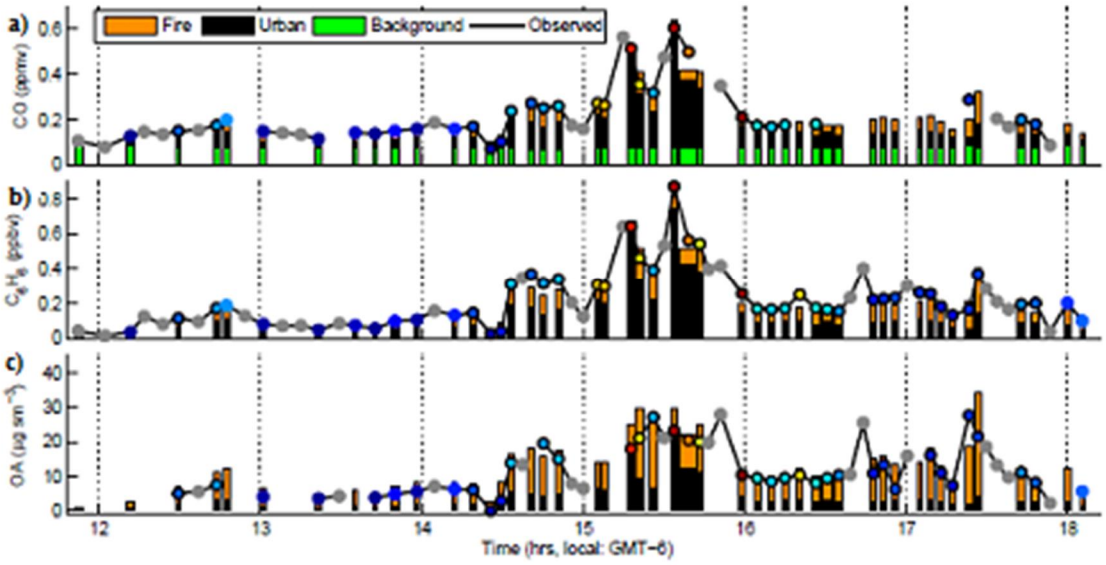

Figure 2.14 Timeline from the flight of 8 March 2006.
The observed (dots) and reconstructed (bars) CO, benzene, and organic aerosol concentrations, are shown in panels (bï c), respectively. From Crounse et al. (2009).

During the MILAGRO campaign, levoglucosan was quantified by different groups over similar periods of time. Stone et al. (2008) used gas chromatography-mass spectrometry and Aiken et al. (2009) used positive matrix factorization analysis of the high resolution OA spectra from aerosol mass spectrometer measurements to identify biomass burning organic aerosols and correlated them with levoglucosan and acetonitrile. Both groups found consistent levoglucosan concentrations for the shared urban site T0. The latter group also derived hydrocarbon-like OA, local nitrogen-containing reduced OA and oxygenated OA contributions and their diurnal profiles. The direct biomass burning mass contribution to PM_1 OA was estimated as 16% (Figure 2.15). Also from OC, LEV, and WSOC concentrations reported by Stone et al. (2008) measured at a peripheral site from MCMA, we calculated an average LEV/WSOC ratio of 0.017 and a LEV/OC ratio of 0.010.

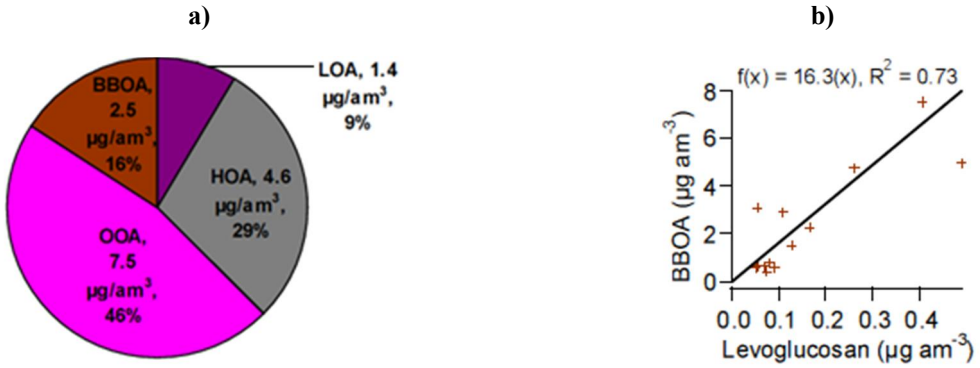

Figure 2.15 a) BBOA Mass contributions to PM_1 OA. b) BBOA vs. levoglucosan concentrations.
From Aiken et al. (2009).

Additionally, Querol et al. (2008) used observed potassium, OC+EC (organic carbon + elemental carbon) and aluminum to determine the contribution of biomass burning and crustal material to $PM_{2.5}$ concentrations. They estimated that biomass burning contributed between 5-15% and crustal material between 15-28% to the total $PM_{2.5}$ ambient concentrations.

3. PROBLEM STATEMENT

The fire season in Mexico occurs during the last part of the dry-warm season and the beginning of the wet season (March through June). From Figure 3.1 we can observe that April and May (warm-dry season) are on average the months with the most reported wildfires nationwide (CONAFOR, 2009). The fires decrease by the beginning of the wet season (June) and start increasing at the end of the dry-cold season (February).

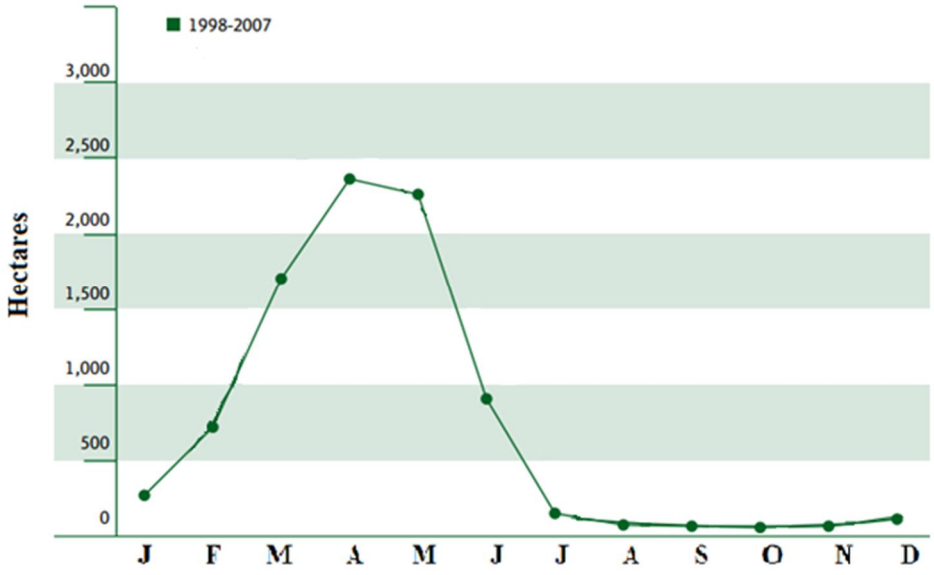

Figure 3.1 Monthly area burned by wildfires over Mexico (1998-2007). Adapted from CONAFOR (2009).

Looking more closely at the fire season in Mexico, during 2013 the central and southern parts of the country presented active fires that affected the air quality of the entire region. To give a sense of the magnitude of this fire season compared with previous years, we used the Fire INventory from the National Center for Atmospheric Research (FINN) and estimate the $PM_{2.5}$ emissions from fires comprising a quadrangular region delimited by latitudes 15 to 23 degrees and longitudes -103 to -195 degrees (covering approximately a radius of 400 km from MCMA).

FINN reports global, daily emission estimates at a horizontal resolution of ~1km^2 for 16 species emitted from wildfires, prescribed burns and agricultural burning. The inventory uses the MODIS Thermal Anomalies Product to identify the location and timing of active fires detected by the MODIS instruments onboard the NASA Terra and Aqua polar orbiting satellites (Wiedinmyer et al., 2011).

As we can see in Figure 3.2, the $PM_{2.5}$ emissions (ton/season) from fires during the fire season of 2013 not only exceed the average over 2002-2013, but also ranked as the year with the second highest emissions of $PM_{2.5}$.

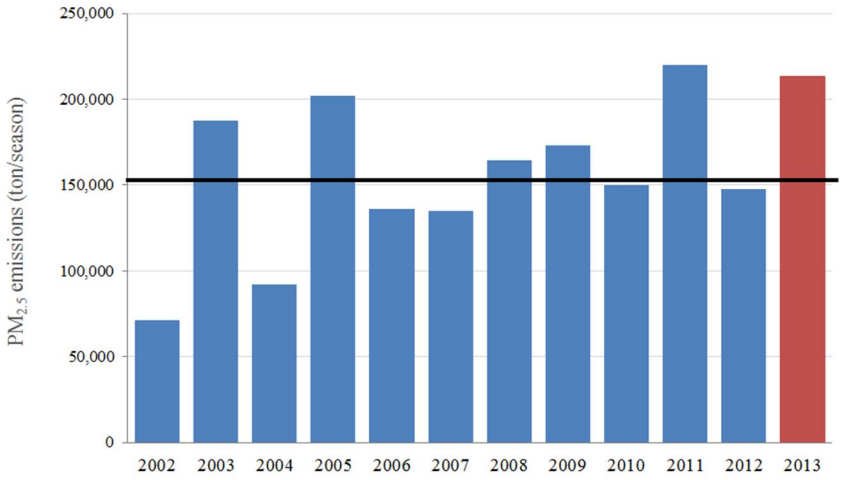

Figure 3.2 $PM_{2.5}$ emissions (ton/season) per fire season from 2002 to 2013. The solid black line represents the average from 2002 to 2012. Fire data from FINN (Wiedinmyer et al., 2011).

If we analyze the monthly emissions per fire season during the same 2002-2013 period, May represents the month with the maximum $PM_{2.5}$ emissions (ton/month). Figure 3.3 shows that May, 2013 exceeds by 40% the average monthly $PM_{2.5}$ emissions of the fire seasons from 2002 to 2013. Furthermore, comparing only the $PM_{2.5}$ emissions (ton/month) for the month of May for the same period, 2013 had as well the maximum emissions of $PM_{2.5}$ (Figure 3.4).

Based on these data, we requested PM filter samples from monitoring stations in MCMA for May 2013, hypothesizing that smoke markers should be readily detected in these samples from fires influencing MCMA air quality during the burning season. We also expected to see variable impacts on pollutant concentrations in the basin, depending on meteorology and fire activity, and proposed to use marker species to estimate the impacts of fires on particulate matter.

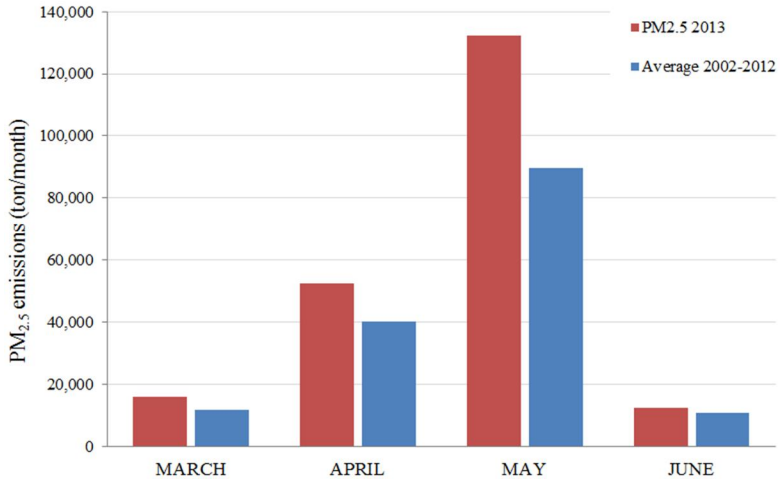

Figure 3.3 Monthly $PM_{2.5}$ emissions (ton/month) during the 2013 fire season and seasonal averages from 2002 to 2013, considering a quadrangular region defined by latitudes 15 to 23 degrees and longitudes -103 to -195 degrees.
Fire data from FINN (Weidenmyer, 2011).

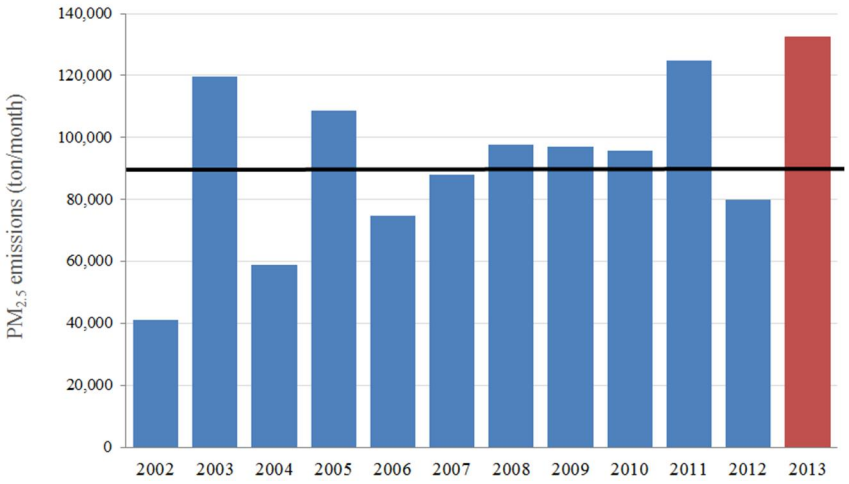

Figure 3.4 $PM_{2.5}$ emissions (ton/month) during the month of May from 2002 to 2013, inside the area of interest.
The solid black line represents the average from 2002 to 2012.
Fire data from FINN (Weidenmyer, 2011).

4. METHODS

Ambient aerosol samples were collected inside MCMA during May 2013. The methodology for the sample collection, the smoke marker laboratory analysis and the methods for estimating the relevant fire sources are presented in this chapter.

Table 4.1 presents the characteristics and sources of the information analyzed in this study. In addition to filter samples, we used monitoring data from the Mexico Cityôs atmospheric monitoring network, SIMAT (Sistema de Monitoreo Atmosférico).

Table 4.1 Source and characteristics of the species analyzed in this study.

SOURCE	TYPE	CO	PM_{10}	$PM_{2.5}$	LEV	WSOC	WSK^+
SIMAT (SIMAT, 2013)	Ambient concentrations	ppm	$\mu g/m^3$	$\mu g/m^3$	-	-	-
FINN (Wiedinmyer et al., 2011)	Total fire emissions	ton/day	-	ton/day	-	-	-
LABORATORY ANALYSIS (CSU)	Ambient concentrations (PM_{10} samples)	-	-	-	$\mu gC/m^3$	$\mu gC/m^3$	$\mu g/m^3$

4.1 HI-VOLUME FILTER SAMPLE COLLECTION

Hi-volume air samplers were used to collect ambient PM_{10} onto glass fiber filters for a 24 hour period (sampling started at 00:00 hours and finished at 24:00 hours, local time). The samples were taken every 6 days during May 2013, at six stations belonging to the atmospheric monitoring network of Mexico City (SIMAT) (Table 4.2). Collection dates were May 4^{th}, 10^{th}, 16^{th}, 22^{nd}, and 28^{th}, and the stations were La Presa (LPR), Merced (MER), Nezahualcóyotl (NEZ), Tlalnepantla (TLA), UAM Iztapalapa (UAM), and Xalostoc (XAL) (see Figure 4.1). A

total of 29 samples were collected (XAL station did not sample on May 4th). The sampling characteristics for each day and station are presented in Table 4.3.

Table 4.2 Characteristics of each sampling site (SIMAT stations).
Station characteristics from SIMAT (2013). Population data from INEGI (2012).

STATION	ID	LATITUDE	LONGITUDE	MASL	COUNTY	COUNTY POPULATION	LOCATION TYPE
La Presa	LPR	19.535	-99.118	2302	Tlalnepantla	653,410	Residential and industrial
Merced	MER	19.425	-99.120	2232	Venustiano Carranza	430,978	Residential
Nezahualcóyotl	NEZ	19.392	-99.028	2237	Nezahualcóyotl	1,104,585	Residential
Tlalnepantla	TLA	19.529	-99.205	2289	Tlalnepantla	653,410	Residential and industrial
UAM-Iztapalapa	UAM	19.361	-99.074	2242	Iztapalapa	1,815,786	Residential
Xalostoc	XAL	19.526	-99.082	2246	Ecatepec de Morelos	1,655,015	Residential and industrial

Table 4.3 Hi-volume air sampling characteristics for the sampling period in May 2013, at six stations belonging to SIMAT.
Data from SIMAT (2013).

DATE	FILTER ID	PM_{10} ($\mu g/m^3$)	VOLUME (m^3)	AVERAGE PRESSURE (mmHg)	AVERAGE TEMPERATURE (°C)
La Presa (LPR)					
4-May-13	16430	88	1848	582	19.3
10-May-13	16444	79	1865	583	21.0
16-May-13	16457	40	1891	584	19.2
22-May-13	16470	51	1876	584	19.0
28-May-13	16484	35	1872	581	18.6
Merced (MER)					
4-May-13	16425	87	1915	587	18.7
10-May-13	16439	81	1961	585	27.8
16-May-13	16452	42	1955	586	25.0
22-May-13	16465	48	1949	587	23.2
28-May-13	16479	38	1967	584	25.7

DATE	FILTER ID	PM_{10} ($\mu g/m^3$)	VOLUME (m^3)	AVERAGE PRESSURE (mmHg)	AVERAGE TEMPERATURE (°C)
Netzahualcóyotl (NEZ)					
4-May-13	16437	81	1931	587	23.0
10-May-13	16450	81	1904	588	21.4
16-May-13	16463	44	1930	587	24.0
22-May-13	16477	50	1946	587	25.0
28-May-13	16490	27	1959	586	27.0
Tlalnepantla (TLA)					
4-May-13	16429	84	1901	582	19.3
10-May-13	16443	80	1926	583	21.0
16-May-13	16456	54	1918	584	19.2
22-May-13	16469	58	1874	584	19.0
28-May-13	16483	43	1753	581	18.6
UAM Iztapalapa (UAM)					
4-May-13	16435	77	1908	587	23.0
10-May-13	16449	83	1903	588	21.4
16-May-13	16462	42	1917	588	24.0
22-May-13	16475	49	1911	587	25.0
28-May-13	16489	32	1992	586	27.0
Xalostoc (XAL)					
4-May-13	--	--	--	--	--
10-May-13	16441	114	1886	587	18.4
16-May-13	16454	76	1943	585	26.0
22-May-13	16467	70	1947	585	23.5
28-May-13	16481	54	1925	585	22.3

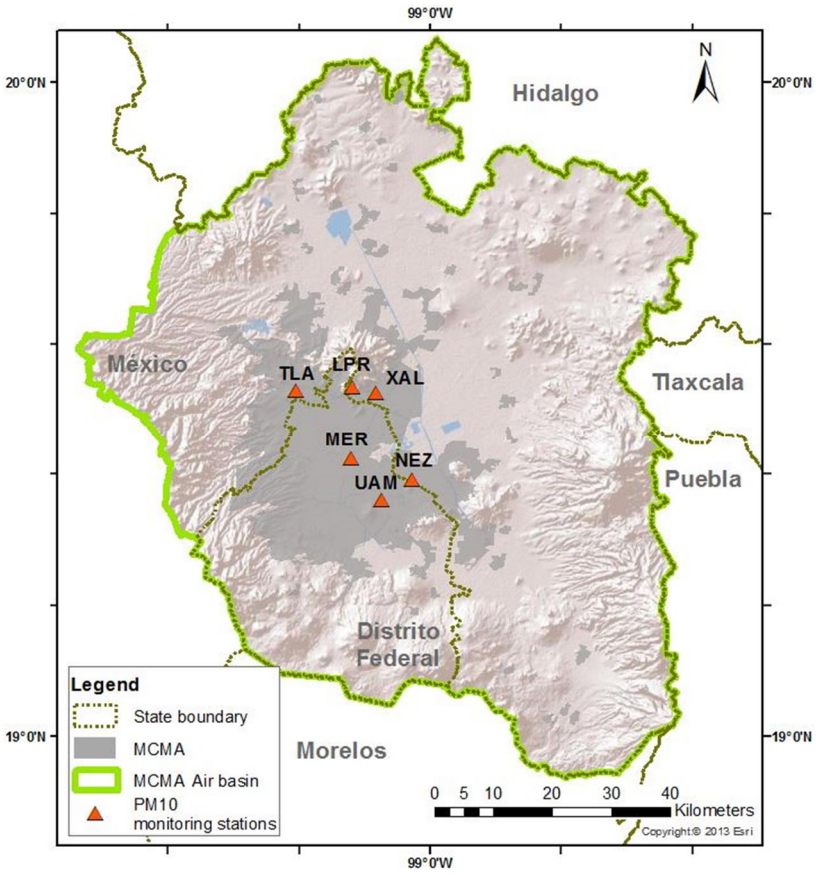

Figure 4.1 SIMAT PM_{10} monitoring stations where 24-hour samples were taken during May 2013.
Station locations from SIMAT (2013). Map created using ArcMap (ESRI, 2012).

Ambient concentrations of CO, PM_{10}, and $PM_{2.5}$

SIMAT also has automated monitoring stations located at the same sites where the PM_{10} samples were taken. The automated stations report hourly ambient concentrations for several air pollutants. The daily mean ambient concentrations of CO (ppm), PM_{10} ($\mu g/m^3$), $PM_{2.5}$ ($\mu g/m^3$), and coarse mode (PM_{10}-$PM_{2.5}$ ($\mu g/m^3$)) are presented in APPENDIX A.

The mean concentrations for the selected SIMAT stations during May 2013 for CO, PM_{10}, and $PM_{2.5}$ were 1.0 ppm, 73 $\mu g/m^3$, and 41 $\mu g/m^3$, respectively. Note that on average,

$PM_{2.5}$ concentrations accounted for 55% of the average PM_{10} ($PM_{10}/PM_{2.5}$ ratio of 1.83 ± 0.22 $\mu g/m^3$ at 95% confidence interval (CI)) with a standard deviation (σ) of 0.06 $\mu g/m^3$.

Degree of homogeneity across the MCMA

In order to determine the degree of homogeneity across the MCMA air basin in ambient concentrations of CO, PM_{10}, and $PM_{2.5}$ during May 2013 (see APPENDIX A), correlation coefficients were calculated for each station and pollutant (for the measurements available in each station) (SIMAT, 2013).

Table 4.4 Correlation coefficients for CO ambient concentrations during sampling dates.
Data from SIMAT (2013).

STATION	LPR	MER	NEZ	TLA	UAM	XAL
LPR	1.00					
MER	0.81	1.00				
NEZ	0.76	0.78	1.00			
TLA	0.81	0.66	0.54	1.00		
UAM	-	0.69	0.64	0.65	1.00	
XAL	0.87	0.68	0.38	0.66	0.27	1.00

Table 4.5 Correlation coefficients for PM_{10} ambient concentrations during sampling dates.
Data from SIMAT (2013).

STATION	MER	TLA	UAM	XAL
MER	1.00			
TLA	0.94	1.00		
UAM	0.96	0.94	1.00	
XAL	0.86	0.91	0.88	1.00

Table 4.6 Correlation coefficients for $PM_{2.5}$ ambient concentrations during sampling dates.
Data from SIMAT (2013).

STATION	MER	NEZ	TLA	UAM	XAL
MER	1.00				
NEZ	0.95	1.00			
TLA	0.96	0.90	1.00		
UAM	0.97	0.96	0.92	1.00	
XAL	0.96	0.95	0.93	0.96	1.00

Table 4.7 Correlation coefficients for coarse fraction ambient concentrations during sampling dates.
Data from SIMAT (2013).

STATION	MER	TLA	UAM	XAL
MER	1.00			
TLA	0.89	1.00		
UAM	0.94	0.93	1.00	
XAL	0.67	0.84	0.75	1.00

Table 4.4 shows relatively low correlation coefficients for CO between the six SIMAT stations compared to the rest of the pollutants. The low correlation can be explained by the multiple sources that CO has in MCMA, where vehicle emissions are its main source (SEDEMA, 2012b). In contrast, the high values for correlation coefficients estimated for the ambient concentrations of PM_{10}, $PM_{2.5}$, and coarse fraction (Table 4.5, Table 4.6, and Table 4.7, respectively) suggest that the MCMA air basin was well-mixed for these pollutants. Furthermore, the high correlation between all the stations also suggests air quality impacts coming from the same sources.

Finally, assuming most of the biomass burning mass concentrations of particle emissions is contained in the $PM_{2.5}$ fraction (discussed in section 2.4.1) the high correlation of course particles between sites (except XAL) might be due to particles derived also from biomass burning sources, photochemistry reactions, and regional dust.

4.2 FILTER SAMPLE ANALYSIS

From each PM_{10} glass fiber filter, two 25 mm diameter punches were extracted in 10 ml of deionized water, then sonicated with heat for 1 hour and 15 minutes and finally filtered with a 0.2 µm PTFE syringe filter to remove possible fiber glass residues. The aqueous extracts were analyzed for 12 carbohydrates (most of them associated with biomass burning particles: levoglucosan, mannosan, galactosan, galactose, glucose, mannose, glycerol, inositol, theritol, mannitol, arabinose, and xylose) the same day they were extracted. The technique used coupled high-performance anion-exchange chromatography with pulsed amperometric detection (HPAEC-PAD). We used a Dionex DX-500 series ion chomatrograph with a Dionex GP-50 pump and a Dionex ED-50 electrochemical detector operating in integrating amperometric mode using waveform A. The waveform is used to alternate between the oxidation of the analytes on the surface of a gold electrode via a positive potential and a second potential that cleans the electrode (Holden et al., 2011). The full description of this method is provided in Sullivan et al. (2008). The limit of detection (LOD) for measuring carbohydrates by this technique was 2.26 µg or $0.00118 \pm 7.7 \times 10^{-5}$ µg/m^3 (considering the air volumes shown in Table 4.3).

Seven ions including water-soluble potassium (WSK^+) were also analyzed from the liquid extract during the same day of extraction using a Dionex DX-500 series ion chromatograph with a Dionex CD-20 conductivity detector, Dionex IP-20 isocratic pump and self-regenerating cation SRS-ULTRA suppressor. To separate the inorganic cations a Dionex IonPac CS12A analytical column was used. Also for this measurement, a 20-mM methanesulfonic acid eluent at a flowrate of 0.5 ml/min was used (Sullivan et al., 2008). The LOD for the ion measurements was 0.36 µg/m^3. Two blanks were run to correct ion

concentrations. The ion concentrations measured on the filter blanks were substracted from the filter samples.

Finally, water-soluble organic carbon (WSOC) concentrations were measured using a Portable Total Organic Carbon Analyzer (Sievers Turbo). In turbo mode, this instrument has a lower LOD of 100 ppb and an upper LOD of 2500 ppb. For the filter samples from May 4th and 10th, 200 µl of the aqueous extract were diluted in 9 ml of deionized water, because the concentrations exceeded the upper LOD of the instrument. The rest of the sampling dates (May 16th, 22nd, and 28th) showed lower concentrations of WSOC and therefore 1 ml of the aqueous extract was diluted in 9 ml of deionized water.

4.3 METEOROLOGY AND BIOMASS BURNING IMPACT

4.3.1 FIRE COUNTS

In order to estimate the biomass burning sources that impacted the six stations where the air samples were taken, two combined analyses were done. The first analysis was aimed at determining the range of air mass pathways that occurred during the 24 hours of sampling (ending at 0600 UTC) and might have impacted MCMA during the sampling periods. For each sampling date, hourly 24-hour backward trajectories from the center of the grid at 3500 MASL were run using the NOAA HYSPLIT model (Draxler and Rolph, 2013, Rolph, 2013). The meteorological field selected was the North American Mesoscale Forecast System (NAM) by the National Centers for Environmental Prediction, which reports data on a 12 km grid. The 3500 MASL height was chosen assuming a mean boundary layer height of 4000 MASL, which was estimated by analyzing the different heights of the lifting condensation level from soundings at 12Z and 00Z for each sampling date (Oolman, 2013). The skew-t diagrams and meteorology

characteristics for each sounding are shown in APPENDIX B. The center of the grid corresponded to Merced station at latitude: 19.4245 N and longitude: 99.1195 W.

In Figure 4.2 we can see a shift of winds coming from the west on May 4th and 10th, to winds coming primarily from the north for the rest of the sampling days.

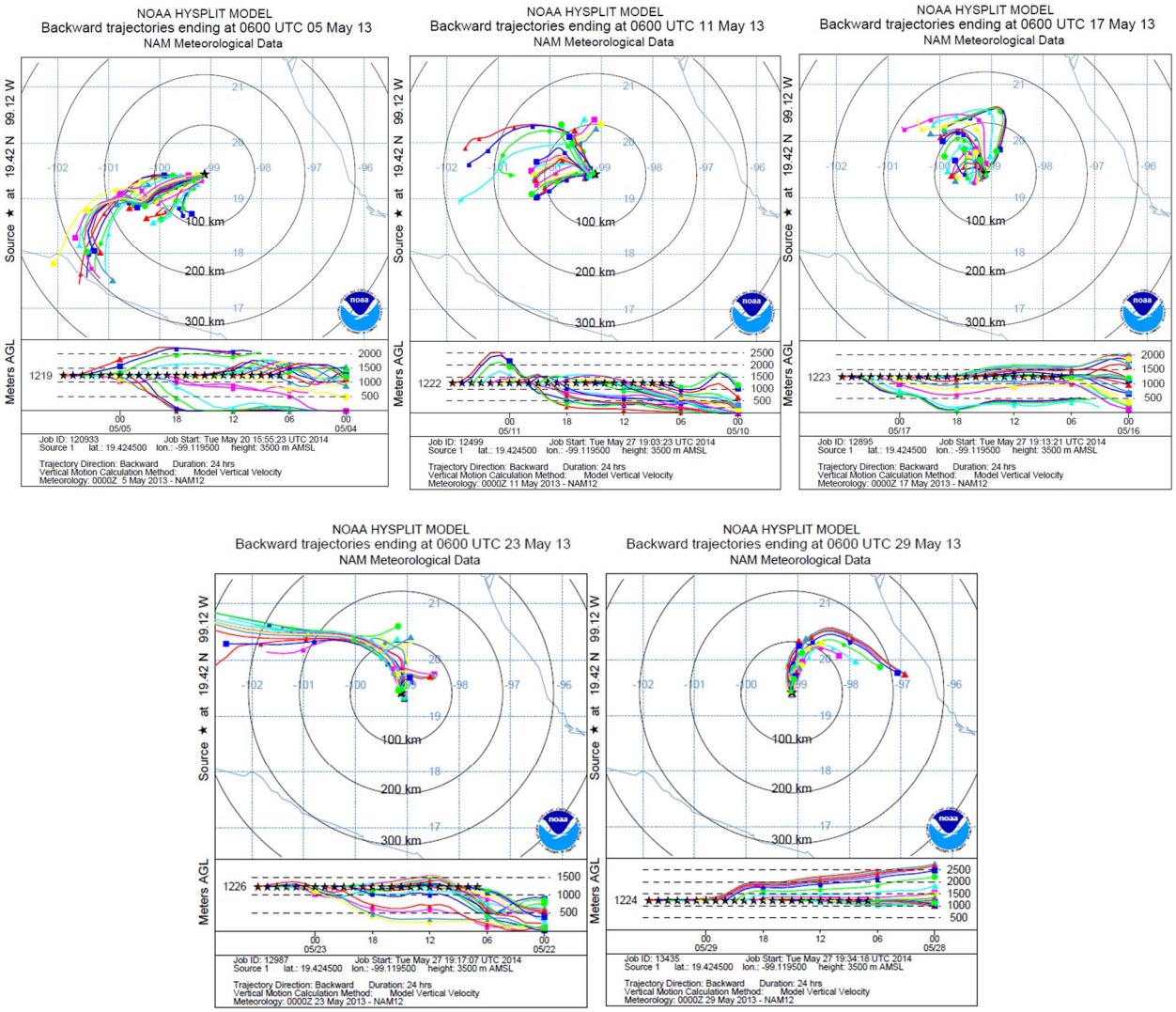

Figure 4.2 Hourly 24-hour backward trajectories from the center of MCMA. NOAA HYSPLIT MODEL with NAM meteorology was used (Draxler and Rolph, 2013).

Considering the range of air mass pathways shown in Figure 4.2, the active fires that were assumed to directly impact MCMA for each sampling day were the ones located over one or more of the eight intercardinal directions (north, north east, east, south east, south, south west, west and north west) within a 400 km radius from MCMA. The fire information from FINN (Wiedinmyer et al., 2011) was used to geographically locate wildfires, prescribed burns and agricultural burning using the geographic information system ArcMap (main component of ArcGIS developed by Environmental Systems Research Institute, ESRI). Figure 4.3 shows the spatial distribution of fires in the region surrounding MCMA and the sectors used to estimate the number of fires that impacted Mexico Cityôs air basin over each sampling day.

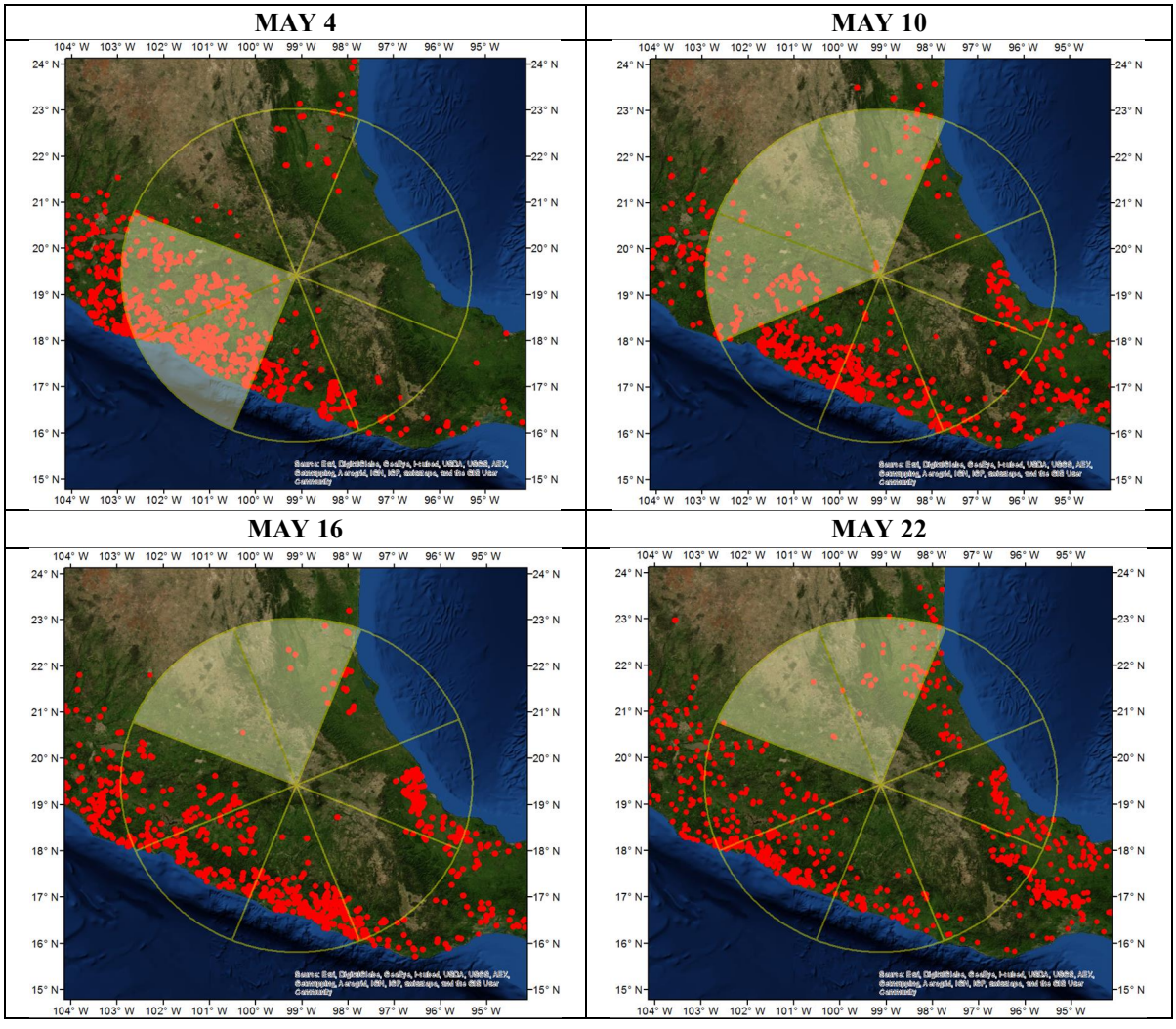

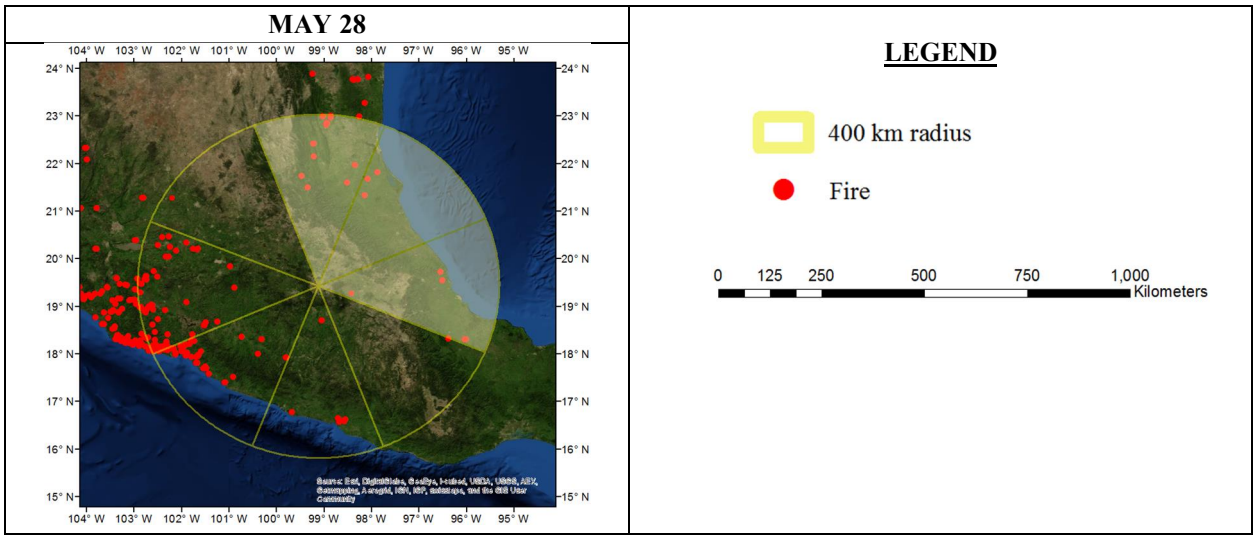

Figure 4.3 Fire spatial distribution in the region surrounding MCMA. Shaded regions are the intercardinal directions used to estimate the number of fires that impacted MCMA each sampling day. Fire information from FINN (Wiedinmyer et al., 2011). Maps were created using ArcMap (ESRI, 2012).

Table 4.8 Fire characteristics over relevant spatial area surrounding MCMA for each sampling day.
Fire counts and emissions from FINN (Wiedinmyer et al., 2011).

DAY	RADIUS	WIND DIRECTION	FIRE COUNT	AREA BURNED (km^2)	CO (ton/day)	$PM_{2.5}$ (ton/day)
4	400	W,SW	425	419	21,976	3,017
10	400	W, NW, N	104	98	3,368	498
16	400	NW, N	12	10	506	50
22	400	NW, N	46	38	843	96
28	400	N, NE, E	21	17	454	49
		TOTAL	**608**	**582**	**27,147**	**3,710**

The fire spatial distributions (Figure 4.3) show that during the sampling dates, most of the fires occurred to the west and south west of MCMA, therefore a change in winds blowing from the west to winds blowing from the north, and reduced fire counts overall in the region, suggest a lower fire impact for May 16th, 22th and 28th. Compared to the MILAGRO campaign, the fires in May 2013, where farther away from MCMA. Aiken et al. (2010) found that 63% of the fires

where located within a 60 km radius from MCMA during the MILAGRO campaign, whereas in May 2013 ~81% of the fires occurred between a 200 to 400 km radius from MCMA.

From Table 4.8, we can see that May 4th was the sampling day when most fires impacted the MCMA air basin. 608 fires were located over a 400 km radius, which represented 72% of the total area burned during the sampling dates. Also, the CO and $PM_{2.5}$ emitted from these fires were the highest with 22,000 and 3,000 tons per day, respectively.

4.3.2 SATELLITE IMAGES

To give a qualitative idea of the biomass burning impact on Mexico Cityôs airshed, satellite images showing active fires over approximately a 400 km radius from MCMA for each sampling date are shown in Figure 4.4 (NASA-Worldview, 2014). The images depict an active fire period across the area with visible smoke plumes affecting not only MCMA but the entire selected region. On May 10th and 16th, we can observe a smoke plume being transported southwards into the Pacific Ocean.

Another meteorological phenomenon that we can observe from satellite images is the development of Hurricane Barbara (Figure 4.5). Barbara developed from a low pressure area (System 92E) during May 28th (last sampling day), 2013 into a Category 1 hurricane (on the Saffir-Simpson Hurricane Wind Scale) on May 29th in the south part of Mexico. Barbara made landfall on May 29th with winds of 130 km/h and dissipated on May 30th (Brown, 2013). Barbaraôs precipitation enhancement did not affect MCMA during our sampling period (see Section 4.3.3). However, in subsequent days, the regional precipitation enhancement and strong winds due to Barbara, potentially helped remove and disperse pollutants from smoke plumes and reduced fires in southern Mexico.

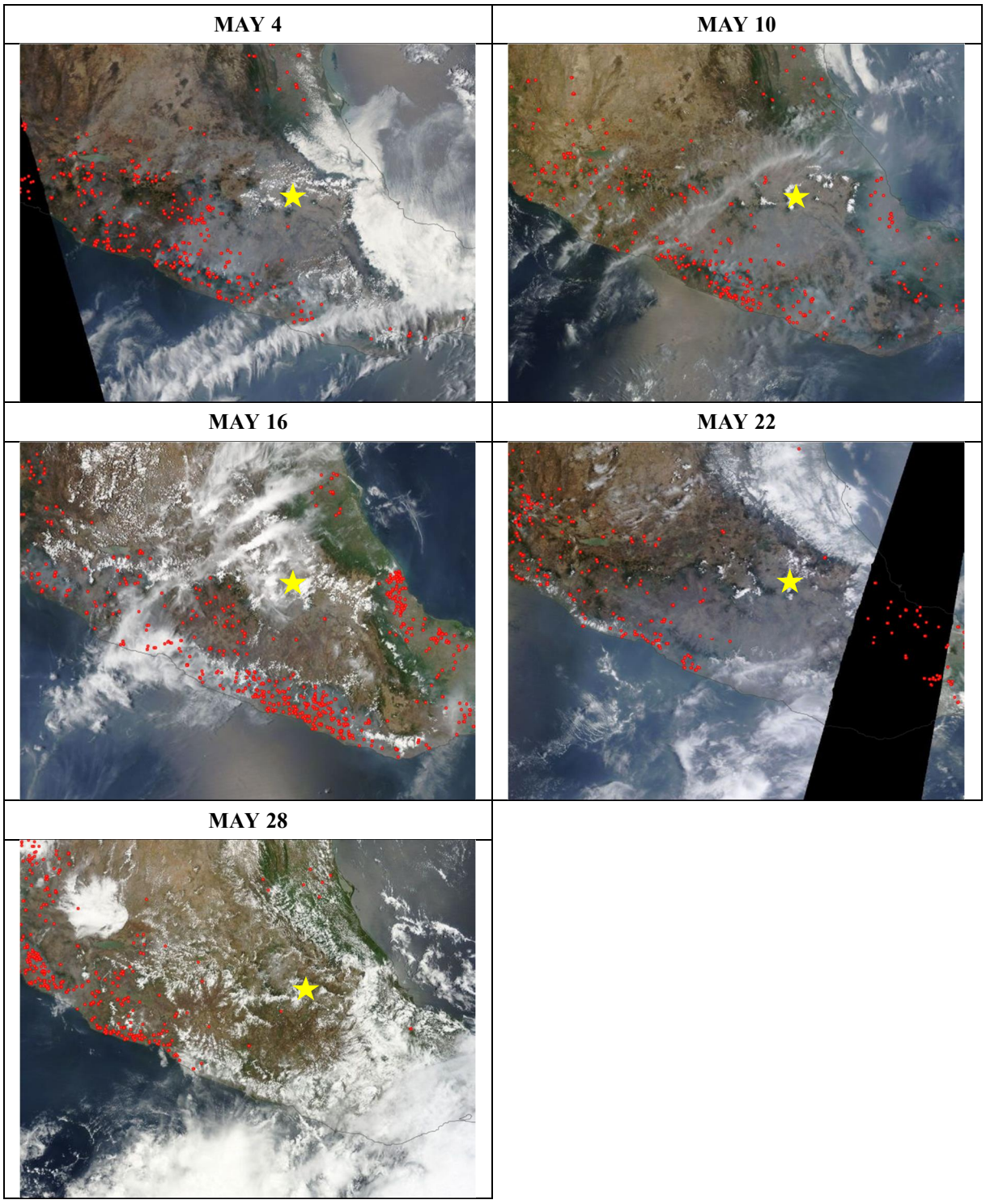

Figure 4.4 Satellite images for the sampling period (NASA-Worldview, 2014).
The area shown corresponds approximately to a 400 km radius from MCMA. Red dots represent active fires. The yellow star shows the approximate location of MCMA.

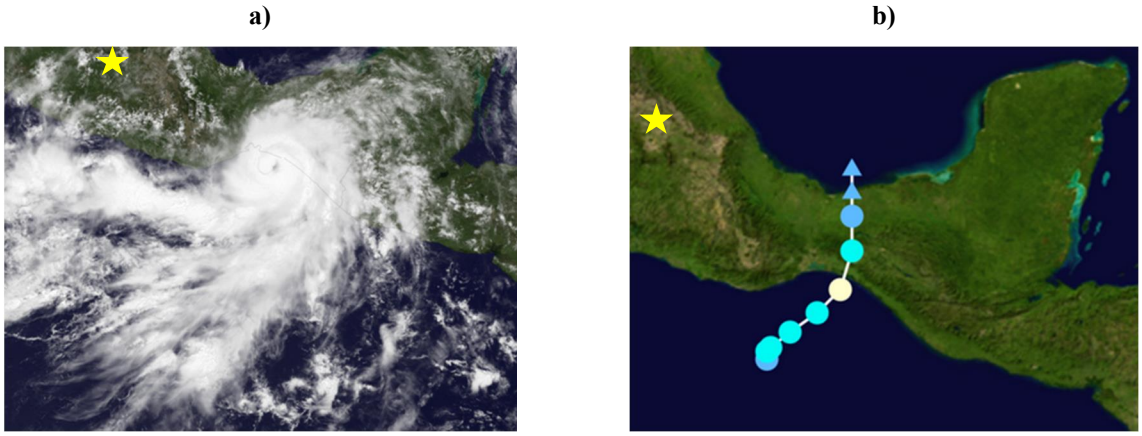

Figure 4.5 Satellite image and storm path of Hurricane Barbara (Brown, 2013).
a) Satellite image of Hurricane Barbara at 1815 UTC, May 29th. b) Storm path. The yellow star shows the approximate location of MCMA.

4.3.3 PRECIPITATION PATTERN

Precipitation patterns over MCMA during May 2013, seemed to have a strong influence over the daily average ambient concentrations of CO (ppm), PM_{10} ($\mu g/m^3$) and $PM_{2.5}$ ($\mu g/m^3$). Daily average precipitation rates during May 2013 showed a dry period early in the month until May 11th, followed by a wet period through May 26th. No precipitation was reported over the last 5 days of the month. Concentrations of CO, PM_{10} and $PM_{2.5}$ at the SIMAT stations were high relative to the rest of the month and increasing while the dry conditions persisted (especially from May 7th through May 11th); they showed a clear decrease basin-wide when the wet period began on May 12th (see Figure 4.6, Figure 4.7, and Figure 4.8). The calculated mean $PM_{2.5}$ ambient concentration for the dry period was 59 $\mu g/m^3$, compared to 39 $\mu g/m^3$ during the wet period.

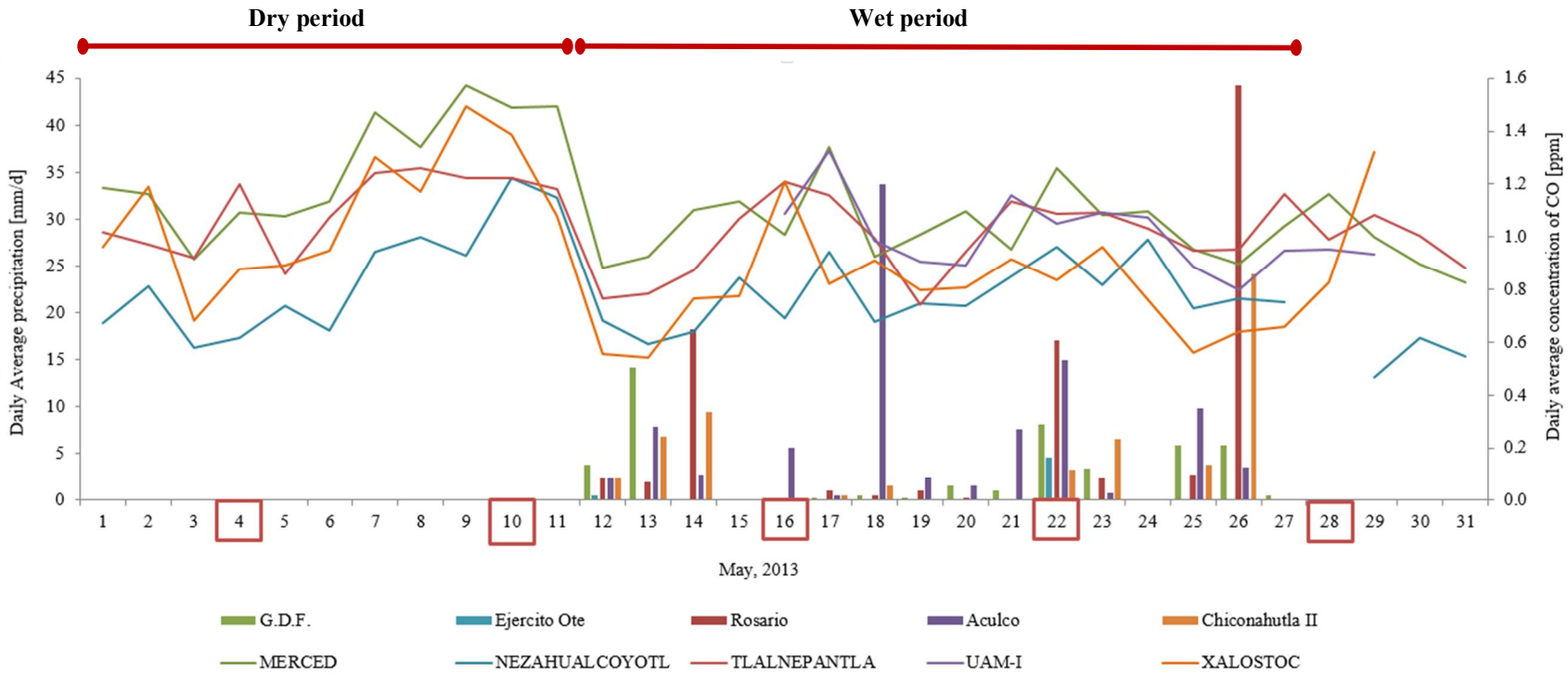

Figure 4.6 Daily average precipitation rates (SACMEX, 2013) and CO daily mean ambient concentrations (SIMAT, 2013) during May 2013.
The nearest rain gauges from SACMEX to the SIMAT stations were considered. The names of the SACMEX stations selected are presented with the same color of the associated SIMAT station.
Dates within red boxes correspond to sampling dates.

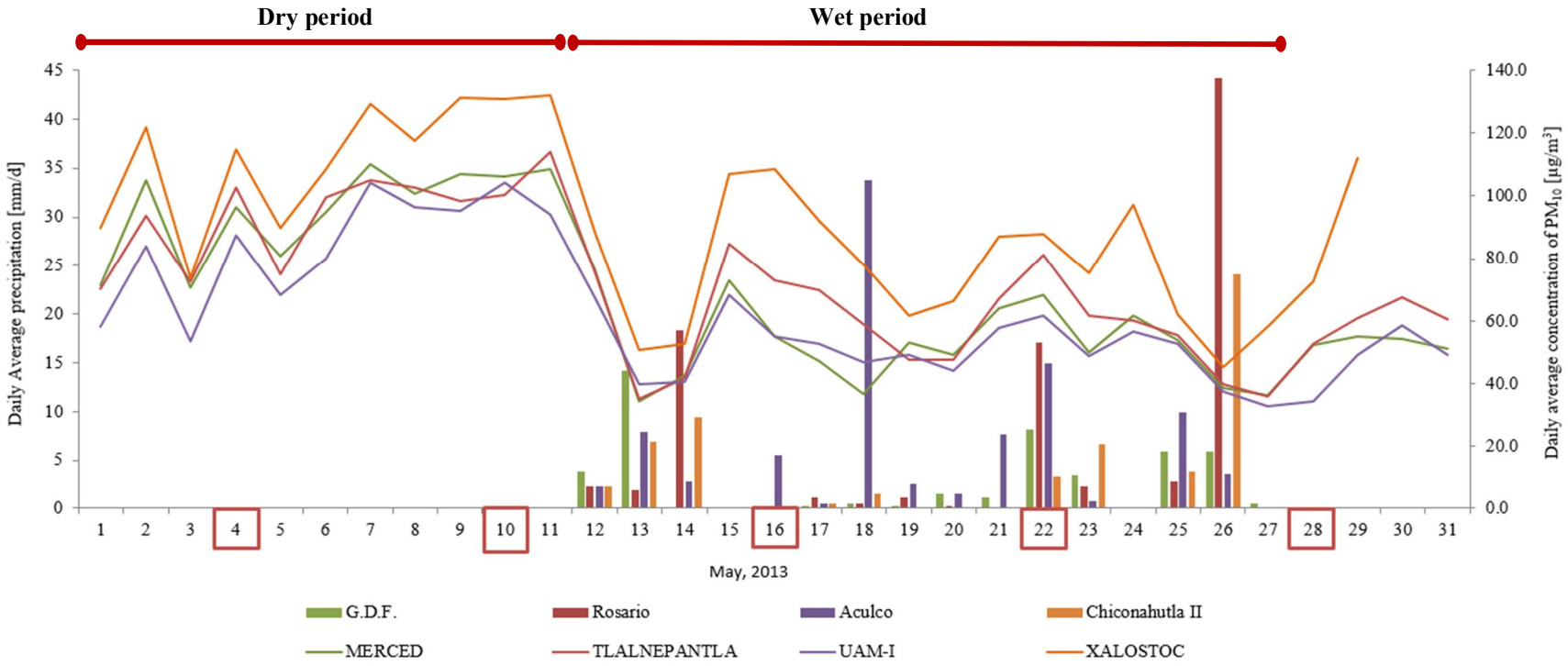

Figure 4.7 Daily average precipitation rates (SACMEX, 2013) and PM_{10} daily mean ambient concentrations (SIMAT, 2013) during May 2013.
The nearest rain gauges from SACMEX to the SIMAT stations were considered. The names of the SACMEX stations selected are presented with the same color of the associated SIMAT station.
Dates within red boxes correspond to sampling dates.

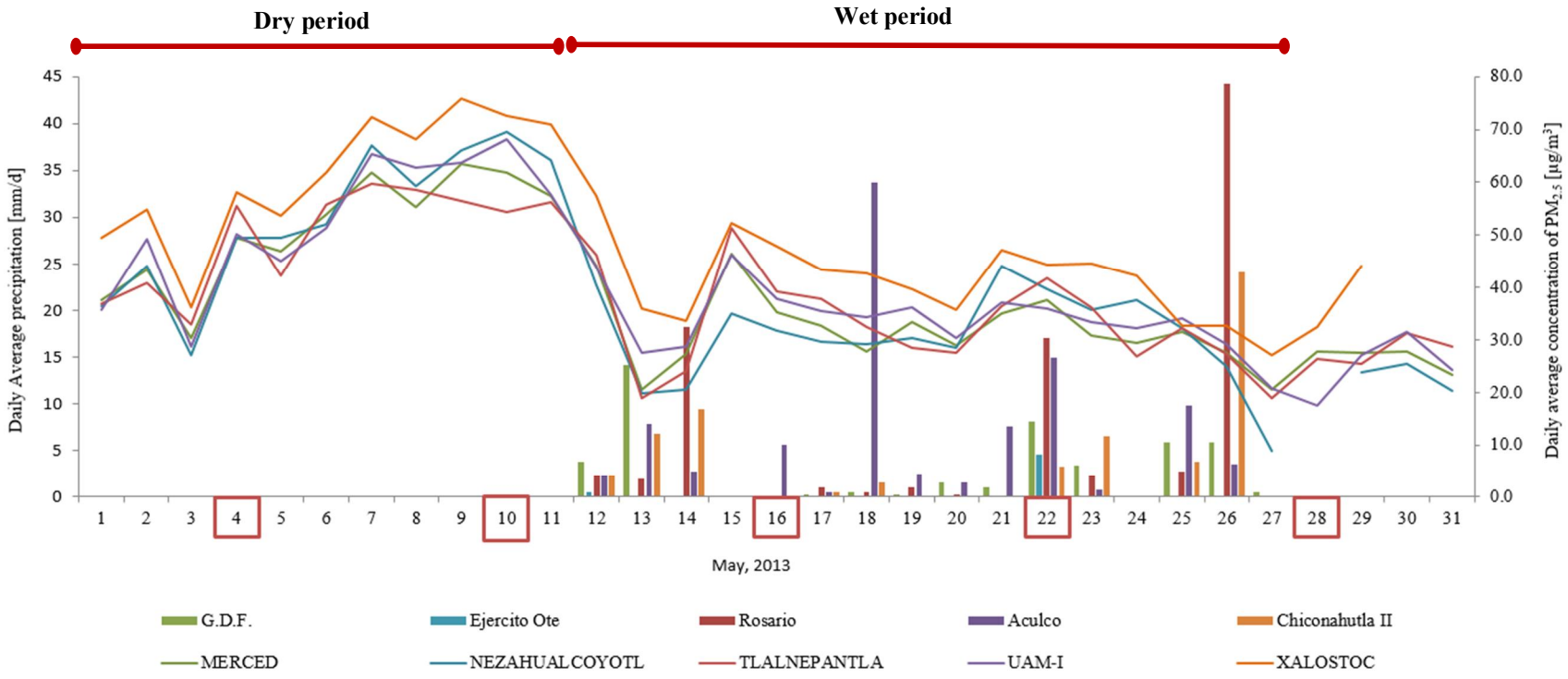

Figure 4.8 Daily average precipitation rates (SACMEX, 2013) and $PM_{2.5}$ daily mean ambient concentrations (SIMAT, 2013) during May 2013.
The nearest rain gauges from SACMEX to the SIMAT stations were considered. The names of the SACMEX stations selected are presented with the same color of the associated SIMAT station.
Dates within red boxes correspond to sampling dates.

4.3.4 METEOROLOGICAL REGIMES

Considering the number of satellite derived fire counts and the change in air mass pathways for each sampling day, as well as the ambient concentrations of CO (ppm), PM_{10} ($\mu g/m^3$) and $PM_{2.5}$ ($\mu g/m^3$), and the mean precipitation rates for each sampling site and day on May 2013, we established two regimes, as shown in Table 4.9. Regime 1 had no precipitation, was more strongly impacted by fire emissions, and had higher mean $PM_{2.5}$ concentrations throughout MCMA.

Table 4.9 Characteristics of the meteorological regimes.

REGIME	SAMPLING DAYS (MAY)	PREDOMINANT AIR MASS PATHWAY	MEAN FIRE COUNT	MEAN PRECIPITATION RATE (mm/day)	MEAN AMBIENT CONCENTRATION		
					CO (ppm)	PM_{10} ($\mu g/m^3$)	$PM_{2.5}$ ($\mu g/m^3$)
1	4, 10	W	265	0	1.1	105	59
2	16, 22, 28	N	26	4	1.0	67	35

5. RESULTS AND DISCUSSION

5.1 BIOMASS BURNING SOURCES

Coupling FINN data with the vegetation and land use geographic information from INEGI (2005), we can estimate the contributions of various fuel types to the total emissions from the 608 fires that happened during the 5 sampling days in May 2013.

Table 5.1 shows that 64% of the total area burned corresponded to wildfires, which contributed ~77% to the total emissions of CO and $PM_{2.5}$. Agricultural burning emissions contributed about 22% and 23% of CO and $PM_{2.5}$ respectively, and trash burning estimated emissions accounted for less than 0.5% of the total emissions. The percentage distributions of CO and $PM_{2.5}$ emissions for each source category are presented in Figure 5.1 and Figure 5.2. Wildfires that occurred in pine and oak forests and in deciduous and semi-deciduous forests were the source categories that contributed the most (~70%) to CO and $PM_{2.5}$ emissions.

Overall, wildfires represented the most important fuel category (~80% of the total CO and $PM_{2.5}$ emissions) and were considered as the most important vegetation burned when estimating the biomass burning contributions to WSOC in section 0.

Table 5.1 Vegetation and land use analysis for the fires during the sampling dates.
Vegetation and land use information from INEGI (2005).
Fire locations from FINN (Wiedinmyer et al., 2011).

VEGETATION AND LAND USE	AREA [km^2]	CO [ton/d]	$PM_{2.5}$ [ton/d]
Wildfires			
Pine and oak forest	179	13,002	1,698
Deciduous and semi-deciduous forest	174	6,127	943
Cloud forest	13	1,796	195
Juniper and gallery forest	2	29	5
Grassland and scrub	4	85	9

VEGETATION AND LAND USE	AREA [km^2]	CO [ton/d]	$PM_{2.5}$ [ton/d]
Total wildfires	372	21,040	2,850
Percent of total	64	78	77
Agricultural burning			
Induced and cultivated pasture	121	3,989	559
Rainfed and irrigated agriculture	83	2,015	292
Total agricultural burning	204	6,003	851
Percent of total	35	22	23
Trash burning			
Urban zone	6	105	11
Percent of total	1	0.4	0.3
TOTAL	**582**	**27,148**	**3,711**

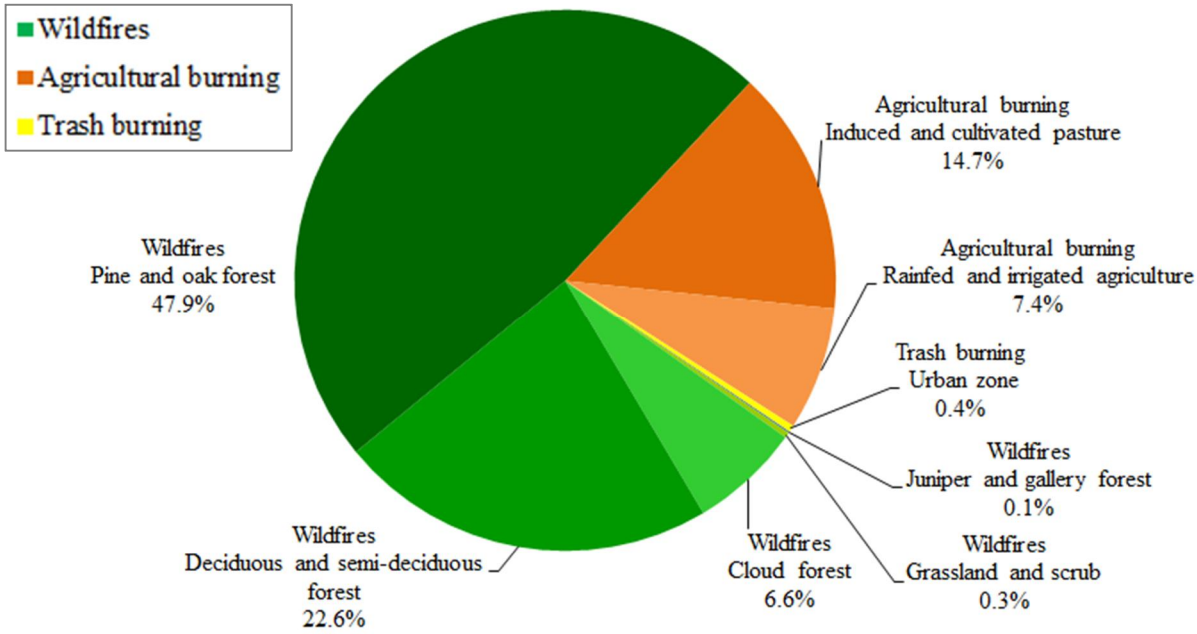

Figure 5.1 Percentage distributions of CO emissions for wildfires, agricultural burning and trash burning source categories.
Vegetation and land use information from INEGI (2005).
Fire locations from FINN (Wiedinmyer et al., 2011).

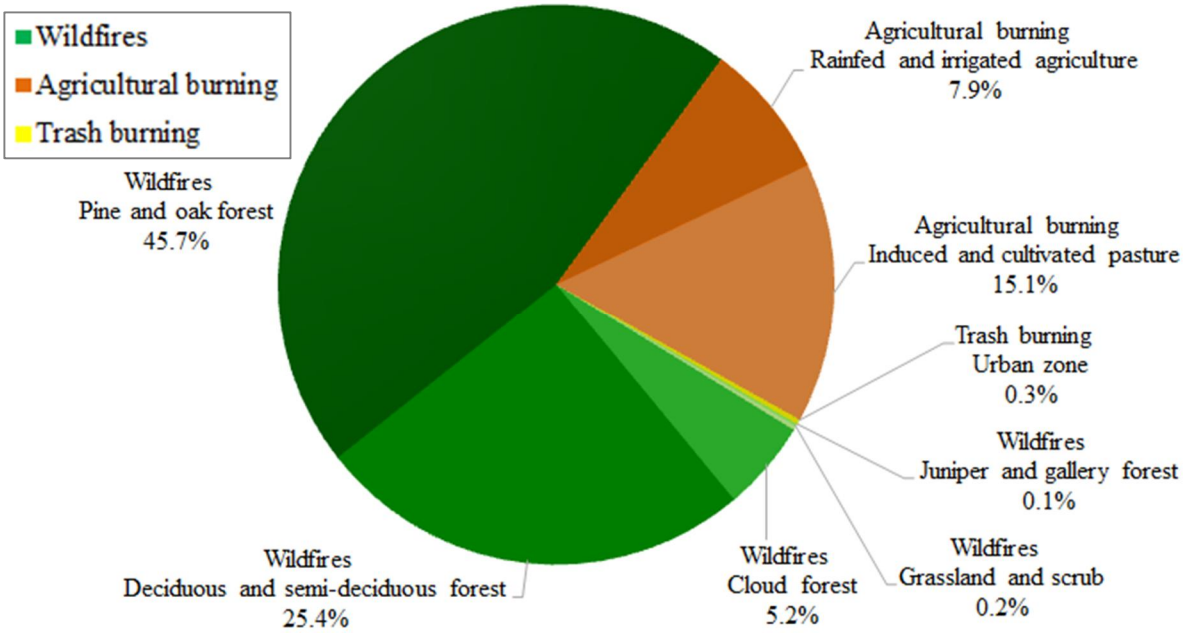

Figure 5.2 Percentage distributions of $PM_{2.5}$ emissions for wildfires, agricultural burning and trash burning source categories. Vegetation and land use information from INEGI (2005). Fire locations from FINN (Wiedinmyer et al., 2011).

5.2 CARBOHYDRATE AND ION CONCENTRATIONS

Between August 2013 and January 2014, 29 PM_{10} filter samples from the six SIMAT stations within MCMA were analyzed for 12 carbohydrates, 7 ions and WSOC. As expected, levoglucosan (LEV) was detected in all the PM_{10} filter samples analyzed. The measured carbohydrate concentrations are presented in Table 5.2, while concentrations of ions, WSOC, LEV as µgC/m^3, and LEV/WSOC ratios (µgC/µgC) are shown in Table 5.3. All concentration data presented are at local temperature and pressure.

In general, the highest concentrations for all the carbohydrates were found on May 4th and May 10th, while most of the lowest concentrations were observed on May 16th. LEV had the highest ambient concentrations for all sampling days and sites, among all the analyzed carbohydrates. The mean LEV concentration was 0.158 ± 0.046 µg/m^3 at 95% confidence

interval (CI) (0.070 ± 0.020 μgC/m^3 at 95% CI) with a standard deviation of 0.146 μg/m^3 (0.065 μgC/m^3). Our results are consistent with the concentrations found by Stone et al. (2008) during the MILAGRO campaign in 2006, which reported an average concentration of 0.151 μg/m^3 (0.067 μgC/m^3) and a standard deviation of 0.136 μg/m^3 (0.060 μgC/m^3) for an urban site (results reported at local temperature and pressure).

The highest and lowest LEV concentrations were found on May 4th and May 16th, respectively. Recalling the meteorological regimes described in section 4.3.4, the average LEV concentration for Regime 1 was 0.335 ± 0.018 μg/m^3 at 95% CI (0.149 ± 0.008 μgC/m^3 at 95% CI) and 0.049 ± 0.005 μg/m^3 at 95% CI (0.022 ± 0.002 μgC/m^3 at 95% CI) for Regime 2, representing a decrease from the first to second regime of about a factor of 7 in mass concentration. The highest LEV concentrations coincided with the highest fire count day (May 4th). Furthermore, the mean LEV concentrations were positively correlated with fire counts for all sampling dates (R^2=0.66, Figure 5.3-a), and with other FINN modeled products such as area burned (R^2=0.66, Figure 5.3-b), CO emissions rate (R^2=0.59, Figure 5.3-c) and $PM_{2.5}$ emissions rate (R^2=0.61, Figure 5.3-d). Combined with the observed homogeneity across the basin for $PM_{2.5}$ (Table 4.6), these findings suggest that the whole MCMA basin was affected by transported emissions from fires occurring in the surrounding regions.

Table 5.2 Carbohydrate ambient concentrations in µg/m^{3}for PM_{10} 24-hour filter samples from six SIMAT stations within MCMA.

May	Station ID	Levoglucosan (µg/m^3)	Mannosan (µg/m^3)	Galactosan (µg/m^3)	Galactose (µg/m^3)	Glucose (µg/m^3)	Mannose (µg/m^3)	Glycerol (µg/m^3)	Inositol (µg/m^3)	Threitol (µg/m^3)	Mannitol (µg/m^3)	Arabinose (µg/m^3)	Xylose (µg/m^3)
4	LPR	0.3314	0.0360	0.0143	0.0036	0.0400	0.0008	0.0060	0.0013	0.0123	0.0088	0.0092	0.0105
	MER	0.4093	0.0465	0.0159	0.0037	0.0503	0.0002	0.0059	0.0042	0.0168	0.0112	0.0107	0.0085
	NEZ	0.3748	0.0427	0.0156	0.0035	0.0370	0.0007	0.0175	0.0048	0.0137	0.0082	0.0097	0.0118
	TLAL	0.3413	0.0366	0.0141	0.0036	0.0663	0.0009	0.0048	0.0005	0.0068	0.0096	0.0096	0.0100
	UAM	0.3786	0.0406	0.0153	0.0035	0.0292	0.0004	0.0182	0.0034	0.0183	0.0076	0.0091	0.0116
10	LPR	0.2664	0.0358	0.0114	0.0026	0.0252	0.0034	0.0241	0.0003	0.0094	0.0055	0.0063	0.0069
	MER	0.3437	0.0495	0.0150	0.0031	0.0615	0.0107	0.0312	0.0040	0.0153	0.0089	0.0075	0.0031
	NEZ	0.4023	0.0533	0.0194	0.0027	0.0322	0.0044	0.0156	0.0031	0.0194	0.0059	0.0085	0.0105
	TLAL	0.2208	0.0285	0.0093	0.0028	0.0696	0.0083	0.0043	0.0011	0.0082	0.0056	0.0070	0.0018
	UAM	0.3665	0.0462	0.0146	0.0029	0.0407	0.0043	0.0204	0.0008	0.0117	0.0078	0.0085	0.0104
	XAL	0.2987	0.0415	0.0146	0.0032	0.0413	0.0039	0.0019	0.0002	0.0115	0.0071	0.0078	0.0089
16	LPR	0.0278	0.0028	0.0012	0.0017	0.0176	0.0008	0.0027	0.0005	0.0013	0.0102	0.0007	0.0005
	MER	0.0240	0.0025	0.0010	0.0016	0.0205	0.0019	0.0045	0.0014	0.0026	0.0087	0.0005	0.0006
	NEZ	0.0356	0.0031	0.0011	0.0016	0.0203	0.0033	0.0059	0.0014	0.0019	0.0119	0.0020	0.0020
	TLAL	0.0332	0.0030	0.0012	0.0019	0.0309	0.0020	0.0068	0.0009	0.0021	0.0098	0.0013	0.0008
	UAM	0.0360	0.0032	0.0012	0.0018	0.0241	0.0029	0.0064	0.0010	0.0026	0.0117	0.0020	0.0011
	XAL	0.0357	0.0034	0.0015	0.0018	0.0261	0.0003	0.0014	0.0009	0.0028	0.0122	0.0016	0.0002
22	LPR	0.0437	0.0040	0.0017	0.0017	0.0179	0.0007	0.0061	0.0008	0.0032	0.0045	0.0017	0.0006
	MER	0.0716	0.0091	0.0019	0.0018	0.0259	0.0025	0.0069	0.0018	0.0055	0.0120	0.0024	0.0015
	NEZ	0.0495	0.0044	0.0020	0.0019	0.0184	0.0014	0.0073	0.0016	0.0047	0.0051	0.0017	0.0011
	TLAL	0.0601	0.0084	0.0026	0.0019	0.0419	0.0008	0.0052	0.0018	0.0106	0.0148	0.0024	0.0006
	UAM	0.0643	0.0089	0.0023	0.0018	0.0235	0.0012	0.0223	0.0014	0.0038	0.0141	0.0023	0.0010
	XAL	0.0565	0.0086	0.0023	0.0019	0.0396	0.0009	0.0088	0.0011	0.0148	0.0132	0.0023	0.0007
28	LPR	0.0588	0.0088	0.0035	0.0031	0.0235	0.0016	0.0042	0.0020	0.0015	0.0108	0.0029	0.0012
	MER	0.0694	0.0075	0.0033	0.0030	0.0307	0.0022	0.0192	0.0020	0.0014	0.0143	0.0031	0.0012
	NEZ	0.0558	0.0075	0.0032	0.0029	0.0278	0.0022	0.0199	0.0017	0.0010	0.0123	0.0031	0.0015
	TLAL	0.0438	0.0061	0.0035	0.0032	0.0473	0.0029	0.0090	0.0020	0.0008	0.0138	0.0033	0.0017
	UAM	0.0552	0.0071	0.0032	0.0030	0.0316	0.0017	0.0097	0.0015	0.0010	0.0145	0.0028	0.0014
	XAL	0.0698	0.0092	0.0038	0.0028	0.0281	0.0021	0.0035	0.0019	0.0021	0.0129	0.0028	0.0017

Table 5.3 Ion, WSOC, and LEV as µgC/m^3 ambient concentrations, and LEV/WSOC ratio (µgC/m^3/µgC/m^3) for PM_{10} 24-hour filter samples from six SIMAT stations within MCMA.

May	Station ID	Sodium (µg/m^3)	Ammonium (µg/m^3)	WSK^+ (µg/m^3)	Magnesium (µg/m^3)	Calcium (µg/m^3)	Nitrate (µg/m^3)	Sulfate (µg/m^3)	WSOC (µg C/m^3)	LEV (µgC/m^3)	LEV/WSOC (µgC/µgC)
4	LPR	1.12	0.71	0.69	0.13	1.38	3.10	2.80	10.49	0.14	0.014
	MER	1.04	0.96	0.71	0.10	1.26	2.95	2.89	11.49	0.18	0.015
	NEZ	0.97	0.90	0.67	0.09	1.10	2.06	2.94	10.77	0.16	0.015
	TLAL	1.18	0.92	0.74	0.16	1.62	3.16	4.54	8.04	0.15	0.018
	UAM	1.08	0.93	0.67	0.08	0.95	2.30	2.73	10.58	0.16	0.016
10	LPR	0.43	0.96	0.68	0.12	1.26	3.47	4.95	8.76	0.12	0.014
	MER	0.51	1.19	0.75	0.10	1.30	3.39	5.79	10.05	0.15	0.015
	NEZ	0.52	1.26	0.86	0.09	1.18	3.59	5.37	11.73	0.18	0.015
	TLAL	0.40	1.23	0.60	0.09	1.31	2.83	6.05	8.04	0.10	0.012
	UAM	0.36	1.03	0.76	0.09	1.20	3.71	4.75	11.04	0.16	0.015
	XAL	0.44	1.19	0.71	0.15	1.76	4.07	5.28	10.15	0.13	0.013
16	LPR	0.19	0.97	0.33	0.09	0.71	2.80	4.78	3.70	0.01	0.003
	MER	0.53	1.24	0.43	0.08	0.78	2.26	7.23	3.17	0.01	0.003
	NEZ	0.53	0.93	0.43	0.07	0.97	2.20	6.65	3.20	0.02	0.005
	TLAL	0.44	1.62	0.42	0.08	1.01	3.36	7.00	4.40	0.01	0.003
	UAM	0.45	1.21	0.44	0.06	0.76	2.31	6.60	3.65	0.02	0.004
	XAL	0.48	1.29	0.43	0.10	1.15	3.80	6.21	3.42	0.02	0.005
22	LPR	0.21	0.54	0.35	0.07	0.85	2.38	3.99	3.91	0.02	0.005
	MER	0.35	0.72	0.48	0.06	0.73	1.92	5.22	4.56	0.03	0.007
	NEZ	0.32	0.69	0.43	0.06	0.85	2.07	5.17	4.14	0.02	0.005
	TLAL	0.43	0.81	0.50	0.07	1.13	2.61	5.55	4.87	0.03	0.005
	UAM	0.44	1.02	0.54	0.05	0.72	2.52	5.30	5.08	0.03	0.006
	XAL	0.41	0.75	0.45	0.10	1.29	2.56	5.49	4.45	0.03	0.006
28	LPR	0.00	0.40	0.19	0.04	0.49	2.18	2.72	2.96	0.03	0.009
	MER	0.24	0.45	0.29	0.05	0.67	2.78	3.17	2.96	0.03	0.010
	NEZ	0.17	0.26	0.19	0.02	0.42	2.48	2.14	3.48	0.02	0.007
	TLAL	0.14	0.71	0.26	0.08	0.90	2.03	5.47	4.35	0.02	0.004
	UAM	0.12	0.26	0.18	0.03	0.44	2.71	1.97	2.36	0.02	0.010
	XAL	0.11	0.37	0.21	0.05	0.70	1.66	3.29	2.38	0.03	0.013

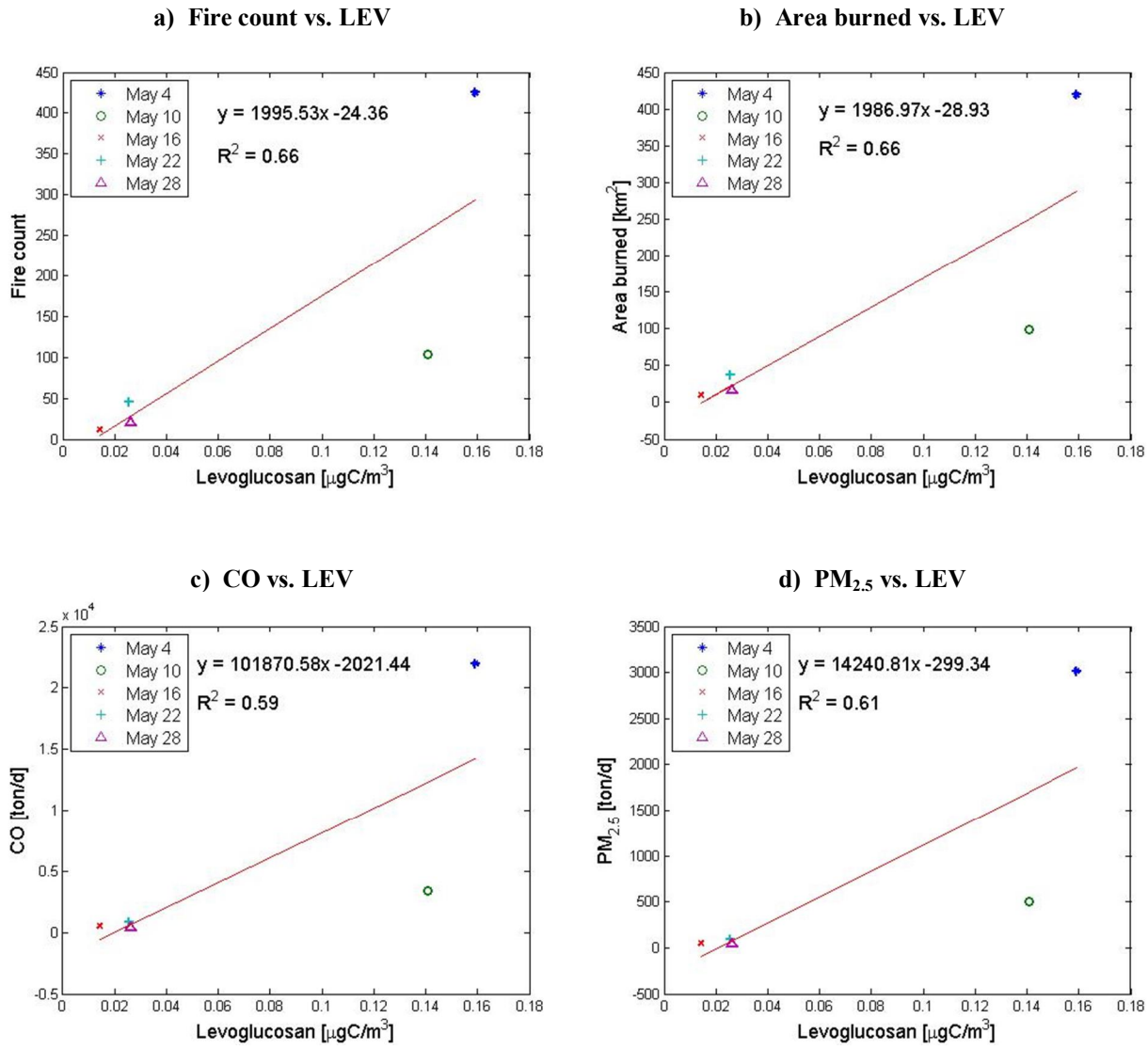

Figure 5.3 Correlation between FINN products and mean LEV (μgC/m^3) concentrations for each day, averaged over all the sampling sites. Fire emissions from FINN (Wiedinmyer et al., 2011).

Relationships between concentrations of CO, PM_{10}, and $PM_{2.5}$ and LEV are presented in Figure 5.4 through Figure 5.9. The results showed low coefficients of determination of CO with LEV ambient concentrations for all sampling dates and all SIMAT sites (R^2 ranged from 0.08 to 0.5), with an overall correlation of R^2=0.06 (Figure 5.4). In Figure 5.5 we can distinguish the ambient concentrations of CO between the two meteorological regimes (Table 4.9). We found a

CO concentration decrease of 9% from Regime 1 to Regime 2, with a mean CO ambient concentration was 1.1 ppm (standard deviation, σ =0.3 ppm) for the first regime and 1.0 ppm (σ=0.2 ppm) for the second. The generalized low correlation suggests multiple local sources of CO that are not related to biomass burning sources. In fact, within MCMA vehicle emissions are the main source of CO (98% of the CO emissions (SEDEMA, 2012b)) and depend on the time and weekday (SEDEMA, 2011).

Stronger correlations were found between particulate matter (PM_{10} and $PM_{2.5}$) and LEV concentrations. PM_{10} and LEV coefficients of determination for each site ranged between R^2=0.55 and R^2=0.89, with an overall R^2 of 0.42 (Figure 5.6). Figure 5.7 shows the concentrations of PM_{10} ($\mu g/m^3$) during both meteorological regimes. On average, PM_{10} concentrations during Regime 1 were 55% higher than during Regime 2. The mean PM_{10} concentration for Regime 1 was 104 ± 4 $\mu g/m^3$ at 95% CI (σ=13) and 67 ± 6 $\mu g/m^3$ at 95% CI (σ=20) for the second regime. We expect PM_{10} to be influenced by local sources of primary particle emissions, such as dust from paved and unpaved roads (SEDEMA, 2012b), while biomass burning primary emissions are mostly in the $PM_{2.5}$ fraction. The strongest correlations were found between $PM_{2.5}$ and LEV coefficients of determination for each SIMAT site ranging between R^2=0.69 and R^2=0.78 and with an overall R^2 of 0.62 (Figure 5.8). Likewise, less spread of $PM_{2.5}$ concentrations between sites was found during both meteorological regimes. For Regime 1 (characterized by higher fire count, predominant winds coming from the west, and no precipitation), the mean $PM_{2.5}$ concentration was 59 ± 3 $\mu g/m^3$ at 95% CI with a smaller standard deviation than PM_{10} (σ=9). For Regime 2 (with lower fire counts, predominant winds coming from the north and a mean precipitation of 4 mm/day), the mean $PM_{2.5}$ concentration was 35 ± 2 $\mu g/m^3$ at 95% CI (σ=8) (Figure 5.9).

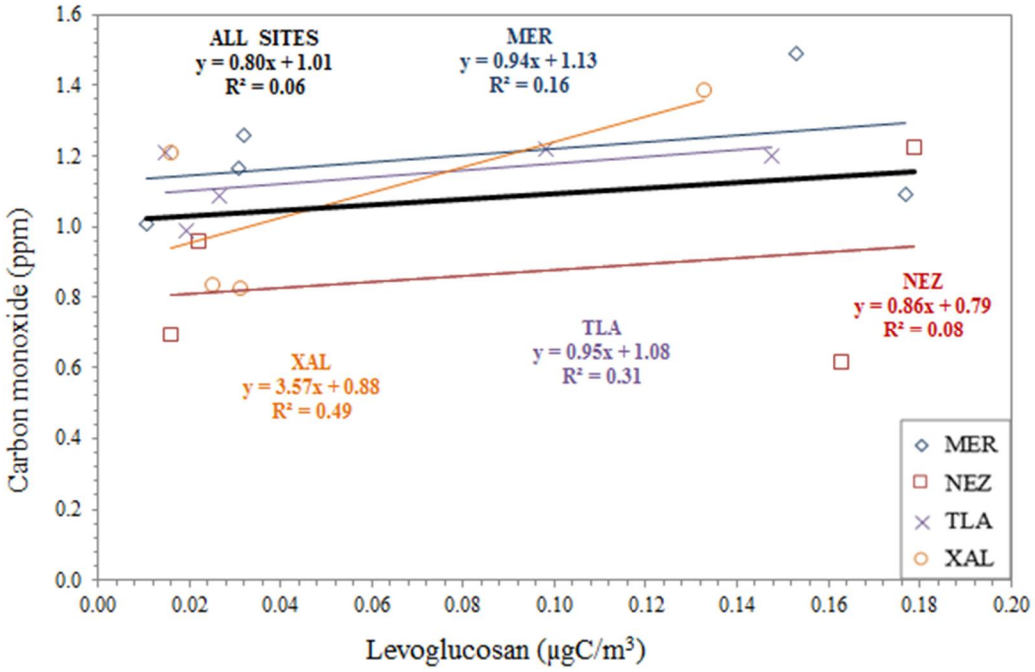

Figure 5.4 Coefficients of determination between CO (ppm) and LEV (µgC/m^3) ambient concentrations for all sampling dates for each and for all SIMAT sites.
Ambient CO concentrations from SIMAT (2013).

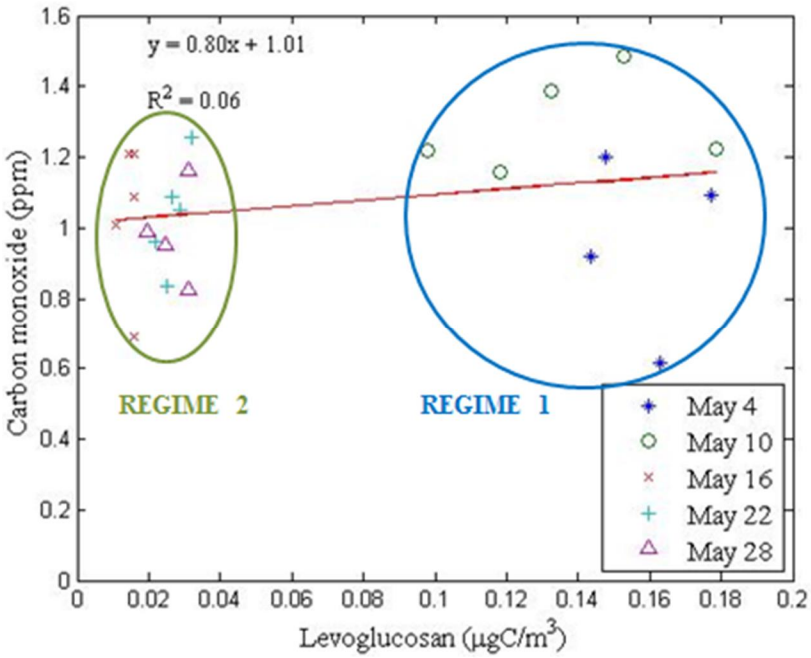

Figure 5.5 CO (ppm) vs. LEV (µgC/m^3) ambient concentrations during the two meteorological regimes.

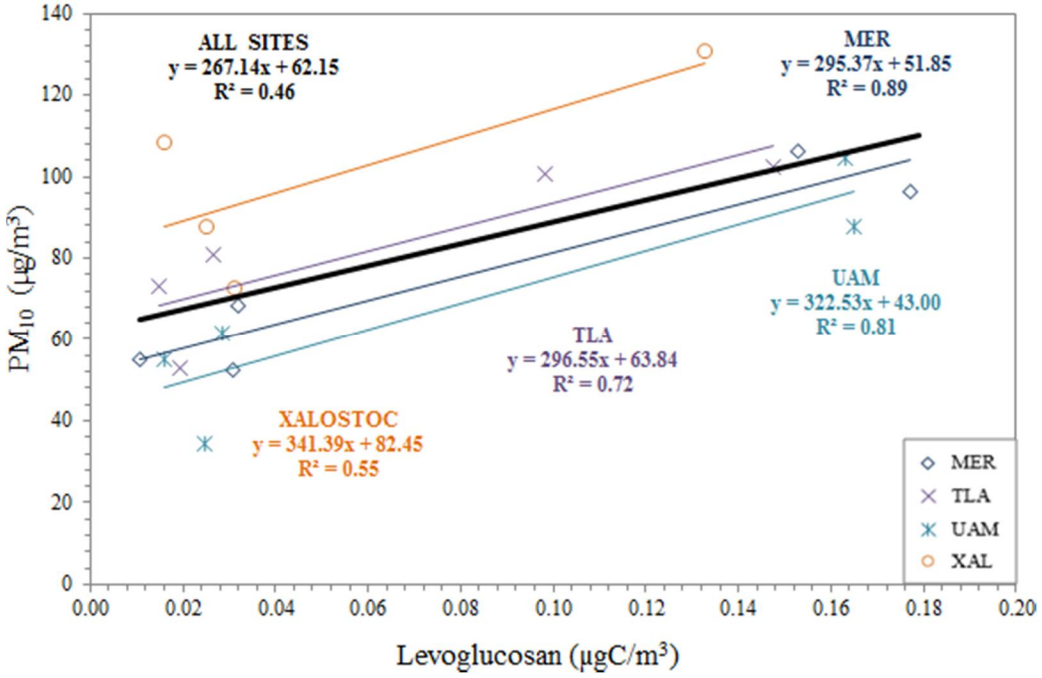

Figure 5.6 Coefficients of determination between LEV (µgC/m^3) and PM_{10} (µg/m^3) ambient concentrations for each and for all SIMAT sites. Ambient PM_{10} concentrations from SIMAT (2013).

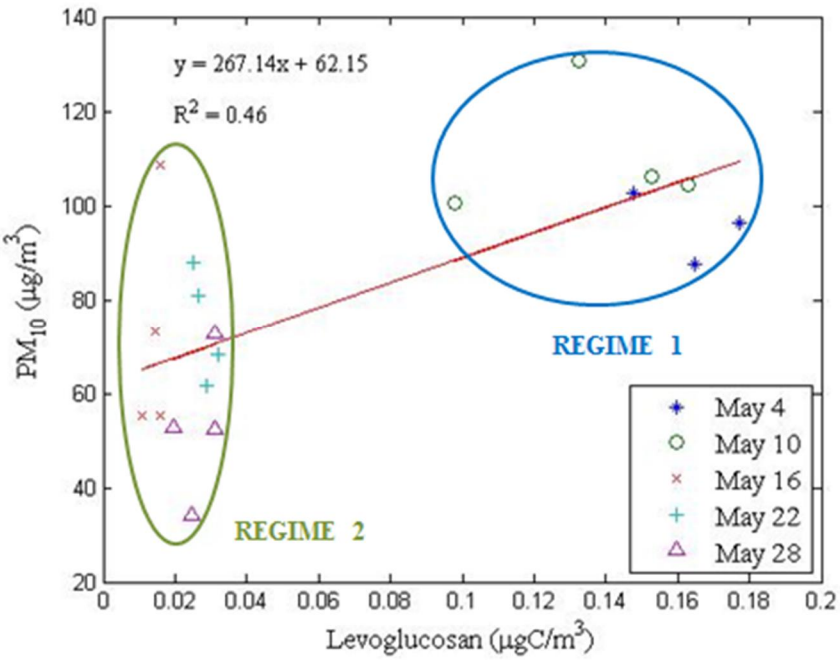

Figure 5.7 PM_{10} (µg/m^3) vs. LEV (µgC/m^3) ambient concentrations during the two meteorological regimes.

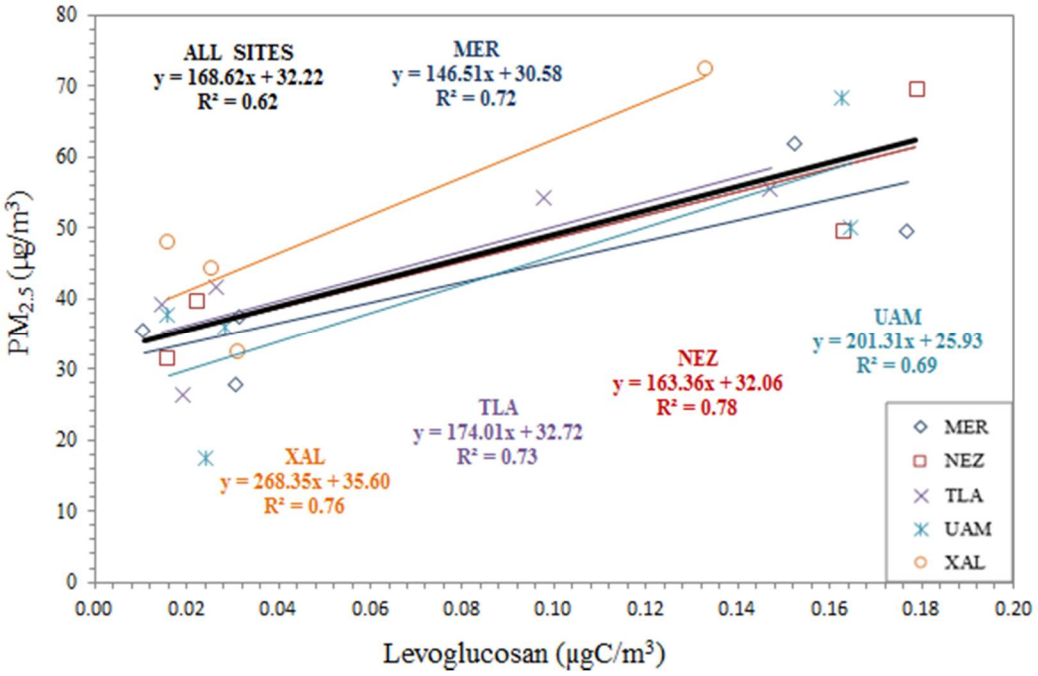

Figure 5.8 Coefficients of determination between $PM_{2.5}$ (µg/m^3) and LEV (µgC/m^3) ambient concentrations for each and for all SIMAT sites. Ambient $PM_{2.5}$ concentrations from SIMAT (2013).

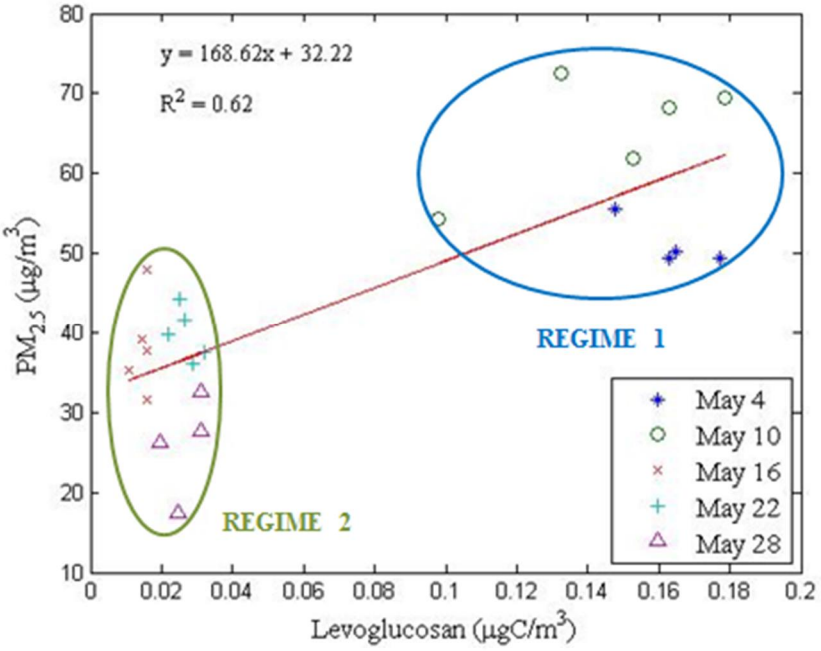

Figure 5.9 $PM_{2.5}$ (µg/m^3) vs. LEV (µgC/m^3) ambient concentrations during the two meteorological regimes.

Since potassium is one of the soluble ions emitted in largest concentrations during biomass burning combustion, we estimated WSK^+ concentrations and correlate them with LEV concentrations. For WSK^+, the estimated concentrations found were higher than LEV concentrations (Table 5.3) (mean concentration of 0.50 ± 0.63 µg/m^3 at 95% CI) and were positively correlated with LEV (R^2=0.75) in all the samples (Figure 5.10). WSK^+ concentrations in Regime 1 were twice as high as those found during Regime 2, with an average concentration in Regime 1 of 0.71 ± 0.02 µg/m^3 at 95% CI, compared to 0.36 ± 0.04 µg/m^3 at 95% CI during Regime 2. Our results show stronger correlations between WSK^+ and LEV than recent studies of ambient samples during fire periods in other countries (Brazil: R^2=0.38 by Urban et al. (2012) and no linear correlation found by Schkolnik et al. (2005); China: no linear correlation found by Cheng et al. (2013)), which generally find no or weak linear correlations. Due to the multiple potassium sources, future studies are suggested to apportion them in the MCMA region.

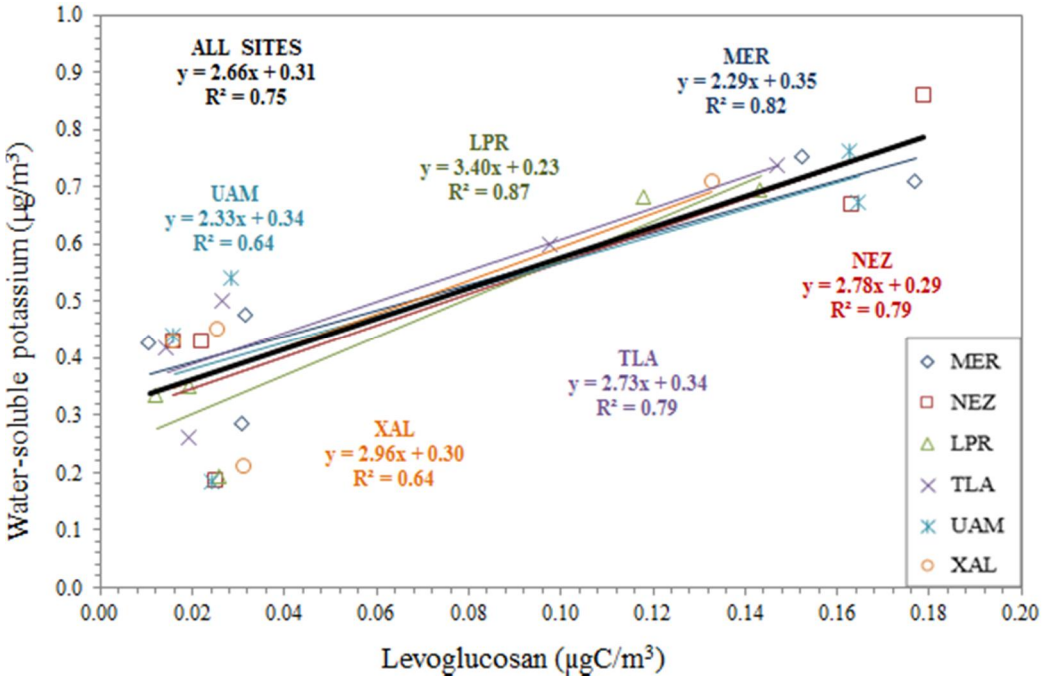

Figure 5.10 Coefficients of determination between WSK^+ (µg/m^3) and LEV (µgC/m^3) ambient concentrations for each and for all SIMAT sites.

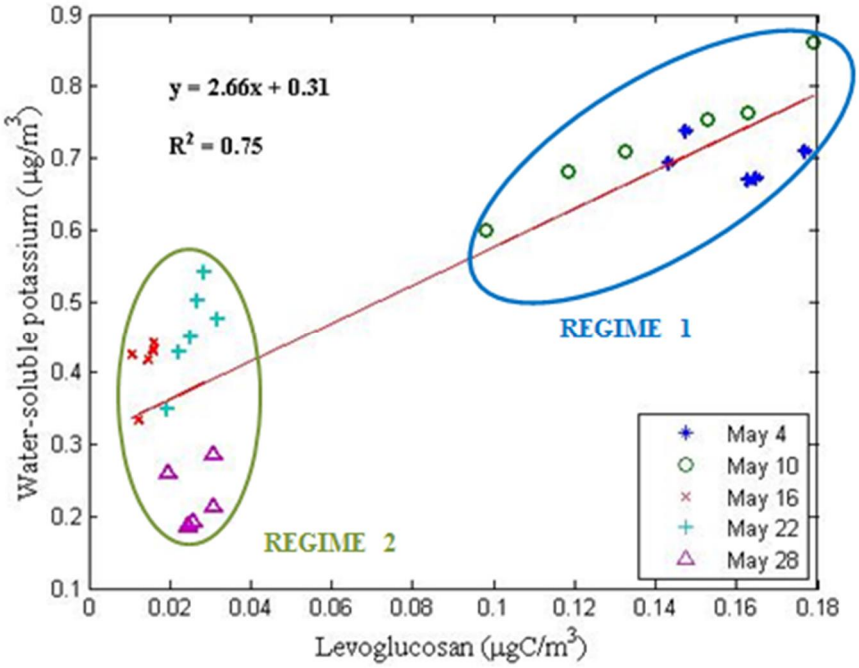

Figure 5.11 WSK^+ (µg/m^3) vs. LEV (µgC/m^3) ambient concentrations during the two meteorological regimes.

The WSOC (µgC/m^3) concentrations also showed a strong correlation (R^2=0.94) with LEV (µgC/m^3) concentrations among all the SIMAT sites (Figure 5.12). Also, the highest WSOC concentrations were found during the first regime with a mean concentration of 10.10 ± 0.41 µgC/m^3 at 95% CI, and the lowest during the second regime with a mean concentration of 3.72 ± 0.26 µgC/m^3 at 95% CI (Figure 5.13).

The mean LEV/WSOC (µgC/µgC) ratios for each sampling date are shown in Figure 5.14. Again, the highest ratios occurred during Regime 1. Comparing our results to calculated LEV/WSOC ratios from LEV and WSOC ambient concentrations reported by Stone et al. (2008) for a non-urban site outside MCMA during the MILAGRO campaign, their ratios are on average two times higher than ours. The difference might be due to the site location, since all of our sampling sites were located in residential and industrial areas (see Table 4.2), as well as

proximity to the fires. Future work is needed to study the differences in ratios and concentrations between urban and non-urban sites inside the MCMA air basin.

The mean LEV/WSOC ratios show an increasing tendency during Regime 2, that might be due to transport of smoke plumes from other regions farther than the 400 km radius from MCMA that was considered. Figure 5.15 shows the smoke surface concentrations as predicted by the NAAPS (Navy Aerosol Analysis and Prediction System) Global Aerosol Model (Hogan et al., 2014) for the entire country starting 30 hours prior to the last sampling day (00 UTC on May 27th) and ending by the end of the sampling period (06 UTC on May 29th). Panel a) shows high smoke concentrations over Peninsula de Yucatan due to active fires in the region. From panel b) to i) the smoke concentrations decrease over Peninsula de Yucatan and are transported towards the west, covering a vast area that contains MCMA. Hurricane Barbara moved across the region on May 29 and 30, as discussed in the previous chapter. Furthermore, if we focus on the average LEV/WSOC ratio on May 28th (Figure 5.14), we can observe that the standard deviation is the highest among all sampling days, suggesting impact from local sources to some sampling sites. Figure 5.16 shows the spatial distribution of the LEV/WSOC ratios across the area that encompasses the considered SIMAT stations. As we can see for May 28th, the highest ratio (0.0131 µgC/µgC) corresponds to the XAL station (north east part of MCMA) and the minimum to TLA (north west part of MCMA). The high variation among LEV/WSOC ratios for this day can be explained due to local sources impacting the sampling sites.

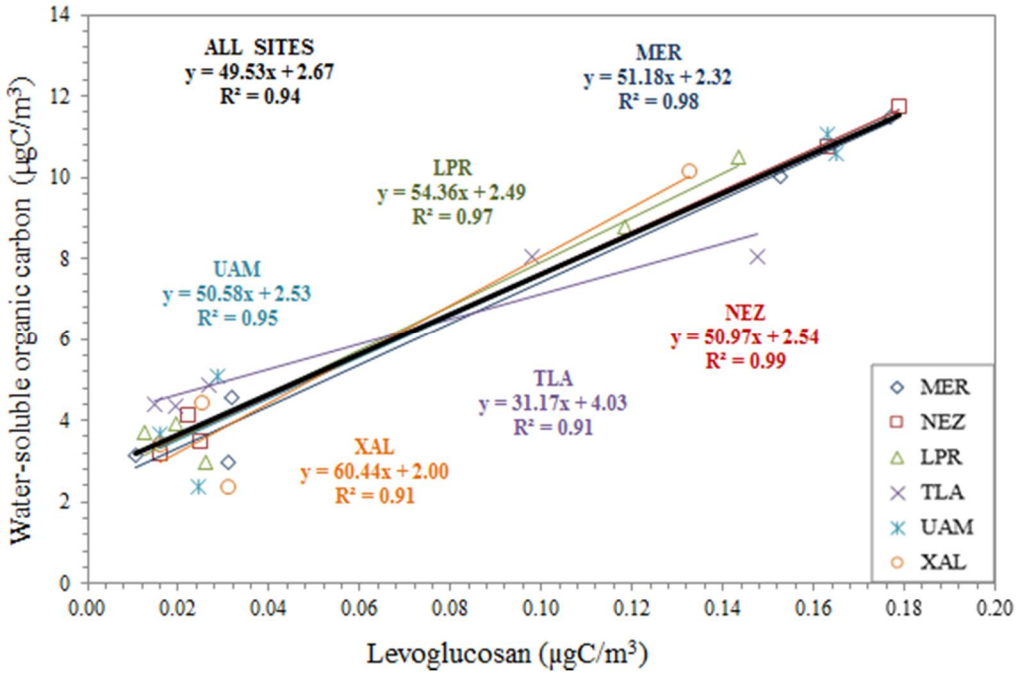

Figure 5.12 Coefficients of determination between WSOC (µgC/m^3) and LEV (µgC/m^3) ambient concentrations for each and for all SIMAT sites.

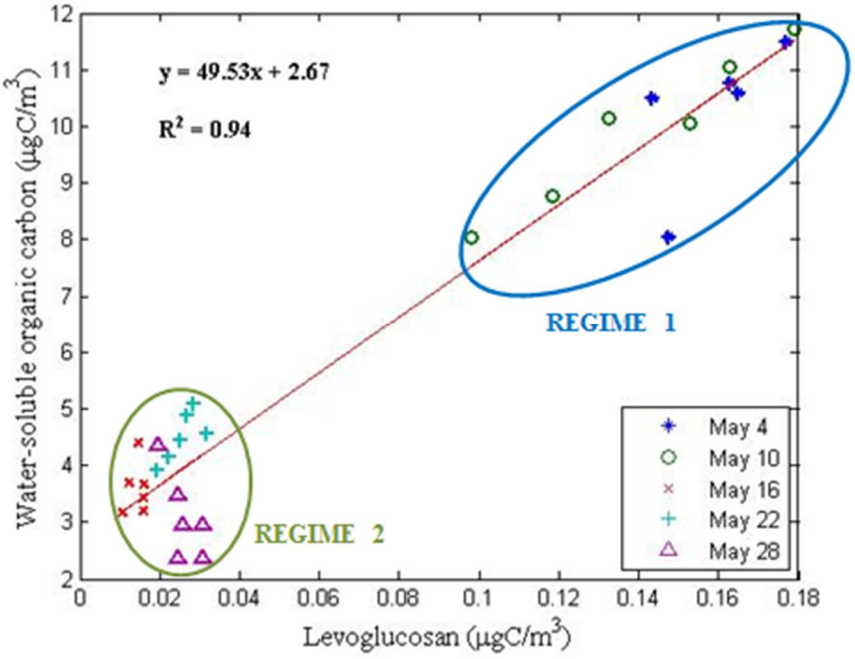

Figure 5.13 WSOC (µgC/m^3) vs. LEV (µgC/m^3) ambient concentrations during the two meteorological regimes.

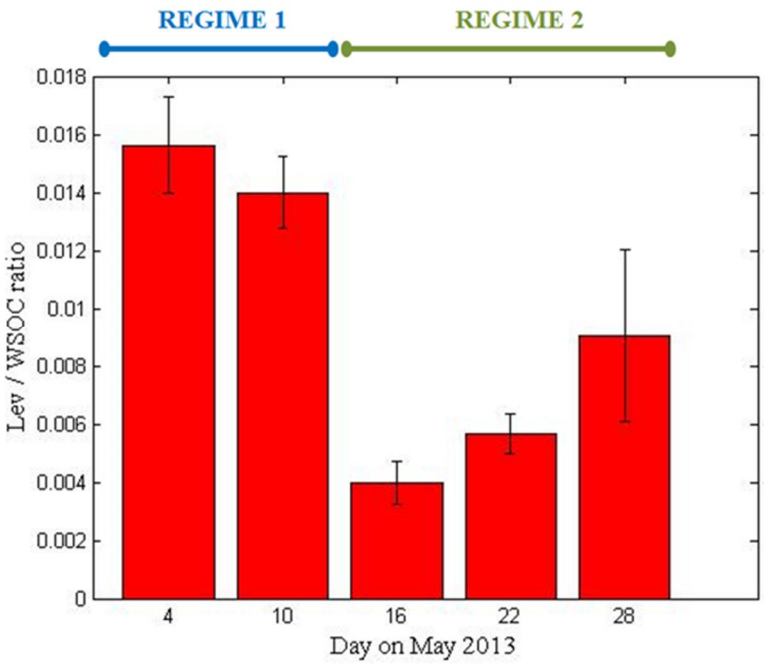

Figure 5.14 LEV/WSOC (µgC/µgC) mean ratios for each sampling date. Error bars indicate the standard deviation for each day.

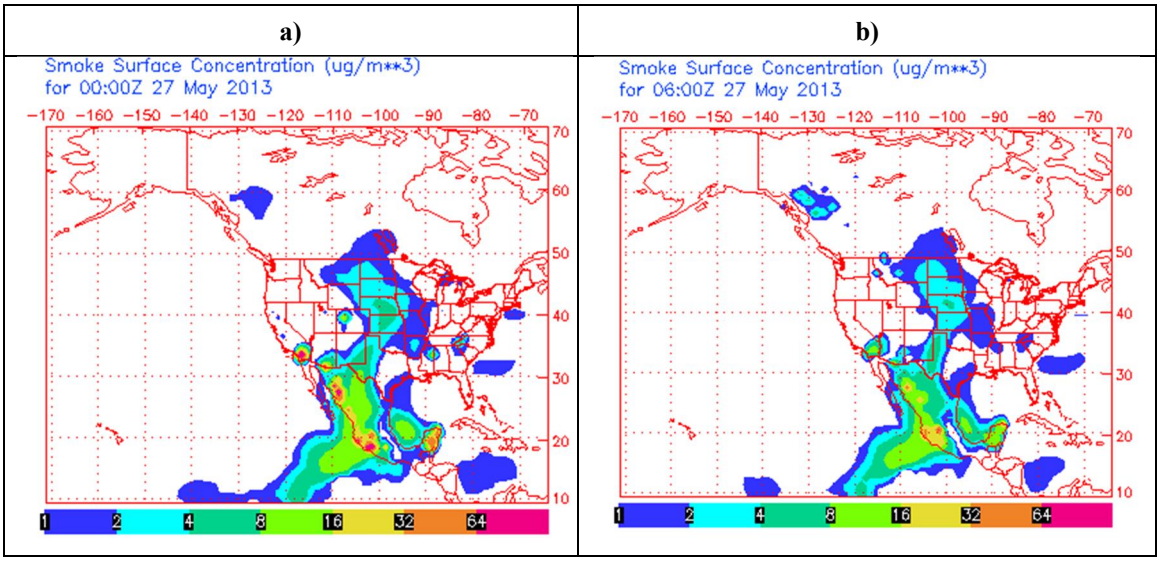

c)	d)
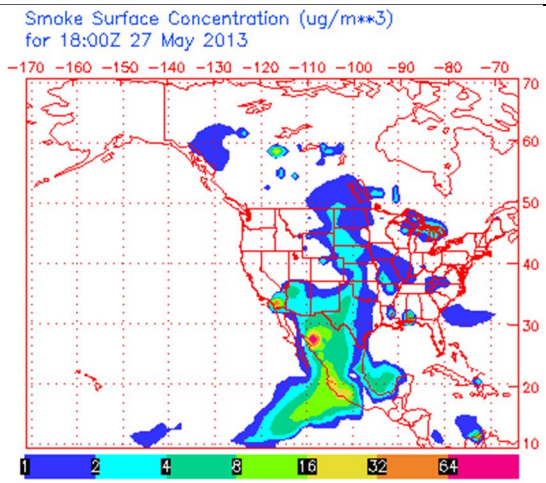 Smoke Surface Concentration (ug/m**3) for 18:00Z 27 May 2013 -170 -160 -150 -140 -130 -120 -110 -100 -90 -80 -70 70 60 50 40 30 20 10 1 2 4 8 16 32 64	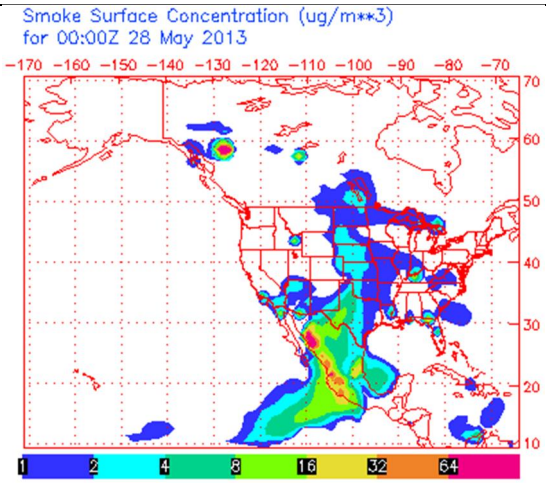 Smoke Surface Concentration (ug/m**3) for 00:00Z 28 May 2013 -170 -160 -150 -140 -130 -120 -110 -100 -90 -80 -70 70 60 50 40 30 20 10 1 2 4 8 16 32 64
e)	**f)**
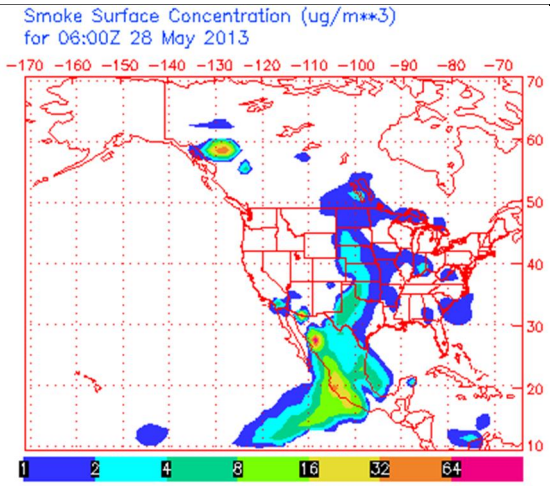 Smoke Surface Concentration (ug/m**3) for 06:00Z 28 May 2013 -170 -160 -150 -140 -130 -120 -110 -100 -90 -80 -70 70 60 50 40 30 20 10 1 2 4 8 16 32 64	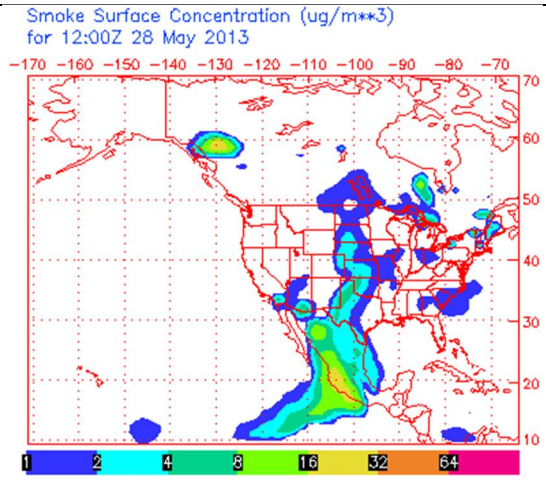 Smoke Surface Concentration (ug/m**3) for 12:00Z 28 May 2013 -170 -160 -150 -140 -130 -120 -110 -100 -90 -80 -70 70 60 50 40 30 20 10 1 2 4 8 16 32 64
g)	**h)**
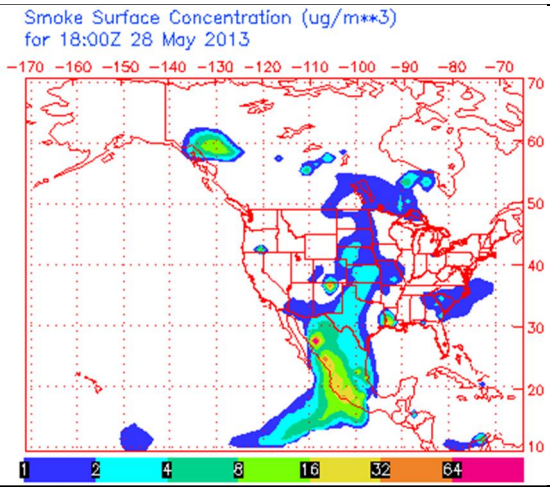 Smoke Surface Concentration (ug/m**3) for 18:00Z 28 May 2013 -170 -160 -150 -140 -130 -120 -110 -100 -90 -80 -70 70 60 50 40 30 20 10 1 2 4 8 16 32 64	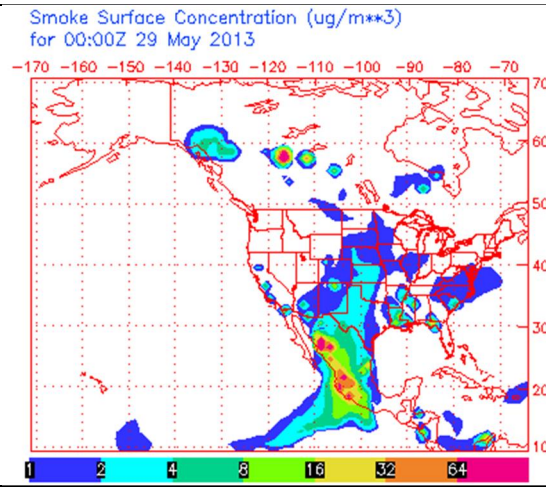 Smoke Surface Concentration (ug/m**3) for 00:00Z 29 May 2013 -170 -160 -150 -140 -130 -120 -110 -100 -90 -80 -70 70 60 50 40 30 20 10 1 2 4 8 16 32 64

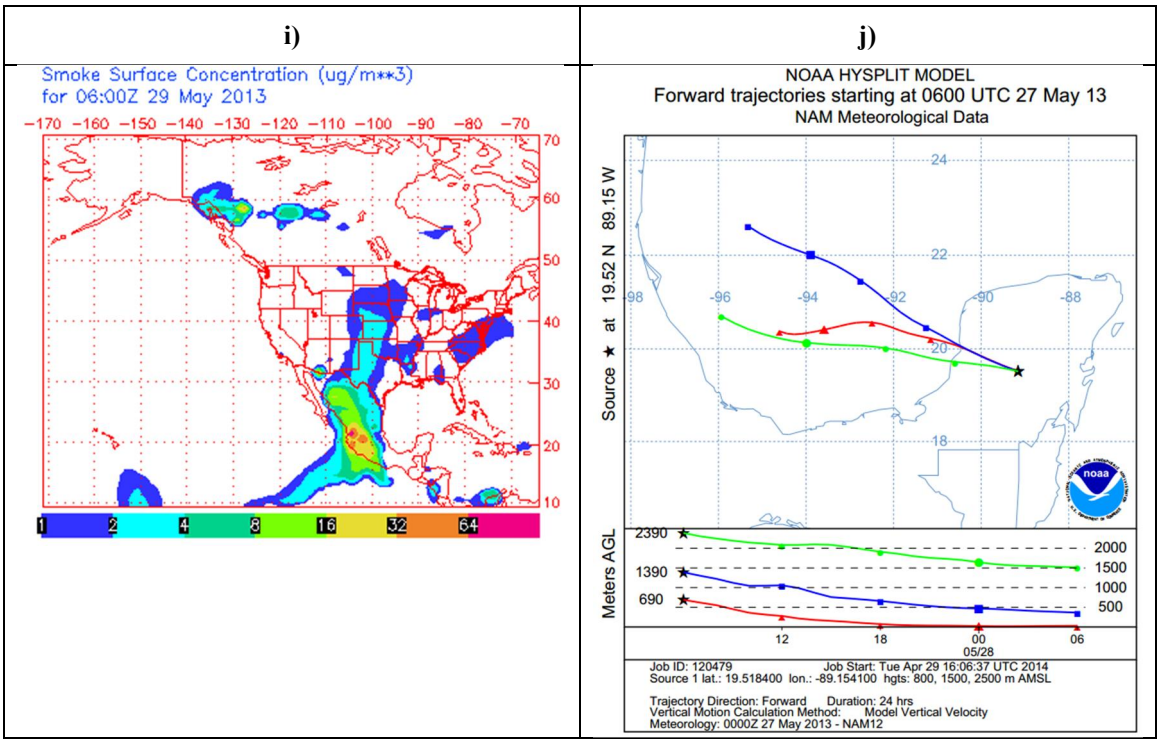

Figure 5.15 Smoke plume transport from Peninsula de Yucatan.
a) Smoke surface concentration in μg/m^3 for 06Z on May 27th,
b) Smoke surface concentration in μg/m^3 for 12Z on May 27th,
c) Smoke surface concentration in μg/m^3 for 18Z on May 27th,
d) Smoke surface concentration in μg/m^3 for 00Z on May 28th,
e) Smoke surface concentration in μg/m^3 for 06Z on May 28th,
f) Smoke surface concentration in μg/m^3 for 12Z on May 28th,
g) Smoke surface concentration in μg/m^3 for 18Z on May 28th,
h) Smoke surface concentration in μg/m^3 for 00Z on May 29th,
i) Smoke surface concentration in μg/m^3 for 06Z on May 29th,
j) 24hour HYSPLIT forward trajectory starting 24 hours prior to sampling on May 28th. Maps shown in a) to i) from NAAPS (Hogan et al., 2014). Panel j) shows a 24-hour forward trajectory from NOAA HYSPLIT MODEL (Draxler and Rolph, 2013).

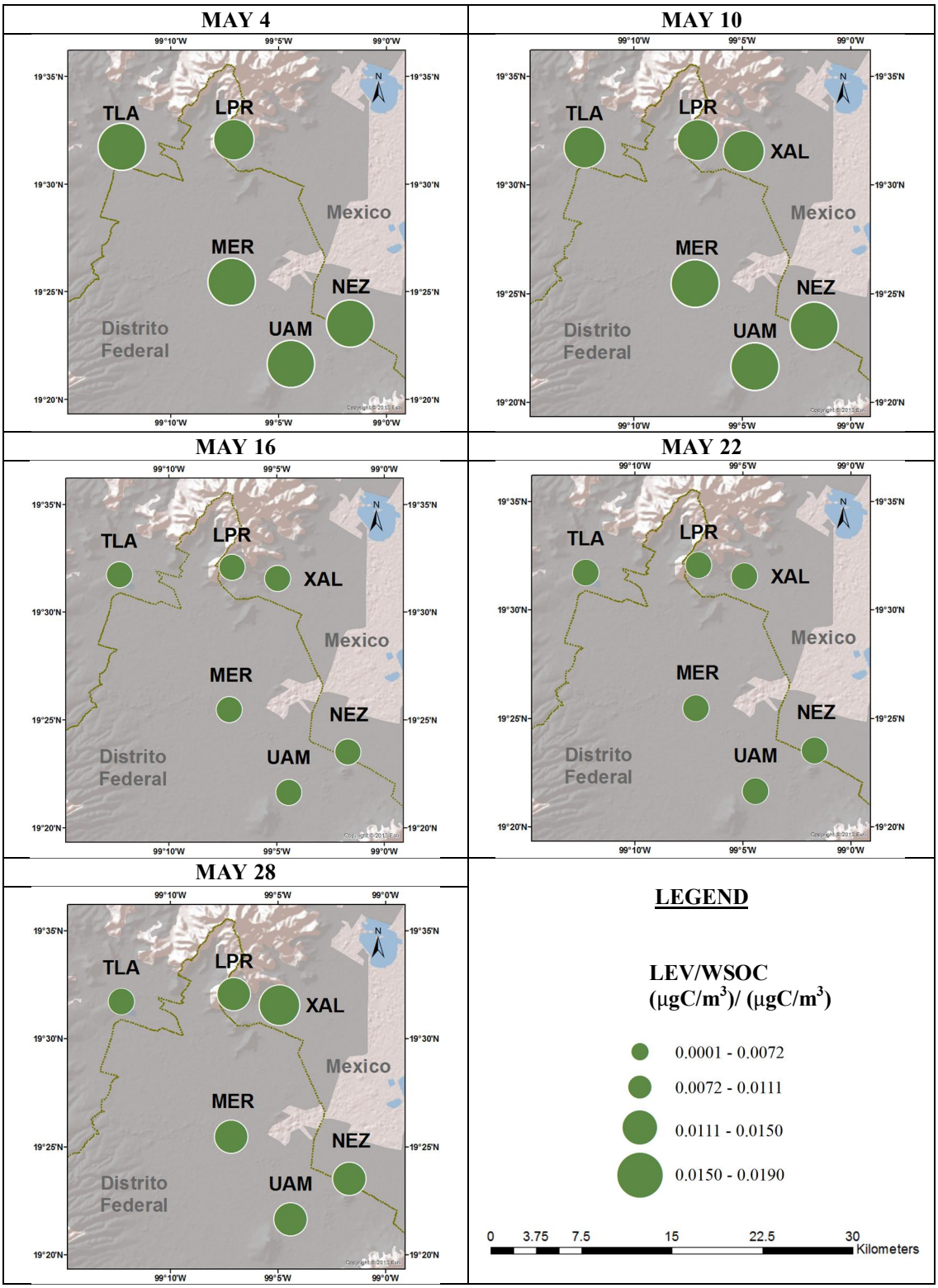

Figure 5.16 Spatial distribution of LEV/WSOC ratios within MCMA for each sampling day.
Maps were created using ArcMap (ESRI, 2012).

5.3 PARTICULATE MATTER ANALYSIS

5.3.1 GRAVIMETRIC MASS CONCENTRATIONS

From reported gravimetric mass concentrations of 24 hour PM_{10} and $PM_{2.5}$ samples for each sampling day at selected SIMAT stations, we found that $PM_{2.5}$ accounted for 60% of the PM_{10} mass concentration. The PM_{10} to $PM_{2.5}$ mass ratio was 1.68, estimated from a zero-intercept linear regression (Figure 5.17). Our estimate was higher than the PM_{10} to $PM_{2.5}$ mass ratio calculated from data reported by Querol et al. (2008) during the MILAGRO campaign at an urban site (T0) inside MCMA, where the average PM_{10} to $PM_{2.5}$ mass ratio was 1.25 ($PM_{2.5}$ accounted on average for 80% of the PM_{10} mass concentration). The higher $PM_{10}/PM_{2.5}$ mass ratio might be due to the differences in the sampling proximity to the fires during the MILAGRO campaign, where 76% of the fires occurred within a 120 km radius of MCMA (Aiken et al., 2010) compared to our study where 81% of the fires were located father away, between a 200 to 400 km radius from MCMA (see section 4.3.1). The lower PM_{10} to $PM_{2.5}$ mass ratio estimated during the MILAGRO campaign was similar to a source ratio of 1.09 reported by McMeeking et al. (2009) for biomass burning source filter samples obtained during chamber burns conducted during the FLAME 1 and FLAME 2 studies.

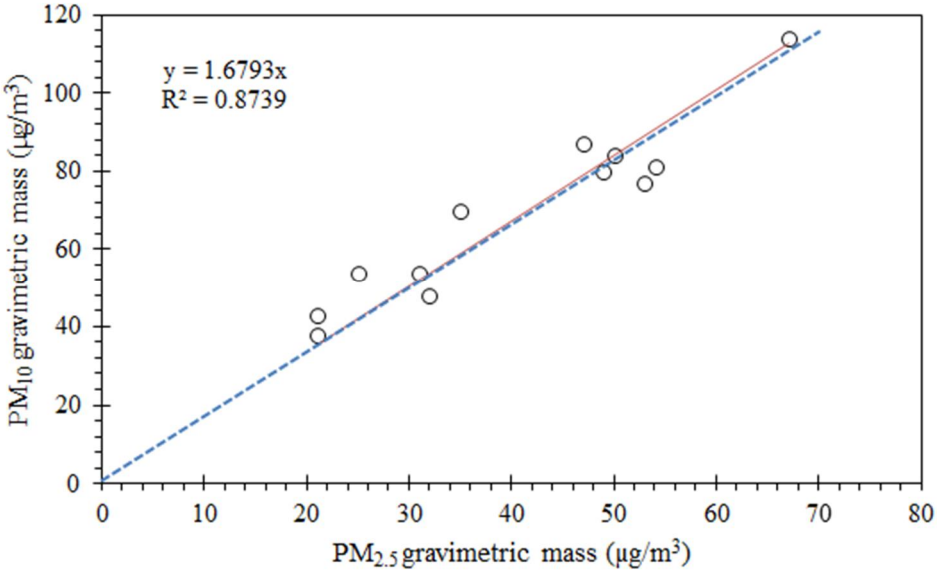

Figure 5.17 Comparison of gravimetric mass concentrations of PM_{10} and $PM_{2.5}$ ($\mu g/m^3$) for available selected SIMAT stations during the sampling period.
Solid line is the linear regression of PM_{10} mass onto $PM_{2.5}$ mass forced through the origin. Dashed line is the 1:1 line.
Gravimetric mass concentration data from SIMAT (2013).

5.3.2 PM_{10} ANALYZED

Hand and Malm (2006) computed the dry $PM_{2.5}$ mass concentrations ($\mu g/m^3$) using Equation 1. They assumed that the sulfate is fully neutralized ammonium sulfate ($(NH_4)_2SO_4$), nitrate is in the form of ammonium nitrate (NH_4NO_3), and organic carbon is included as particulate organic material (POM), computed by multiplying organic carbon (OC) concentrations by a molecular weight per carbon weight ratio (Roc). They also considered light-absorbing carbon (LAC) and sea salt.

Equation 1

$$PM_{2.5} = (NH_4)_2SO_4 + NH_4NO_3 + POM + LAC + Soil + Sea\ salt$$

where:
POM = Roc·OC
Roc = average molecular weight per carbon weight for the organic aerosol constituents
Roc ~ 1.4 ï 2.2
LAC = EC (elemental carbon)
Soil = 2.2Al + 2.49Si + 1.94Ti + 1.63Ca + 2.42Fe

Using the same approach, we estimated the percentage of PM_{10} characterized in this study. We used Equation 2 and assumed that the sodium was in form of sodium chloride and accounted for the total sea salt concentration. The gravimetric mass concentrations reported by SIMAT (2013) were considered as the total PM_{10} mass concentration, therefore the percentage of PM_{10} characterized can be calculated using Equation 3. Results show that the average PM_{10} characterized in this study was 37% ± 2.11% at a 95% CI. The rest of the concentrations might be related to crustal material (soil or dust) and carbon compounds.

Equation 2

$$PM_{10\ study} = \sum [ionic\ species] + 2 \cdot [WSOC] + [Sea\ salt]$$

where:
[Sea salt] = NaCl

Equation 3

$$\frac{PM_{10\ study}}{PM_{10\ SIMAT}} \times 100 = \%\ PM_{10\ characterized}$$

5.4 ESTIMATES OF BIOMASS BURNING CONTRIBUTIONS TO WSOC

To estimate the portion of WSOC observed in MCMA PM_{10} samples that could be attributed to biomass burning primary emissions, we used LEV/WSOC source ratios obtained in the Fire Lab at Missoula Experiments (FLAME). This series of experiments was aimed at measuring chemical, physical and optical properties of biomass burning smoke, and obtaining source marker profiles for a wide range of North American and other fuels (Sullivan et al., 2008). To represent the most important vegetation burned during our study (see section 5.1), we used reported FLAME LEV/WSOC ratios for needles (LEV/WSOC = 0.064 µgC/µgC, low estimate) and leaves (LEV/WSOC = 0.095 µgC/µgC, high estimate) (Table 2.1). We then estimated the percentage of WSOC attributable to biomass burning sources ($WSOC_{BB}$) using Equation 4.

Equation 4

$$\frac{\frac{LEV}{WSOC_{study}}}{\frac{LEV}{WSOC_{FLAME}}} \times 100 = \%\, WSOC_{BB}$$

Table 5.4 presents the range of $WSOC_{BB}$ percentage contributions calculated in this study, averaged over each meteorological regime. The biomass burning contribution to WSOC ranged from 7% to 23 %. As expected, the first meteorological regime had a higher estimated biomass burning contribution, more than twice that computed for Regime 2. From LEV and WSOC concentrations reported by Stone et al. (2008) for a non-urban site within the MCMA air basin during the MILAGRO campaign, we estimated a range of $WSOC_{BB}$ from 10 to 36 %. The similar but slightly higher contribution during the MILAGRO campaign might be related to a closer proximity to most of the active fires (Aiken et al., 2010), compared to this study.

Table 5.4 Percentage of WSOC from biomass burning ($WSOC_{BB}$).

REGIME	UPPER (%)	LOWER (%)
1	23	16
2	10	7

The estimated $WSOC_{BB}$ percentages from the previous table were calculated assuming that LEV is inert in the atmosphere. However, as discussed in Section 2.4.2.1, recent studies have proposed that LEV can degrade in the atmosphere in both clear air and in-cloud conditions. Therefore, the calculated $WSOC_{BB}$ contributions shown in Table 5.4might underestimate the influence of biomass burning. We used an average LEV lifetime of 1.1 days (the time for its decay to 1/e of the initial concentration) estimated by Hennigan et al. (2010) as our maximum (upper limit) LEV degradation rate. For the minimum LEV degradation rate, we used a LEV lifetime of 5 days, estimated from the Hoffmann et al. (2009) results. Assuming a pseudo first order reaction for the rate of decay (Equation 5), we calculated the initial LEV concentrations ($\mu g/m^3$) considering our measurements as the LEV final concentrations (Equation 6). After correcting the LEV concentrations, we recomputed $WSOC_{BB}$ for the revised LEV/WSOC concentrations (Table 5.5). The revised estimates of $WSOC_{BB}$ percentages showed an average increase of biomass burning direct emission contributions by about 80% (Figure 5.18). However, this finding depends on the source profile used in the apportionment. Source profiles specific to the regions in Mexico in which fires occur in the springtime are needed to increase confidence in this estimate.

Equation 5

$$\frac{d[LEV]}{dt} = -k\,[LEV]$$

Equation 6

$$[LEV]_{init} = \frac{[LEV]_{final}}{e^{-kt}}$$

Table 5.5 Corrected LEV concentrations (µgC/m^3), LEV/WSOC ratios (µgC/µgC) and percentages of WSOC from biomass burning ($WSOC_{BB}$) considering LEV degradation rates.
Upper LEV degradation rate from Hennigan et al. (2010).
Lower LEV degradation rate from Hoffmann et al. (2009).

REGIME	LEV (µgC/m^3)		LEV/WSOC (µgC/µgC)		$WSOC_{BB}$ (%)	
	UPPER	LOWER	UPPER	LOWER	UPPER	LOWER
1	0.37	0.18	0.04	0.02	57	19
2	0.05	0.03	0.01	0.01	23	8

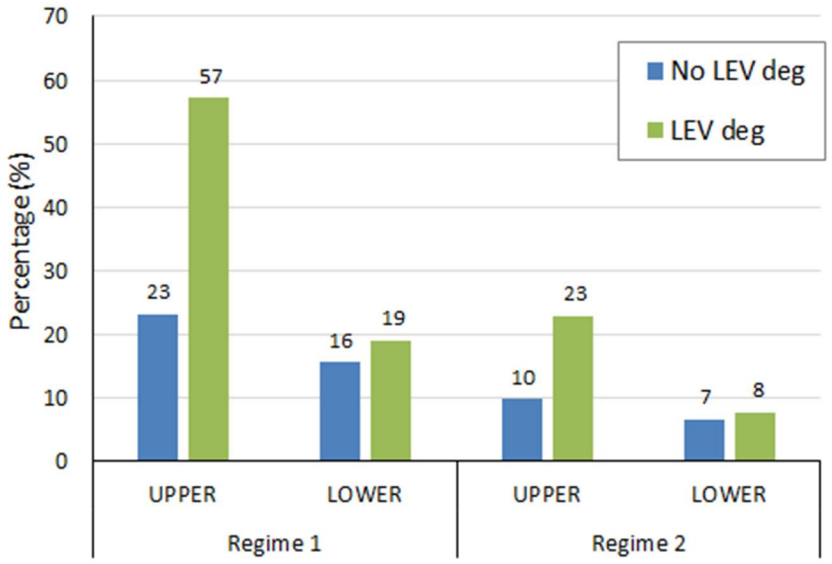

Figure 5.18 $WSOC_{BB}$ percentages estimated for Regime 1 and Regime 2.

6. FUTURE WORK

The biomass burning contribution to WSOC estimated in this study adds to the limited number of estimates of primary emissions from this source to carbonaceous aerosols in the MCMA. However, a broader characterization of carbonaceous compounds could potentially allow the estimation of the biomass burning contribution not only to the water-soluble fraction, but also to ambient concentrations of PM_{10} and $PM_{2.5}$. Providing estimates of the contribution of biomass burning to PM_{10} and $PM_{2.5}$ would be more useful to decision makers tasked with improving emission inventories and air quality policies. Likewise, a longer sampling period and spatial distributions of biomass burning sources could also provide information about seasonal patterns and ñhot spotsò of biomass burning that could ultimately be used to improve and create emission source controls.

We have provided a recommended suite of future measurements that would allow us to estimate the biomass burning contribution to ambient concentrations of PM_{10} and $PM_{2.5}$ inside MCMA, and this is shown in Figure 6.1. Ambient and source samples of PM_{10} and $PM_{2.5}$ (as well as blanks for each one) should be collected on quartz filters in order to estimate the concentrations of EC, OC, WSOC, carbohydrates and water-soluble ions. From the LEV/WSOC ratios of ambient and source samples, the biomass burning contribution to WSOC could be determined and then used to estimate the OC from biomass burning sources (OC_{BB}) using a WSOC/OC ratio. The total carbon (TC) from ambient samples could be estimated using the OC and EC concentrations. Finally, both the LEV/WSOC, WSOC/OC and OC/PM_{10} (or $PM_{2.5}$) ratio from source and ambient samples, will be used to estimate the contributions of biomass burning to PM_{10} and $PM_{2.5}$ ambient concentrations.

Considering the ambient samples taken inside MCMA, the duration of the sampling period suggested in order to obtain representative seasonal patterns is two years. The number and location of the sites should be determined considering the seasonal wind patterns in the MCMA air basin, where during the day air masses move from the northern part of the basin towards the south (see section 2.3.2). Moreover, the periodicity of sampling should emphasize the fire season (see section 3) in order to have a detailed estimate of the biomass burning contribution during that period. Regarding the source samples, since wildfires and agricultural burning were found to represent the most important fuel categories in this study (see section 5.1), specific source profiles for their main fuel types are needed to increase confidence in the estimation of their contributions to carbonaceous aerosols. For both fuel categories, the source samples should be collected at the edge of the burn itself. These source profiles would be used for estimating the biomass burning fraction to PM_{10} and $PM_{2.5}$ ambient concentrations.

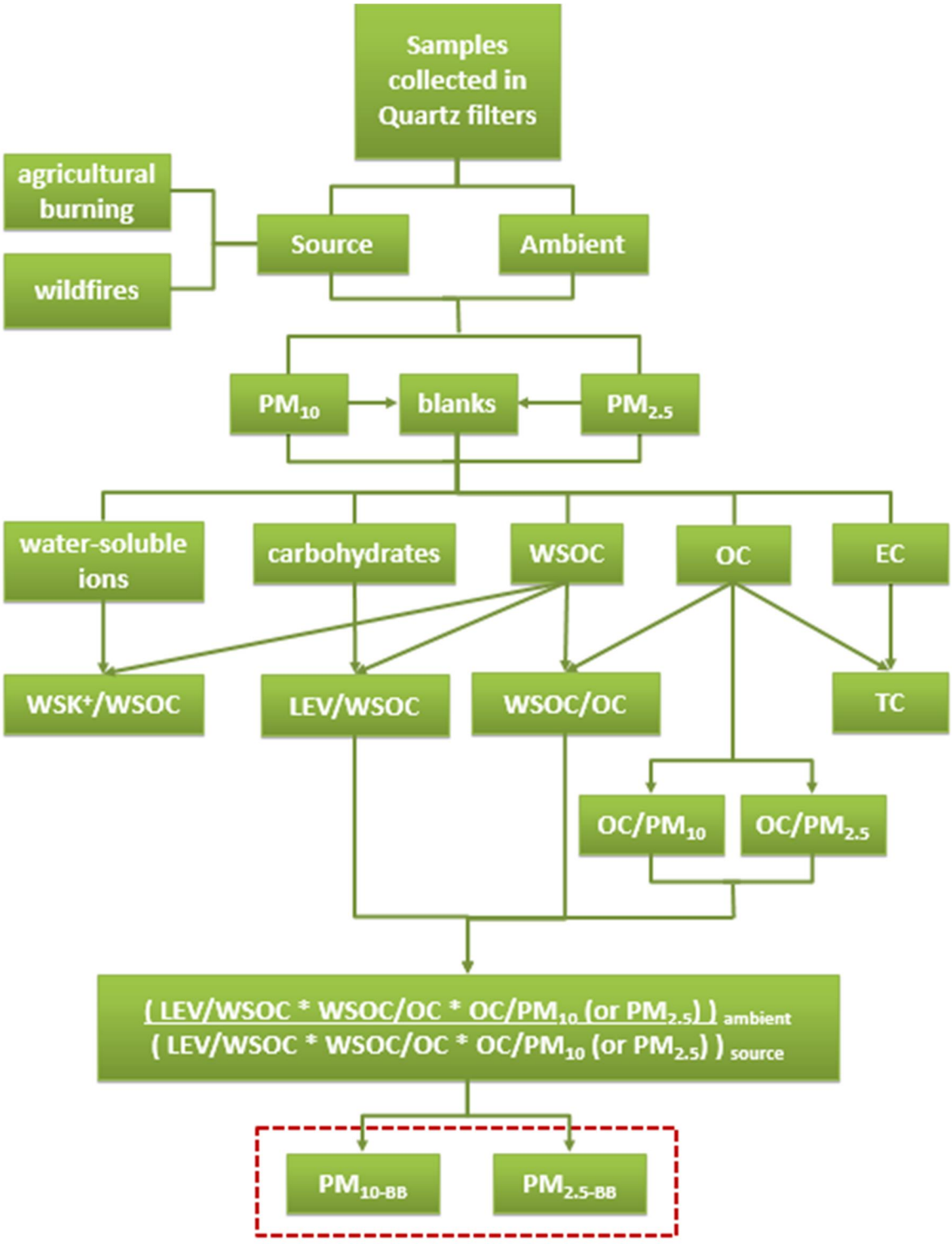

Figure 6.1 Flow chart describing the types of analyses to estimate the biomass burning contribution to ambient concentrations of PM_{10} and $PM_{2.5}$.

7. SUMMARY AND CONCLUSIONS

May 2013 represented a particularly active fire month in Mexico, with emissions from biomass burning having the potential to affect the air quality of the entire region in which MCMA is located. We obtained and analyzed PM_{10} filter samples from six sites within MCMA for 5 sampling days over the month, focusing on detection of species that could be used to apportion some of the observed particulate matter to biomass burning sources. Two meteorological regimes were defined by considering variations in the number of satellite derived fire counts, predominant air mass pathways, ambient concentrations of CO (ppm), PM_{10} ($\mu g/m^3$) and $PM_{2.5}$ ($\mu g/m^3$), and precipitation patterns during May 2013. The first regime (May 1-11) had predominant winds coming from the west, no precipitation, and high fire counts; two filter samples were obtained during this regime. The second regime (May 12-28) had winds mostly coming from the north, lower fire counts and a mean precipitation rate of 4 mm/day; three filter samples were obtained during this period.

Modeled biomass burning sources, using vegetation and land use information input to the FINN model, attributed 64% of the total area burned to wildfires that contributed ~77% of the total fire emissions of CO and $PM_{2.5}$. Agricultural burning was the second most important fire source, with an estimated 35% of the total area burned and about 22% of the emissions for both CO and $PM_{2.5}$.

As expected, results from laboratory PM_{10} filter analysis showed that species associated with biomass burning emissions, namely LEV, WSK^+ and WSOC, had mass concentrations in ambient air that were about 7, 2 and 3 times higher respectively, during the first meteorological regime than during the second. Correlations were found between LEV concentrations and FINN products (fire counts, R^2=0.66; area burned, R^2=0.66; and daily emissions of CO and $PM_{2.5}$

R^2=0.59 and 0.61), which together with site-to-site correlations for $PM_{2.5}$ concentrations suggested that the whole air basin was affected by transported emissions from fires occurring in the surrounding region. Correlations between LEV concentrations and ambient concentrations of $PM_{2.5}$ (R^2=0.62) also suggested a strong biomass burning influence. However, a low correlation between LEV and CO ambient concentrations was found, suggesting multiple non-biomass burning local sources of CO, consistent with MCMA emission inventories that attribute most basin-wide CO emissions to automotive sources.

A strong correlation (R^2=0.75) was observed between LEV and WSK^+ concentrations on the PM_{10} filters that were analyzed. For both WSOC (µgC/m^3) concentrations and LEV/WSOC (µgC/µgC) ratios, the highest values were found during the first regime when fire activity was highest, and WSOC concentrations were strongly correlated with LEV (R^2=0.94). However, LEV/WSOC mean ratios had an increasing tendency during the second regime that might be due to transport of smoke plumes from other regions farther than a radius of 400 km from MCMA. Furthermore, the LEV/WSOC ratio on May 28th was the highest of the samples obtained during Regime 2, and this sampling day also had the greatest standard deviation in LEV/WSOC among all sampling days, suggesting that local sources may have impacted some of the sampling sites.

Analysis of gravimetric mass concentrations from filters collected each sampling day at the SIMAT stations, showed that $PM_{2.5}$ accounted for 60% of the PM_{10} mass concentration with an estimated $PM_{10}/PM_{2.5}$ ratio of 1.68. Additionally, we calculated that on average our laboratory characterization measured 37% of the total PM_{10} mass concentration. The rest of the concentration might be related to crustal material (soil or dust) and carbonaceous aerosols that were not segregated into the water-soluble fraction. Future work is needed to measure more constituents in order to explain the possible sources of the remaining mass.

The biomass burning contributions to WSOC ($WSOC_{BB}$) were estimated using laboratory-based source smoke marker profiles, assuming that LEV is stable in the atmosphere during transport. The estimates ranged from 7-23% of the total WSOC attributed to primary biomass burning emissions, depending on the source profile selected, with the highest percentage contributions during Regime 1. When the possibility of LEV degradation in the atmosphere during transport was considered, by applying 1.1 to 5 day LEV lifetimes as reported in the literature, the $WSOC_{BB}$ contributions increased on average by 80%. Thus, we conclude that biomass burning sources had a large impact on WSOC and $PM_{2.5}$ during May 2013, potentially explaining up to half of the measured WSOC.

The results from this study contribute to the limited number of estimates of the relative contributions of primary emissions from biomass burning to carbonaceous aerosols in MCMA during an active fire season. One limitation of this work is the lack of smoke marker source profiles that are specific to MCMA. Sampling closer to active fires, for different vegetation and different burn phases, is thus needed, and/or laboratory studies using fuels from the surrounding regions. Another limitation to estimating total impacts of biomass burning is that SOA formation from biomass burning sources is highly likely. To date there are no specific molecular markers for smoke-derived SOA, but work in this arena is ongoing, and other methods such as modeling could be used to bound the fire contributions to SOA. Finally, FINN and MCMA databases may be missing some local fire sources, such as burning to clear the verges of roads and highways. Since these sources occur within MCMA they may have strong impacts on air quality, despite being much smaller in emissions magnitude than large wildfires. Given the importance of understanding sources contributing to MCMA air quality degradation in order to develop sound and effective mitigation strategies, further work is needed to estimate biomass burning

contributions to total carbon and ambient concentrations of particulate matter in MCMA. Such studies will ultimately be used to improve the emission inventories that are commonly used by decision makers to design air quality policies and emission source controls.

8. REFERENCES

AIKEN, A. C., DE FOY, B., WIEDINMYER, C., DECARLO, P. F., ULBRICH, I. M., WEHRLI, M. N., SZIDAT, S., PREVOT, A. S. H., NODA, J., WACKER, L., VOLKAMER, R., FORTNER, E., WANG, J., LASKIN, A., SHUTTHANANDAN, V., ZHENG, J., ZHANG, R., PAREDES-MIRANDA, G., ARNOTT, W. P., MOLINA, L. T., SOSA, G., QUEROL, X. & JIMENEZ, J. L. 2010. Mexico city aerosol analysis during MILAGRO using high resolution aerosol mass spectrometry at the urban supersite (T0) ï Part 2: Analysis of the biomass burning contribution and the non-fossil carbon fraction. *Atmos. Chem. Phys.,* 10**,** 5315-5341.

AIKEN, A. C., SALCEDO, D., CUBISON, M. J., HUFFMAN, J. A., DECARLO, P. F., ULBRICH, I. M., DOCHERTY, K. S., SUEPER, D., KIMMEL, J. R., WORSNOP, D. R., TRIMBORN, A., NORTHWAY, M., STONE, E. A., SCHAUER, J. J., VOLKAMER, R., FORTNER, E., DE FOY, B., WANG, J., LASKIN, A., SHUTTHANANDAN, V., ZHENG, J., ZHANG, R., GAFFNEY, J., MARLEY, N. A., PAREDES-MIRANDA, G., ARNOTT, W. P., MOLINA, L. T., SOSA, G. & JIMENEZ, J. L. 2009. Mexico City aerosol analysis during MILAGRO using high resolution aerosol mass spectrometry at the urban supersite (T0) ï Part 1: Fine particle composition and organic source apportionment. *Atmos. Chem. Phys.,* 9**,** 8377-8427.

BROWN, D. P. 2013. Hurrucane Barbara (EP022013). *Tropical Cyclone Report.* National Hurricane Center.

CHENG, Y., ENGLING, G., HE, K. B., DUAN, F. K., MA, Y. L., DU, Z. Y., LIU, J. M., ZHENG, M. & WEBER, R. J. 2013. Biomass burning contribution to Beijing aerosol. *Atmos. Chem. Phys. Discuss.,* 13**,** 8387-8434.

CONAFOR 2009. Programa Nacional de Protección contra Incendios Forestales. Resultados 2008. Comision Nacional Forestal, Secretaría de Medio Ambiente y Recursos Naturales.

COSTA, M. A. M., CARVALHO JR, J. A., SOARES NETO, T. G., ANSELMO, E., LIMA, B. A., KURA, L. T. U. & SANTOS, J. C. 2012. Real-time sampling of particulate matter smaller than 2.5 ε m from Amazon forest biomass combustion. *Atmospheric Environment,* 54**,** 480-489.

CROUNSE, J. D., DECARLO, P. F., BLAKE, D. R., EMMONS, L. K., CAMPOS, T. L., APEL, E. C., CLARKE, A. D., WEINHEIMER, A. J., MCCABE, D. C., YOKELSON, R. J., JIMENEZ, J. L. & WENNBERG, P. O. 2009. Biomass burning and urban air pollution over the Central Mexican Plateau. *Atmos. Chem. Phys.,* 9**,** 2699-2734.

DRAXLER, R. R. & ROLPH, G. D. 2013. HYSPLIT (HYbrid Single-Particle Lagrangian Integrated Trajectory) Model *In:* NOAA AIR RESOURCES LABORATORY, C. P., MD. (ed.). NOAA ARL READY.

ESRI 2012. ArcMap. *In:* ENVIRONMENTAL SYSTEMS RESEARCH INSTITUTE, R., CA (ed.) 10.1 ed.

FENN, M. E., BAUER, M. D. L. & HERNÁNDEZ-TEJEDA, T. 2002. *Urban air pollution and forests resources at risk in the Mexico City Air Basin,* New York, Springer.

FRASER, M. P. & LAKSHMANAN, K. 2000. Using Levoglucosan as a Molecular Marker for the Long-Range Transport of Biomass Combustion Aerosols. *Environmental Science & Technology,* 34**,** 4560-4564.

GAO, S., HEGG, D. A., HOBBS, P. V., KIRCHSTETTER, T. W., MAGI, B. I. & SADILEK, M. 2003. Water-soluble organic components in aerosols associated with savanna fires in southern Africa: Identification, evolution, and distribution. *Journal of Geophysical Research: Atmospheres,* 108**,** 8491.

GRIESHOP, A. P., DONAHUE, N. M. & ROBINSON, A. L. 2009. Laboratory investigation of photochemical oxidation of organic aerosol from wood fires 2: analysis of aerosol mass spectrometer data. *Atmos. Chem. Phys.,* 9**,** 2227-2240.

HAND, J. L. & MALM, W. C. 2006. Review of the IMPROVE Equation for Estimating Ambient Light Extinction Coefficients. Interagency Monitoring of Protected Visual Environments.

HENNIGAN, C. J., SULLIVAN, A. P., COLLETT, J. L. & ROBINSON, A. L. 2010. Levoglucosan stability in biomass burning particles exposed to hydroxyl radicals. *Geophysical Research Letters,* 37**,** L09806.

HOFFMANN, D., TILGNER, A., IINUMA, Y. & HERRMANN, H. 2009. Atmospheric Stability of Levoglucosan: A Detailed Laboratory and Modeling Study. *Environmental Science & Technology,* 44**,** 694-699.

HOGAN, T. F., ROSMOND, T. E. & BRODY, L. R. 2014. *NAAPS (Navy Aerosol Analysis and Prediction System) Global Aerosol Model*. Naval Research Laboratory.

HOLDEN, A. S., SULLIVAN, A. P., MUNCHAK, L. A., KREIDENWEIS, S. M., SCHICHTEL, B. A., MALM, W. C. & COLLETT JR, J. L. 2011. Determining contributions of biomass burning and other sources to fine particle contemporary carbon in the western United States. *Atmospheric Environment,* 45**,** 1986-1993.

HOLMES, B. & PETRUCCI, G. 2007. Oligomerization of levoglucosan by Fenton chemistry in proxies of biomass burning aerosols. *Journal of Atmospheric Chemistry,* 58**,** 151-166.

HOLMES, B. J. & PETRUCCI, G. A. 2006. Water-Soluble Oligomer Formation from Acid-Catalyzed Reactions of Levoglucosan in Proxies of Atmospheric Aqueous Aerosols. *Environmental Science & Technology,* 40**,** 4983-4989.

HOSSEINI, S., URBANSKI, S. P., DIXIT, P., QI, L., BURLING, I. R., YOKELSON, R. J., JOHNSON, T. J., SHRIVASTAVA, M., JUNG, H. S., WEISE, D. R., MILLER, J. W. & COCKER, D. R. 2013. Laboratory characterization of PM emissions from combustion of wildland biomass fuels. *Journal of Geophysical Research: Atmospheres,* 118**,** 9914-9929.

HU, Q.-H., XIE, Z.-Q., WANG, X.-M., KANG, H. & ZHANG, P. 2013. Levoglucosan indicates high levels of biomass burning aerosols over oceans from the Arctic to Antarctic. *Sci. Rep.,* 3.

INEGI 2005. Carta de Uso del Suelo y Vegetación, Serie IV (2005), escala 1:250 000, México. *In:* GEOGRAFÍA, I. N. D. E. Y. (ed.).

INEGI 2012. Delimitación de las Zonas Metropolitanas de México 2010. *In:* GEOGRAFÍA, I. N. D. E. Y. (ed.).

KEHRWALD, N., ZANGRANDO, R., GABRIELLI, P., JAFFREZO, J.-L., BOUTRON, C., BARBANTE, C. & GAMBARO, A. 2012. Levoglucosan as a specific marker of fire events in Greenland snow. *Tellus B,* 64.

KHALIL, M. A. K. & RASMUSSEN, R. A. 2003. Tracers of wood smoke. *Atmospheric Environment,* 37**,** 1211-1222.

LEE, T., SULLIVAN, A. P., MACK, L. E., JIMENEZ, J. L., KREIDENWEIS, S. M., ONASCH, T. B., WORSNOP, D. R., MALM, W. C., WOLD, C. E., HAO, W. M. & COLLETT, J. L. 2010. Chemical Smoke Marker Emissions During Flaming and Smoldering Phases of Laboratory Open Burning of Wildland Fuels. *Aerosol Science and Technology,* 44.

LEVIN, E. J. T. 2013. *Remote continental aerosol characteristics in the Rocky Mountains of Colorado and Wyoming.* Colorado State University. Libraries.

LEVIN, E. J. T., MCMEEKING, G. R., CARRICO, C. M., MACK, L. E., KREIDENWEIS, S. M., WOLD, C. E., MOOSMÜLLER, H., ARNOTT, W. P., HAO, W. M., COLLETT, J. L. & MALM, W. C. 2010. Biomass burning smoke aerosol properties measured during Fire Laboratory at Missoula Experiments (FLAME). *Journal of Geophysical Research: Atmospheres,* 115**,** D18210.

LEVINE, J. S. 1991. *Global biomass burning atmospheric, climatic, and biospheric implications,* Cambridge, Mass., MIT Press.

LOCKER, H. B. 1988. *The use of levoglucosan to assess the environmental impact of residential wood-burning on air quality.* Ph.D. thesis, Dartmouth College, Hanover, N.H.

MACK, L. E., LEVIN, E. J. T., KREIDENWEIS, S. M., OBRIST, D., MOOSMÜLLER, H., LEWIS, K. A., ARNOTT, W. P., MCMEEKING, G. R., SULLIVAN, A. P., WOLD, C. E., HAO, W. M., COLLETT JR, J. L. & MALM, W. C. 2010. *Optical closure experiments for biomass smoke aerosols*.

MARKOWSKI, P. 2010. *Mesoscale meteorology in midlatitudes,* Chichester, West Sussex ;, Wiley-Blackwell.

MAYOL-BRACERO, O. L., GUYON, P., GRAHAM, B., ROBERTS, G., ANDREAE, M. O., DECESARI, S., FACCHINI, M. C., FUZZI, S. & ARTAXO, P. 2002. Water-soluble organic compounds in biomass burning aerosols over Amazonia 2. Apportionment of the chemical composition and importance of the polyacidic fraction. *Journal of Geophysical Research: Atmospheres,* 107**,** 8091.

MCMEEKING, G. R. 2004. *Size distribution measurements of wildfire smoke-influenced aerosol at Yosemite National Park.* Master's thesis, Colorado State University.

MCMEEKING, G. R., KREIDENWEIS, S. M., BAKER, S., CARRICO, C. M., CHOW, J. C., COLLETT, J. L., HAO, W. M., HOLDEN, A. S., KIRCHSTETTER, T. W., MALM, W. C., MOOSMÜLLER, H., SULLIVAN, A. P. & WOLD, C. E. 2009. Emissions of trace gases and aerosols during the open combustion of biomass in the laboratory. *Journal of Geophysical Research: Atmospheres,* 114**,** D19210.

MKOMA, S. L., KAWAMURA, K. & FU, P. 2012. Carbonaceous components, levoglucosan and inorganic ions in tropical aerosols from Tanzania, East Africa: implication for biomass burning contribution to organic aerosols. *Atmos. Chem. Phys.,* 12**,** 28661-28703.

MOCHIDA, M., KAWAMURA, K., FU, P. & TAKEMURA, T. 2010. Seasonal variation of levoglucosan in aerosols over the western North Pacific and its assessment as a biomass-burning tracer. *Atmospheric Environment,* 44**,** 3511-3518.

MOLINA, L. T., MADRONICH, S., GAFFNEY, J. S., APEL, E., DE FOY, B., FAST, J., FERRARE, R., HERNDON, S., JIMENEZ, J. L., LAMB, B., OSORNIO-VARGAS, A. R., RUSSELL, P., SCHAUER, J. J., STEVENS, P. S., VOLKAMER, R. & ZAVALA, M. 2010. An overview of the MILAGRO 2006 Campaign: Mexico City emissions and their transport and transformation. *Atmos. Chem. Phys.,* 10**,** 8697-8760.

MUNCHAK, L. A., SCHICHTEL, B. A., SULLIVAN, A. P., HOLDEN, A. S., KREIDENWEIS, S. M., MALM, W. C. & COLLETT JR, J. L. 2011. Development of wildland fire particulate smoke marker to organic carbon emission ratios for the conterminous United States. *Atmospheric Environment,* 45**,** 395-403.

NASA-WORLDVIEW 2014. Earth Science Data and Information System (ESDIS) Project. Version 0.6.4 ed.

OOLMAN, L. 2013. Upper air soundings. Department of Atmospheric Science University of Wyoming.

PSICHOUDAKI, M. & PANDIS, S. N. 2013. Atmospheric Aerosol Water-Soluble Organic Carbon Measurement: A Theoretical Analysis. *Environmental Science & Technology,* 47**,** 9791-9798.

QUEROL, X., PEY, J., MINGUILLÓN, M. C., PÉREZ, N., ALASTUEY, A., VIANA, M., MORENO, T., BERNABÉ, R. M., BLANCO, S., CÁRDENAS, B., VEGA, E., SOSA, G., ESCALONA, S., RUIZ, H. & ARTÍÑANO, B. 2008. PM speciation and sources in Mexico during the MILAGRO-2006 Campaign. *Atmos. Chem. Phys.,* 8**,** 111-128.

ROLPH, G. D. 2013. Real-time Environmental Applications and Display sYstem (READY) *In:* NOAA AIR RESOURCES LABORATORY, C. P., MD. (ed.).

SACMEX 2013. Red de estaciones pluviométricas de la Ciudad de México. *In:* MÉXICO, S. D. A. D. L. C. D. (ed.).

SCHKOLNIK, G., FALKOVICH, A. H., RUDICH, Y., MAENHAUT, W. & ARTAXO, P. 2005. New Analytical Method for the Determination of Levoglucosan, Polyhydroxy Compounds, and 2-Methylerythritol and Its Application to Smoke and Rainwater Samples. *Environmental Science & Technology,* 39**,** 2744-2752.

SEDEMA 2006. Informe Climatológico Ambiental del Valle de México 2006. Secretaría del Medio Ambiente del Distrito Federal.

SEDEMA 2011. Programa para mejorar la calidad del aire de la zona metropolitana del Valle de México 2011-2020. Secretaría del Medio Ambiente del Distrito Federal.

SEDEMA 2012a. Calidad del Aire en la Ciudad de Mexico, 2011. Secretaría del Medio Ambiente del Distrito Federal.

SEDEMA 2012b. Inventario de Emisiones de la Zona Metropolitana del Valle de México 2010. Secretaría del Medio Ambiente del Distrito Federal.

SHEESLEY, R. J., SCHAUER, J. J., ZHENG, M. & WANG, B. 2007. Sensitivity of molecular marker-based CMB models to biomass burning source profiles. *Atmospheric Environment,* 41**,** 9050-9063.

SIMAT 2013. Bases de datos. *In:* DIRECCIÓN DE MONITOREO ATMOSFÉRICO, S. D. M. A. (ed.). Secretaría del Medio Ambiente del Distrito Federal.

SIMONEIT, B. R. T. & ELIAS, V. O. 2001. Detecting Organic Tracers from Biomass Burning in the Atmosphere. *Marine Pollution Bulletin,* 42**,** 805-810.

SIMONEIT, B. R. T., SCHAUER, J. J., NOLTE, C. G., OROS, D. R., ELIAS, V. O., FRASER, M. P., ROGGE, W. F. & CASS, G. R. 1999. Levoglucosan, a tracer for cellulose in biomass burning and atmospheric particles. *Atmospheric Environment,* 33**,** 173-182.

STONE, E. A., SNYDER, D. C., SHEESLEY, R. J., SULLIVAN, A. P., WEBER, R. J. & SCHAUER, J. J. 2008. Source apportionment of fine organic aerosol in Mexico City during the MILAGRO experiment 2006. *Atmos. Chem. Phys.,* 8**,** 1249-1259.

SULLIVAN, A. P., HOLDEN, A. S., PATTERSON, L. A., MCMEEKING, G. R., KREIDENWEIS, S. M., MALM, W. C., HAO, W. M., WOLD, C. E. & COLLETT, J. L. 2008. A method for smoke marker measurements and its potential application for determining the contribution of biomass burning from wildfires and prescribed fires to ambient PM2.5 organic carbon. *Journal of Geophysical Research: Atmospheres,* 113**,** D22302.

SULLIVAN, A. P., MAY, A. A., LEE, T., MCMEEKING, G. R., KREIDENWEIS, S. M., AKAGI, S. K., YOKELSON, R. J., URBANSKI, S. P. & COLLETT JR, J. L. 2014. Airborne characterization of smoke marker ratios from prescribed burning. *Atmos. Chem. Phys. Discuss.,* 14**,** 11715-11747.

SULLIVAN, A. P., PELTIER, R. E., BROCK, C. A., DE GOUW, J. A., HOLLOWAY, J. S., WARNEKE, C., WOLLNY, A. G. & WEBER, R. J. 2006. Airborne measurements of carbonaceous aerosol soluble in water over northeastern United States: Method development and an investigation into water-soluble organic carbon sources. *Journal of Geophysical Research: Atmospheres,* 111**,** D23S46.

SULLIVAN, A. P., WEBER, R. J., CLEMENTS, A. L., TURNER, J. R., BAE, M. S. & SCHAUER, J. J. 2004. A method for on-line measurement of water-soluble organic carbon in ambient aerosol particles: Results from an urban site. *Geophysical Research Letters,* 31**,** L13105.

TURCO, R. P. 2002. *Earth Under Siege: From Air Pollution to Global Change*, Oxford University Press.

URBAN, R. C., LIMA-SOUZA, M., CAETANO-SILVA, L., QUEIROZ, M. E. C., NOGUEIRA, R. F. P., ALLEN, A. G., CARDOSO, A. A., HELD, G. & CAMPOS, M. L. 2012. Use of levoglucosan, potassium, and water-soluble organic carbon to characterize the origins of biomass-burning aerosols. *Atmospheric Environment,* 61**,** 562-569.

WALLACE, J. M. & HOBBS, P. V. 2006. *Atmospheric science: an introductory survey*, Academic press.

WHO/UNEP 1992. Urban Air Pollution in Megacities of the World. World Health Organization and United Nations Environment Programme, Blackwell, Oxford.

WIEDINMYER, C., AKAGI, S. K., YOKELSON, R. J., EMMONS, L. K., AL-SAADI, J. A., ORLANDO, J. J. & SOJA, A. J. 2011. The Fire INventory from NCAR (FINN): a high resolution global model to estimate the emissions from open burning. *Geosci. Model Dev.,* 4**,** 625-641.

WONASCHÜTZ, A., HERSEY, S. P., SOROOSHIAN, A., CRAVEN, J. S., METCALF, A. R., FLAGAN, R. C. & SEINFELD, J. H. 2011. Impact of a large wildfire on water-soluble organic aerosol in a major urban area: the 2009 Station Fire in Los Angeles County. *Atmos. Chem. Phys.,* 11**,** 8257-8270.

YOKELSON, R. J., BURLING, I. R., URBANSKI, S. P., ATLAS, E. L., ADACHI, K., BUSECK, P. R., WIEDINMYER, C., AKAGI, S. K., TOOHEY, D. W. & WOLD, C. E. 2011. Trace gas and particle emissions from open biomass burning in Mexico. *Atmos. Chem. Phys.,* 11**,** 6787-6808.

YOKELSON, R. J., URBANSKI, S. P., ATLAS, E. L., TOOHEY, D. W., ALVARADO, E. C., CROUNSE, J. D., WENNBERG, P. O., FISHER, M. E., WOLD, C. E., CAMPOS, T. L., ADACHI, K., BUSECK, P. R. & HAO, W. M. 2007. Emissions from forest fires near Mexico City. *Atmos. Chem. Phys.,* 7**,** 5569-5584.

ZHU, T., MELAMED, M., PARRISH, D., GAUSS, M., GALLARDO KLENNER, L., LAWRENCE, M., KONARE, A. & LIOUSSE, C. 2012. WMO/IGAC Impacts of Megacities on Air Pollution and Climate. World Meteorological Organization and International Global Atmospheric Chemistry.

9. APPENDIX A

The daily mean ambient concentrations of CO (ppm), PM_{10} ($\mu g/m^3$), $PM_{2.5}$ ($\mu g/m^3$), and coarse mode for each sampling station during May 2013 (SIMAT, 2013) are presented in the following tables. No information is shown in the tables if the SIMAT station did not report concentrations for a certain pollutant.

Table 9.1 Daily mean ambient concentrations of CO (ppm) for sampling SIMAT stations during May 2013.
Data from SIMAT (2013).

DAY	LPR (ppm)	MER (ppm)	NEZ (ppm)	TLA (ppm)	UIZ (ppm)	XAL (ppm)
1	0.6	1.2	0.7	1.0		1.0
2	1.1	1.2	0.8	1.0		1.2
3	0.8	0.9	0.6	0.9		0.7
4	0.9	1.1	0.6	1.2		0.9
5	0.8	1.1	0.7	0.9		0.9
6	0.9	1.1	0.6	1.1		0.9
7	1.3	1.5	0.9	1.2		1.3
8	1.1	1.3	1.0	1.3		1.2
9	1.2	1.6	0.9	1.2		1.5
10	1.2	1.5	1.2	1.2		1.4
11	1.1	1.5	1.1	1.2		1.1
12	0.7	0.9	0.7	0.8		0.6
13	0.6	0.9	0.6	0.8		0.5
14	0.7	1.1	0.6	0.9		0.8
15	0.8	1.1	0.8	1.1		0.8
16		1.0	0.7	1.2	1.1	1.2
17		1.3	0.9	1.2	1.3	0.8
18		0.9	0.7	1.0	1.0	0.9
19		1.0	0.7	0.7	0.9	0.8
20		1.1	0.7	0.9	0.9	0.8
21		1.0	0.8	1.1	1.2	0.9
22		1.3	1.0	1.1	1.1	0.8
23		1.1	0.8	1.1	1.1	1.0
24		1.1	1.0	1.0	1.1	0.8
25		1.0	0.7	0.9	0.9	0.6
26		0.9	0.8	1.0	0.8	0.6
27		1.0	0.8	1.2	0.9	0.7
28		1.2		1.0	1.0	0.8

DAY	LPR (ppm)	MER (ppm)	NEZ (ppm)	TLA (ppm)	UIZ (ppm)	XAL (ppm)
29		1.0	0.5	1.1	0.9	1.3
30		0.9	0.6	1.0		
31		0.8	0.5	0.9	0.5	

Table 9.2 Daily mean ambient concentrations of PM_{10} ($\mu g/m^3$) for sampling SIMAT stations during May 2013.
Data from SIMAT (2013).

DAY	MER ($\mu g/m^3$)	TLA ($\mu g/m^3$)	UIZ ($\mu g/m^3$)	XAL ($\mu g/m^3$)
1	71	70	58	90
2	105	94	84	122
3	71	73	54	74
4	96	103	88	115
5	81	75	68	90
6	95	100	80	109
7	110	105	104	129
8	101	103	96	118
9	107	98	95	131
10	106	101	104	131
11	108	114	94	132
12	77	76	68	89
13	34	35	40	51
14	43	42	41	53
15	73	85	68	107
16	55	73	55	109
17	47	70	53	92
18	37	59	47	78
19	53	48	49	62
20	49	48	44	66
21	64	67	58	87
22	68	81	62	88
23	50	62	49	75
24	62	60	57	97
25	54	55	53	62
26	39	40	38	45
27	36	36	33	58
28	52	53	34	73
29	55	61	49	112
30	54	68	59	
31	51	61	49	

Table 9.3 Daily mean ambient concentrations of PM2.5 ($\mu g/m^3$) for sampling SIMAT stations during May 2013.
Data from SIMAT (2013).

DAY	MER ($\mu g/m^3$)	NEZ ($\mu g/m^3$)	TLA ($\mu g/m^3$)	UIZ ($\mu g/m^3$)	XAL ($\mu g/m^3$)
1	38	36	37	36	50
2	43	44	41	49	55
3	30	27	33	29	36
4	49	49	56	50	58
5	47	49	42	45	54
6	54	52	56	51	62
7	62	67	60	65	72
8	55	59	59	63	68
9	64	66	57	64	76
10	62	69	54	68	73
11	57	64	56	58	71
12	44	40	46	44	57
13	20	20	19	28	36
14	27	20	24	29	34
15	47	35	51	46	52
16	35	32	39	38	48
17	33	30	38	35	43
18	28	29	32	34	43
19	33	30	28	36	40
20	29	29	27	30	36
21	35	44	36	37	47
22	37	40	42	36	44
23	31	36	36	33	45
24	30	38	27	32	42
25	31	32	32	34	33
26	28	25	27	29	33
27	21	9	19	21	27
28	28		26	17	33
29	27	24	25	27	44
30	28	25	31	32	
31	23	20	29	24	

Table 9.4 Daily mean ambient concentrations of coarse fraction (PM_{10} - $PM_{2.5}$, $\mu g/m^3$) for sampling SIMAT stations during May 2013. Data fromSIMAT (2013).

DAY	MER ($\mu g/m^3$)	TLA ($\mu g/m^3$)	UIZ ($\mu g/m^3$)	XAL ($\mu g/m^3$)
1	34	33	22	40
2	62	53	35	67
3	40	40	25	38
4	47	47	37	57
5	34	33	23	36
6	41	44	29	46
7	48	45	39	57
8	46	44	34	50
9	44	42	31	55
10	44	46	36	58
11	51	58	37	61
12	33	30	24	31
13	14	16	12	15
14	15	18	12	19
15	26	33	22	55
16	20	34	18	61
17	15	32	17	49
18	9	27	13	36
19	20	19	13	22
20	20	20	14	31
21	29	31	21	40
22	31	39	25	43
23	19	26	16	31
24	32	33	25	55
25	22	23	18	30
26	11	12	9	13
27	16	17	12	31
28	25	27	17	40
29	27	35	22	68
30	27	36	27	
31	28	32	25	

10. APPENDIX B

Skew-t diagrams and sounding data for each sampling date at 12Z and 00Z for station number 76679 located at Mexico Cityôs International Airport, obtained from the Department of Atmospheric Science, University of Wyoming (Oolman, 2013).

May 4th

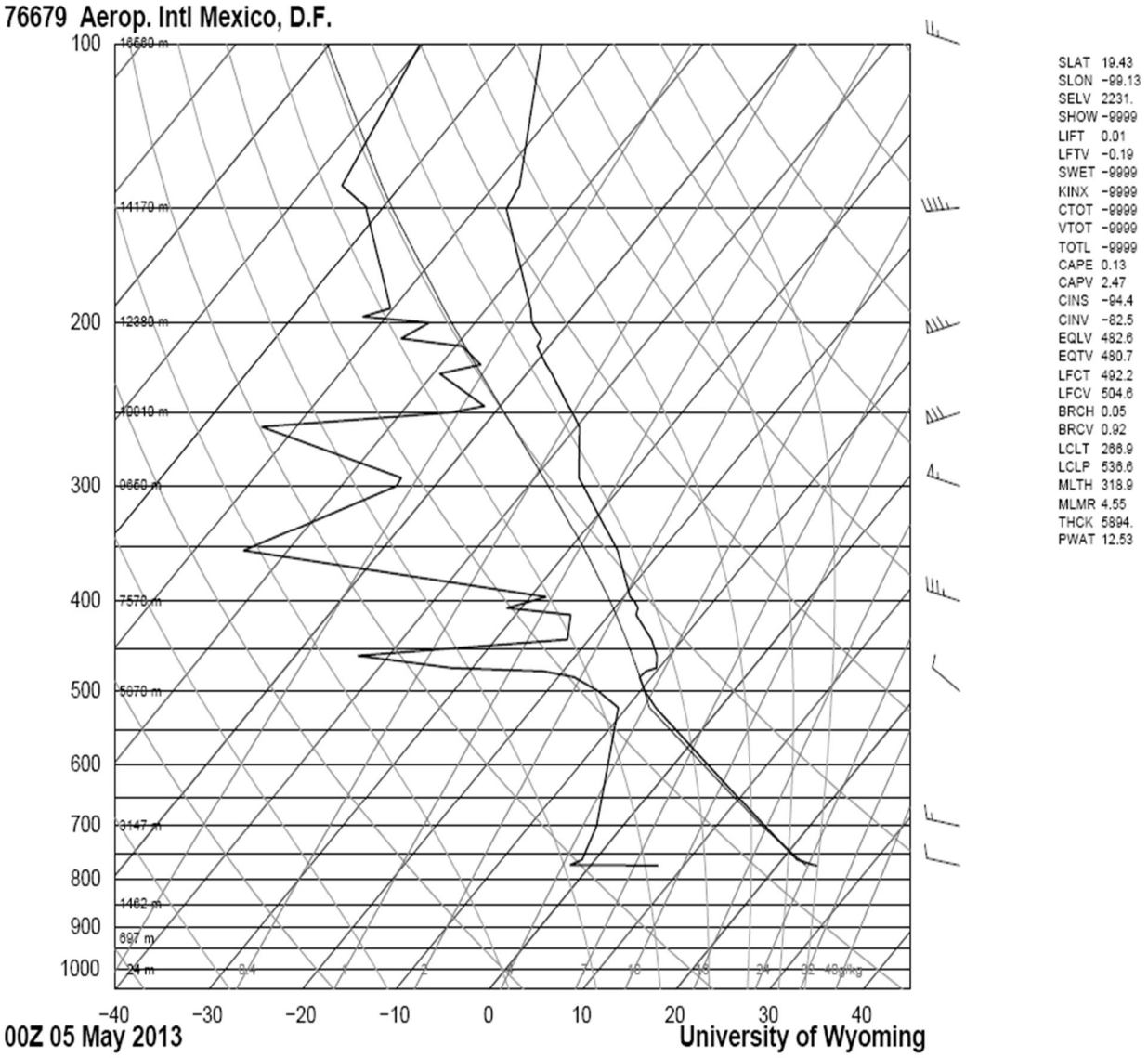

76679 Aerop. Intl Mexico, D.F. Observations at 00Z 05 May 2013

PRES [hPa]	HGHT [m]	TEMP [C]	DWPT [C]	RELH [%]	MIXR [g/kg]	DRCT [deg]	SKNT [knot]	THTA [K]	THTE [K]	THTV [K]
1000	-24									
925	697									
850	1462									
772	2231	24.2	7.2	34	8.32	280	12	320.2	347.1	321.8
771	2243	23.8	-2.2	18	4.24	280	12	319.9	334	320.7
761	2367	21.6	-1.4	21	4.56	280	13	318.7	333.7	319.6
700	3147	15.2	-2.8	29	4.47	280	17	319.3	334.1	320.1
521	5550	-6.9	-10.9	73	3.21	302	9	320.8	331.6	321.4
500	5870	-9.5	-14.5	67	2.5	305	8	321.4	330	321.9
483	6137	-11.3	-18.3	56	1.88	302	13	322.4	328.9	322.7
476	6249	-11.1	-22.1	40	1.38	301	14	324	328.9	324.2
472	6314	-10.3	-32.3	15	0.54	300	15	325.7	327.8	325.8
458	6545	-11.3	-43.3	5	0.18	297	19	327.3	328	327.3
440	6852	-13.3	-22.3	47	1.46	294	25	328.5	333.9	328.8
414	7312	-17.1	-24.1	55	1.32	288	33	329.4	334.3	329.7
407	7440	-17.5	-31.5	28	0.68	287	35	330.5	333.1	330.6
400	7570	-18.5	-29.5	37	0.83	285	37	330.9	334	331
396	7645	-19.3	-28.3	45	0.94	285	38	330.8	334.3	331
353	8490	-24.7	-64.7	1	0.02	285	44	334.5	334.6	334.5
300	9650	-34.1	-54.1	11	0.08	285	54	337.2	337.6	337.2
294	9791	-35.3	-54.3	13	0.08	282	56	337.4	337.8	337.5
259	10669	-39.7	-73.7	1	0.01	261	67	343.4	343.4	343.4
250	10910	-41.7	-54.7	23	0.09	255	70	343.9	344.3	343.9
246	11019	-42.7	-51.7	37	0.13	255	70	344	344.6	344.1
227	11556	-47.3	-59.3	24	0.06	255	71	345	345.2	345
222	11702	-48.7	-55.7	44	0.09	255	72	345.1	345.4	345.1
212	12003	-51.3	-59.3	38	0.06	255	72	345.6	345.9	345.6
208	12127	-51.5	-66.5	15	0.02	255	72	347.1	347.3	347.1
200	12380	-53.9	-64.9	25	0.03	255	73	347.2	347.4	347.3
197	12477	-54.5	-72.5	9	0.01	255	74	347.8	347.9	347.8
193	12608	-55.3	-70.3	14	0.02	255	75	348.6	348.6	348.6
151	14130	-66.5	-81.5	11	0	265	47	354.7	354.7	354.7
150	14170	-66.7	-81.7	10	0	265	46	355	355	355
142	14500	-67.3	-86.3	5	0	268	43	359.6	359.6	359.6
100	16560	-77.3	-90.3	11	0	285	23	378.1	378.1	378.1
82.2	17673	-81.1	-95.1	8	0	260	36	392.1	392.1	392.1
78.1	17962	-80.3	-96.3	6	0	292	25	399.6	399.6	399.6

PRES [hPa]	HGHT [m]	TEMP [C]	DWPT [C]	RELH [%]	MIXR [g/kg]	DRCT [deg]	SKNT [knot]	THTA [K]	THTE [K]	THTV [K]
75.9	18126	-74.1	-93.1	4	0	310	19	415.8	415.8	415.8
73.6	18305	-74.7	-100.7	1	0	329	12	418.2	418.2	418.2
72.2	18417	-73.7	-100.7	1	0	341	8	422.6	422.6	422.6
71.7	18458	-70.3	-98.3	1	0	345	6	430.7	430.7	430.7
70	18600	-70.5	-98.5	1	0	0	1	433.2	433.2	433.2
64.6	19074	-71.9	-99.9	1	0	352	2	440.2	440.2	440.2
60.3	19483	-68.3	-97.3	1	0	344	4	457	457	457
50	20620	-62.7	-92.7	1	0	325	7	495.3	495.3	495.3
45.6	21189	-61.7	-91.7	1	0	354	10	510.9	510.9	510.9
42.2	21667	-63.5	-93.5	1	0	18	12	517.9	517.9	517.9
35.7	22707	-58.3	-89.3	1	0	71	18	556.8	556.8	556.8
33.9	23032	-59.1	-90.1	1	0	87	19	562.9	563	562.9
30	23800	-58.5	-89.5	1	0	125	23	584.6	584.6	584.6
27.3	24393	-58.5	-89.5	1	0	105	20	600.5	600.6	600.5
23.3	25409	-49.7	-83.7	1	0.02	72	16	654.1	654.3	654.1
21.5	25932	-52.1	-85.1	1	0.01	55	13	662.1	662.3	662.1
20	26400	-51.7	-84.7	1	0.02	40	11	677.2	677.3	677.2
15.1	28260	-42.7	-78.7	1	0.05	83	12	763.6	764.2	763.6
13.1	29220	-41.9	-77.9	1	0.07	104	12	798	798.8	798
11.8	29926	-43.3	-79.3	1	0.06	120	13	817.2	818	817.2
10	31050	-39.3	-76.3	1	0.12	145	13	871.7	873.2	871.8
9.4	31476	-37.7	-75.7	1	0.14	138	12	893.3	895.1	893.4
8.7	32008	-39.3	-76.3	1	0.14	129	11	907.1	908.9	907.2
7	33510	-35.9	-73.9	1	0.25	105	9	979.2	982.7	979.4
5.8	34824	-32.9	-71.9	1	0.4	1046.4	1052.3	1046.6		

Station information and sounding indices

Station number	76679
Observation time	130505/0000
Station latitude	19.43
Station longitude	-99.13
Station elevation	2231
Lifted index	0.01
LIFT computed using virtual temperature	-0.19
Convective Available Potential Energy	0.13
CAPE using virtual temperatura	2.47
Convective Inhibition	-94.49

Station information and sounding indices

CINS using virtual temperature	-82.51
Equilibrum Level	482.63
Equilibrum Level using virtual temperature	480.73
Level of Free Convection	492.2
LFCT using virtual temperature	504.66
Bulk Richardson Number	0.05
Bulk Richardson Number using CAPV	0.92
Temp [K] of the Lifted Condensation Level	266.99
Pres [hPa] of the Lifted Condensation Level	536.65
Mean mixed layer potential temperature	318.96
Mean mixed layer mixing ratio	4.55
1000 hPa to 500 hPa thickness	5894
Precipitable water [mm] for entire sounding	12.53

May 10th

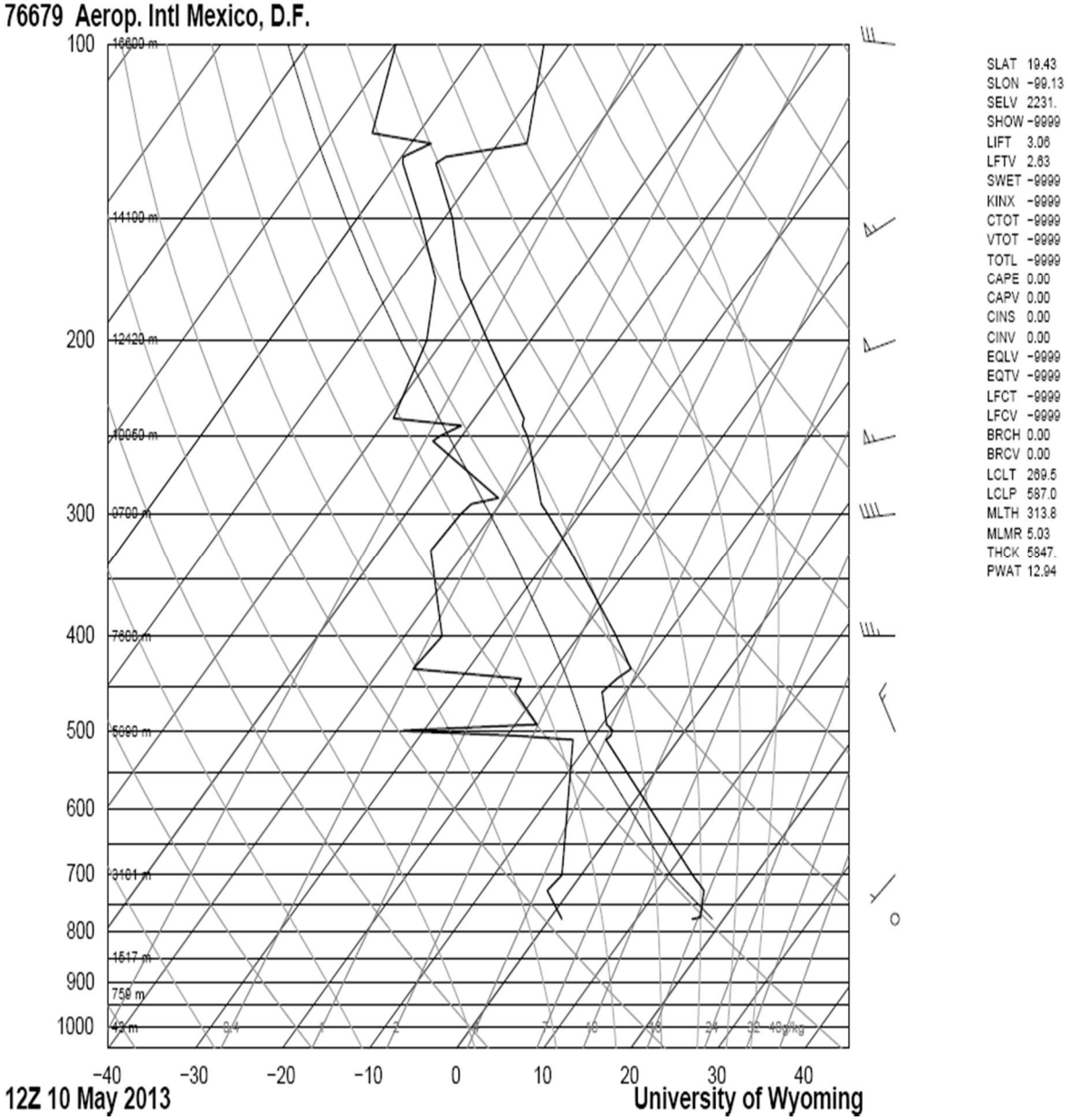
76679 Aerop. Intl Mexico, D.F.
100
200
300
400
500
600
700
800
900
1000
16600 m
14100 m
12420 m
10060 m
9700 m
7660 m
5980 m
3161 m
1517 m
759 m
43 m
−40
−30
−20
−10
0
10
20
30
40
12Z 10 May 2013
University of Wyoming
SLAT 19.43
SLON -99.13
SELV 2231.
SHOW -9999
LIFT 3.06
LFTV 2.63
SWET -9999
KINX -9999
CTOT -9999
VTOT -9999
TOTL -9999
CAPE 0.00
CAPV 0.00
CINS 0.00
CINV 0.00
EQLV -9999
EQTV -9999
LFCT -9999
LFCV -9999
BRCH 0.00
BRCV 0.00
LCLT 289.5
LCLP 587.0
MLTH 313.8
MLMR 5.03
THCK 5847.
PWAT 12.94

76679 Aerop. Intl Mexico, D.F. Observations at 12Z 10 May 2013

PRES [hPa]	HGHT [m]	TEMP [C]	DWPT [C]	RELH [%]	MIXR [g/kg]	DRCT [deg]	SKNT [knot]	THTA [K]	THTE [K]	THTV [K]
1000	43									
925	759									
850	1517									
776	2231	16.4	1.4	36	5.49	0	0	311.3	328.7	312.3
773	2267	17.2	1.2	34	5.43	355	0	312.5	329.8	313.5
726	2847	15.4	-2.6	29	4.37	276	3	316.2	330.5	317
700	3181	12.8	-2.2	35	4.67	230	4	316.6	331.9	317.5
510	5736	-8.3	-12.1	74	2.98	324	12	321	331.1	321.6
505	5813	-8.1	-19.1	41	1.68	327	13	322.2	328.1	322.5
500	5890	-8.3	-31.3	14	0.56	330	13	322.9	325	323
499	5906	-8.3	-32.3	13	0.51	329	13	323	325	323.1
492	6015	-9.5	-17.5	52	1.98	326	15	322.9	329.8	323.3
456	6600	-12.7	-22.7	43	1.36	305	22	326	330.9	326.2
442	6838	-12.1	-23.1	40	1.36	297	25	329.6	334.6	329.9
432	7014	-11.3	-36.3	11	0.4	291	27	332.8	334.4	332.9
400	7600	-15.7	-35.7	16	0.46	270	35	334.5	336.3	334.6
327	9087	-28.1	-44.1	20	0.23	267	39	337.2	338.2	337.3
300	9700	-33.7	-43.7	36	0.27	265	40	337.8	338.9	337.8
293	9864	-35.3	-43.3	44	0.28	264	42	337.8	338.9	337.8
289	9960	-35.9	-40.7	61	0.38	264	43	338.2	339.8	338.3
253	10870	-41.9	-52.9	29	0.11	260	53	342.5	343	342.5
250	10950	-42.5	-52.5	33	0.12	260	54	342.7	343.3	342.8
244	11114	-43.9	-50.9	46	0.15	259	53	343	343.7	343.1
240	11225	-44.3	-59.3	17	0.05	259	53	344.1	344.3	344.1
200	12420	-54.9	-61.9	42	0.05	255	49	345.7	345.9	345.7
173	13327	-63.1	-66	68	0.03	250	53	346.8	346.9	346.8
150	14190	-69.1	-72.8	59	0.01	245	57	350.9	350.9	350.9
132	14944	-75.5	-79.3	55	0.01	255	53	352.5	352.5	352.5
130	15033	-74.9	-79.8	47	0.01	256	52	355.1	355.1	355.1
126	15219	-66.7	-77.7	20	0.01	258	49	373.1	373.2	373.1
123	15365	-67.3	-85.3	6	0	260	48	374.6	374.6	374.6
100	16600	-72.9	-89.9	6	0	275	32	386.6	386.6	386.6
72.6	18452	-78.7	-93.7	7	0	300	7	411.4	411.4	411.4
70	18660	-77.9	-92.9	8	0	250	16	417.4	417.4	417.4
68.7	18767	-78.1	-93.1	7	0	240	16	419.2	419.2	419.2
61.2	19444	-69.1	-92.1	2	0	178	14	453.3	453.3	453.3
56.5	19924	-67.5	-93.5	1	0	135	13	467.4	467.4	467.4
53.2	20286	-69.3	-96.3	1	0	103	13	471.3	471.4	471.3
50	20660	-65.5	-93.5	1	0	70	12	488.7	488.7	488.7

PRES [hPa]	HGHT [m]	TEMP [C]	DWPT [C]	RELH [%]	MIXR [g/kg]	DRCT [deg]	SKNT [knot]	THTA [K]	THTE [K]	THTV [K]
39.3	22130	-63.3	-93.3	1	0	75	19	529.1	529.1	529.1
37	22506	-57.7	-89.7	1	0	76	21	552.6	552.7	552.6
33.8	23073	-60.1	-91.1	1	0	78	24	560.8	560.8	560.8
30	23820	-57.7	-89.7	1	0	80	27	586.8	586.8	586.8
26.4	24628	-57.5	-89.5	1	0	85	24	609.1	609.2	609.1
23.9	25265	-52.1	-85.1	1	0.01	88	21	642.4	642.5	642.4
22.7	25598	-52.9	-85.9	1	0.01	90	20	649.6	649.7	649.6
20	26420	-50.7	-84.7	1	0.02	95	17	680.2	680.4	680.2
16.9	27530	-45.1	-80.1	1	0.04			731.7	732.1	731.7
13.5	29035	-43.5	-79.5	1	0.05			785.7	786.3	785.7

Station information and sounding indices

Station number	76679
Observation time	130510/1200
Station latitude	19.43
Station longitude	-99.13
Station elevation	2231
Lifted index	3.06
LIFT computed using virtual temperature	2.63
Convective Available Potential Energy	0
CAPE using virtual temperature	0
Convective Inhibition	0
CINS using virtual temperature	0
Bulk Richardson Number	0
Bulk Richardson Number using CAPV	0
Temp [K] of the Lifted Condensation Level	269.51
Pres [hPa] of the Lifted Condensation Level	587.09
Mean mixed layer potential temperature	313.83
Mean mixed layer mixing ratio	5.03
1000 hPa to 500 hPa thickness	5847
Precipitable water [mm] for entire sounding	12.94

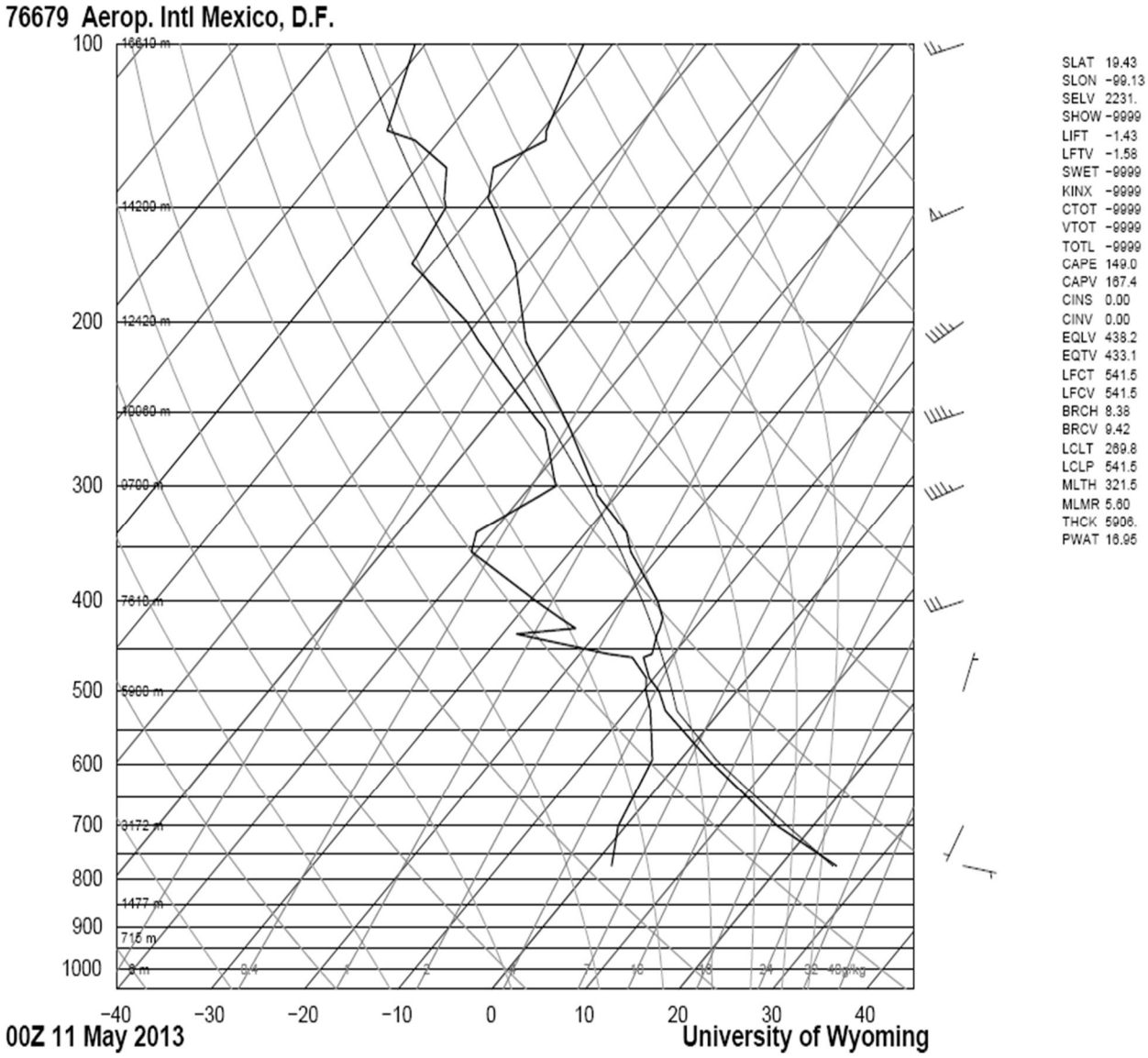

76679 Aerop. Intl Mexico, D.F. Observations at 00Z 11 May 2013

PRES [hPa]	HGHT [m]	TEMP [C]	DWPT [C]	RELH [%]	MIXR [g/kg]	DRCT [deg]	SKNT [knot]	THTA [K]	THTE [K]	THTV [K]
1000	-6									
925	715									
850	1477									
773	2231	26	2	21	5.75	100	7	322	341	323.1
700	3172	16.2	-0.8	31	5.18	210	3	320.4	337.5	321.4
593	4548	3	-3	65	5.2	294	5	320.6	337.8	321.6
525	5519	-5.9	-7.5	88	4.17	355	6	321.3	335.2	322.1

PRES [hPa]	HGHT [m]	TEMP [C]	DWPT [C]	RELH [%]	MIXR [g/kg]	DRCT [deg]	SKNT [knot]	THTA [K]	THTE [K]	THTV [K]
500	5900	-8.3	-9.7	90	3.68	20	7	322.9	335.3	323.6
484	6153	-10.5	-10.8	98	3.49	2	10	323.2	335	323.9
460	6544	-12.9	-14.1	91	2.81	333	16	324.9	334.6	325.4
456	6611	-12.3	-17	68	2.23	328	17	326.5	334.3	326.9
434	6990	-13.5	-28.5	27	0.84	301	22	329.6	332.8	329.8
428	7096	-13.7	-22.7	47	1.45	293	24	330.6	335.9	330.9
417	7294	-14.3	-25.3	39	1.18	278	27	332.3	336.7	332.6
400	7610	-16.3	-29.3	32	0.85	255	31	333.7	337	333.9
354	8515	-23.5	-40.5	19	0.32	253	37	335.9	337.2	335.9
337	8872	-25.7	-41.7	21	0.29	252	39	337.6	338.8	337.7
307	9538	-32.1	-38.1	55	0.47	250	43	337.8	339.6	337.9
300	9700	-33.1	-37.3	66	0.52	250	44	338.6	340.7	338.7
299	9724	-33.5	-37.5	67	0.51	250	44	338.4	340.4	338.5
261	10667	-40.7	-43.4	75	0.32	254	45	341.2	342.5	341.3
250	10960	-43.1	-46.4	70	0.24	255	45	341.9	342.9	341.9
210	12107	-53.1	-58.1	54	0.07	243	47	343.7	344	343.7
200	12420	-55.1	-61.1	47	0.05	240	47	345.4	345.6	345.4
173	13331	-61.1	-72.1	22	0.01	245	51	350.1	350.1	350.1
150	14200	-68.5	-73.5	49	0.01	250	54	351.9	352	351.9
147	14321	-69.7	-74.4	50	0.01	251	53	351.9	351.9	351.9
136	14783	-71.9	-76.9	47	0.01	255	51	355.9	355.9	355.9
127	15191	-68.7	-82.7	12	0	255	46	368.7	368.7	368.7
124	15335	-69.5	-86.5	7	0	255	44	369.8	369.8	369.8
100	16610	-73.1	-91.1	5	0	255	27	386.2	386.2	386.2
94.8	16922	-75.3	-91.3	7	0	255	24	387.9	387.9	387.9
70	18670	-78.3	-95.3	5	0	285	10	416.6	416.6	416.6
69.7	18695	-78.5	-95.5	5	0	283	10	416.6	416.6	416.6
64.9	19108	-73.5	-93.5	3	0	246	12	436.1	436.1	436.1
62.5	19329	-74.3	-95.3	3	0	226	14	439.1	439.1	439.1
56.3	19950	-67.1	-93.1	1	0	172	17	468.8	468.8	468.8
52.7	20351	-66.1	-93.1	1	0	137	19	480	480	480
50	20670	-67.3	-94.3	1	0	110	21	484.5	484.5	484.5
49.2	20767	-67.7	-94.7	1	0	109	21	485.8	485.8	485.8
42.1	21714	-63.9	-92.9	1	0	100	23	517.3	517.3	517.3
39.9	22047	-59.5	-90.5	1	0	97	24	536.3	536.3	536.3
37.8	22384	-61.7	-91.7	1	0	94	24	539.1	539.1	539.1
34.6	22940	-56.1	-88.1	1	0	88	25	567.5	567.5	567.5
31.8	23478	-54.9	-86.9	1	0.01	83	26	584.6	584.6	584.6
30	23850	-55.7	-87.7	1	0.01	80	27	592.2	592.3	592.2
25.4	24913	-53.1	-86.1	1	0.01	86	20	628.5	628.6	628.5
22.9	25575	-55.5	-87.5	1	0.01	90	16	640.3	640.4	640.3

PRES [hPa]	HGHT [m]	TEMP [C]	DWPT [C]	RELH [%]	MIXR [g/kg]	DRCT [deg]	SKNT [knot]	THTA [K]	THTE [K]	THTV [K]
20.5	26288	-49.1	-83.1	1	0.02	94	11	680.3	680.5	680.3
20	26450	-48.9	-82.9	1	0.02	95	10	685.7	686	685.7
16.8	27603	-45.5	-80.5	1	0.04			731.7	732.1	731.7
12.2	29766	-38.9	-75.9	1	0.1			825	826.2	825
10.5	30791	-40.9	-77.9	1	0.09			853.8	854.9	853.8

Station information and sounding indices

Station number	76679
Observation time	130511/0000
Station latitude	19.43
Station longitude	-99.13
Station elevation	2231
Lifted index	-1.43
LIFT computed using virtual temperature	-1.58
Convective Available Potential Energy	149.04
CAPE using virtual temperature	167.42
Convective Inhibition	0
CINS using virtual temperature	0
Equilibrum Level	438.25
Equilibrum Level using virtual temperature	433.14
Level of Free Convection	541.54
LFCT using virtual temperature	541.54
Bulk Richardson Number	8.38
Bulk Richardson Number using CAPV	9.42
Temp [K] of the Lifted Condensation Level	269.88
Pres [hPa] of the Lifted Condensation Level	541.54
Mean mixed layer potential temperature	321.58
Mean mixed layer mixing ratio	5.6
1000 hPa to 500 hPa thickness	5906
Precipitable water [mm] for entire sounding	16.95

May 16th

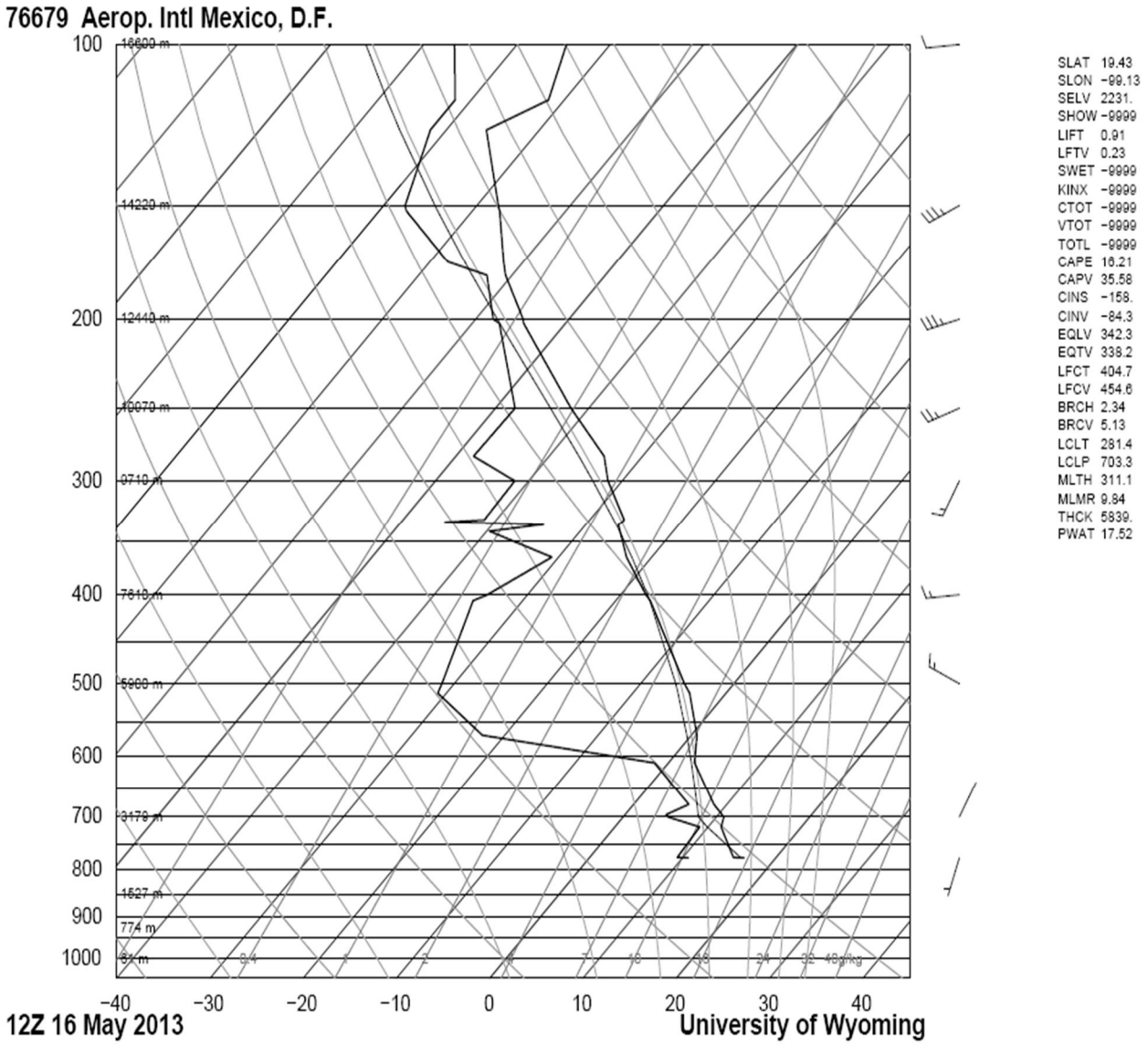

76679 Aerop. Intl Mexico, D.F. Observations at 12Z 16 May 2013

PRES [hPa]	HGHT [m]	TEMP [C]	DWPT [C]	RELH [%]	MIXR [g/kg]	DRCT [deg]	SKNT [knot]	THTA [K]	THTE [K]	THTV [K]
1000	61									
925	774									
850	1527									

PRES [hPa]	HGHT [m]	TEMP [C]	DWPT [C]	RELH [%]	MIXR [g/kg]	DRCT [deg]	SKNT [knot]	THTA [K]	THTE [K]	THTV [K]
776	2231	16.6	10.6	68	10.45	200	3	311.5	343.9	313.5
775	2243	15.4	9.4	67	9.64	198	3	310.4	340.2	312.1
718	2947	11.4	9.1	86	10.2	72	1	312.8	344.6	314.7
700	3179	10.8	4.8	66	7.76	30	1	314.4	339	315.9
696	3227	10.4	4.4	66	7.59	28	1	314.5	338.5	315.9
678	3445	8.6	5.9	83	8.66	21	2	314.8	342.2	316.5
610	4312	2.8	-1.5	73	5.65	351	6	317.8	336.2	318.9
569	4873	0.6	-22.4	16	1.12	332	8	321.6	325.6	321.8
512	5713	-3.9	-30.9	10	0.57	302	12	326	328.2	326.1
500	5900	-5.3	-31.3	11	0.56	295	13	326.5	328.7	326.6
406	7498	-16.3	-35.3	18	0.47	267	15	332.3	334.1	332.4
400	7610	-17.3	-34.3	21	0.53	265	15	332.4	334.5	332.5
364	8311	-22.7	-30.7	48	0.82	247	15	334.3	337.4	334.4
341	8789	-25.7	-39.7	26	0.36	234	16	336.5	337.9	336.6
335	8918	-26.5	-34.5	47	0.62	231	16	337.1	339.5	337.2
333	8961	-26.3	-45.3	15	0.2	230	16	338	338.8	338
331	9005	-26.3	-41.3	23	0.31	229	16	338.6	339.8	338.6
300	9710	-31.5	-41.5	37	0.34	210	16	340.9	342.2	340.9
282	10144	-34.1	-48.1	23	0.17	224	19	343.2	344	343.2
250	10970	-41.9	-47.9	52	0.2	250	24	343.6	344.5	343.7
202	12376	-54.5	-57.1	73	0.08	255	35	345.3	345.7	345.3
200	12440	-54.9	-58.1	67	0.07	255	36	345.7	346	345.7
179	13139	-60.7	-62.7	77	0.05	251	35	347.3	347.5	347.3
173	13350	-62.1	-68.1	44	0.02	250	35	348.4	348.5	348.4
152	14140	-67.1	-77.1	23	0.01	245	34	353	353	353
150	14220	-67.7	-77.7	23	0.01	245	34	353.3	353.3	353.3
124	15342	-75.7	-81.7	39	0	225	28	358.5	358.5	358.5
115	15782	-71.7	-81.7	21	0	239	21	373.7	373.7	373.7
100	16600	-74.7	-86.7	14	0	265	8	383.1	383.2	383.1
82.2	17727	-78.3	-91.3	11	0	235	8	397.9	397.9	397.9
79.5	17919	-76.1	-90.1	10	0	205	10	406.2	406.2	406.2
72.4	18456	-77.9	-92.9	8	0	120	16	413.4	413.4	413.4
70.4	18617	-74.7	-90.7	7	0	95	18	423.6	423.6	423.6
70	18650	-74.7	-90.7	7	0	90	18	424.2	424.3	424.2
50	20660	-64.9	-94.9	1	0	90	25	490.1	490.1	490.1
49.7	20697	-65.3	-94.3	1	0	90	25	490	490	490
47.8	20937	-60.9	-91.9	1	0	88	25	506	506	506
45.5	21243	-62.1	-92.1	1	0	85	25	510.3	510.3	510.3
40.3	21995	-61.7	-91.7	1	0	79	25	529.3	529.3	529.3
38	22363	-58.1	-90.1	1	0	77	24	547.4	547.4	547.4
35	22880	-59.3	-90.3	1	0	73	24	557.3	557.3	557.3

PRES [hPa]	HGHT [m]	TEMP [C]	DWPT [C]	RELH [%]	MIXR [g/kg]	DRCT [deg]	SKNT [knot]	THTA [K]	THTE [K]	THTV [K]
31.3	23589	-54.7	-86.7	1	0.01	67	24	587.8	587.8	587.8
30	23860	-56.1	-88.1	1	0.01	65	24	591.1	591.2	591.1
27.5	24409	-57.5	-89.5	1	0	68	25	602.1	602.1	602.1
25.8	24813	-54.5	-87.5	1	0.01	71	26	621.7	621.8	621.7
23.5	25408	-55.1	-87.1	1	0.01	74	27	636.7	636.8	636.8
22.1	25803	-50.1	-84.1	1	0.02	76	28	662.9	663	662.9
20	26450	-51.9	-84.9	1	0.01	80	29	676.6	676.7	676.6
18.6	26919	-52.7	-85.7	1	0.01			688.2	688.4	688.2
16.8	27582	-48.9	-82.9	1	0.02			720.8	721	720.8
13.9	28828	-47.9	-81.9	1	0.04			764.2	764.6	764.3

Station information and sounding indices

Station number	76679
Observation time	130516/1200
Station latitude	19.43
Station longitude	-99.13
Station elevation	2231
Lifted index	0.91
LIFT computed using virtual temperature	0.23
Convective Available Potential Energy	16.21
CAPE using virtual temperature	35.58
Convective Inhibition	-158.47
CINS using virtual temperature	-84.36
Equilibrum Level	342.34
Equilibrum Level using virtual temperature	338.21
Level of Free Convection	404.75
LFCT using virtual temperature	454.66
Bulk Richardson Number	2.34
Bulk Richardson Number using CAPV	5.13
Temp [K] of the Lifted Condensation Level	281.4
Pres [hPa] of the Lifted Condensation Level	703.34
Mean mixed layer potential temperature	311.19
Mean mixed layer mixing ratio	9.84
1000 hPa to 500 hPa thickness	5839
Precipitable water [mm] for entire sounding	17.52

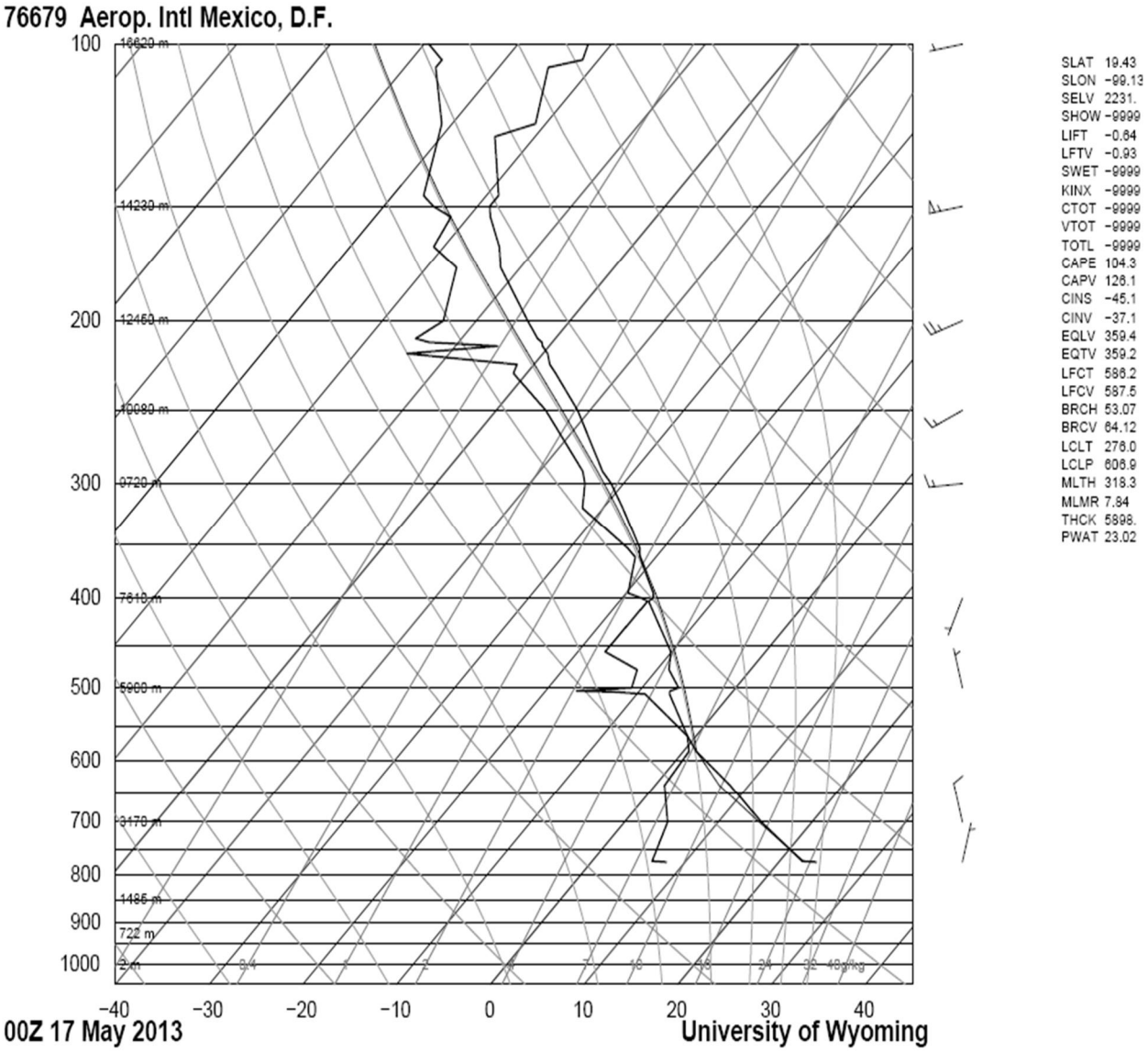

76679 Aerop. Intl Mexico, D.F. Observations at 00Z 17 May 2013

PRES [hPa]	HGHT [m]	TEMP [C]	DWPT [C]	RELH [%]	MIXR [g/kg]	DRCT [deg]	SKNT [knot]	THTA [K]	THTE [K]	THTV [K]
1000	2									
925	722									
850	1485									
774	2231	24	8	36	8.77	15	7	319.7	348	321.4
772	2256	22.4	6.4	35	7.87	14	7	318.2	343.5	319.7
700	3170	14.6	4.6	51	7.65	345	10	318.6	343.3	320.1
638	3946	8	1	61	6.49	345	8	319.7	340.8	320.9

PRES [hPa]	HGHT [m]	TEMP [C]	DWPT [C]	RELH [%]	MIXR [g/kg]	DRCT [deg]	SKNT [knot]	THTA [K]	THTE [K]	THTV [K]
586	4640	1.4	0.6	94	6.87	345	6	319.8	342.1	321.2
564	4948	-0.9	-0.9	100	6.4	345	6	320.6	341.5	321.9
508	5776	-6.5	-9.1	82	3.8	345	3	323.6	336.4	324.3
505	5822	-6.7	-12.7	62	2.87	345	3	323.9	333.7	324.4
504	5838	-6.7	-16.7	45	2.07	345	3	324.1	331.3	324.5
500	5900	-6.1	-11.1	68	3.29	345	3	325.5	336.9	326.2
478	6250	-8.7	-12.1	76	3.18	317	3	326.5	337.5	327.2
457	6598	-10.1	-17.1	57	2.2	289	3	329	336.8	329.4
403	7554	-16.9	-17	99	2.52	210	3	332.2	341.2	332.7
400	7610	-16.7	-17.9	90	2.35	205	3	333.2	341.6	333.7
395	7705	-17.1	-19.8	80	2.03	208	4	333.9	341.2	334.3
361	8377	-21.7	-22.2	96	1.8	226	8	336.4	343.1	336.8
353	8542	-22.5	-23.8	89	1.6	231	9	337.5	343.4	337.8
319	9280	-27.9	-32.2	67	0.81	252	13	339.9	343.1	340.1
300	9720	-31.3	-34.1	76	0.72	265	16	341.1	344	341.3
291	9934	-33.3	-35.4	81	0.65	262	16	341.3	343.9	341.4
250	10980	-41.3	-44.7	69	0.29	245	16	344.5	345.7	344.6
228	11597	-46.9	-51.4	60	0.15	247	20	345.2	345.8	345.2
223	11743	-48.3	-51.8	67	0.14	248	21	345.2	345.9	345.2
217	11922	-49.5	-64.5	16	0.03	248	22	346.1	346.2	346.1
213	12044	-50.7	-55.5	57	0.1	249	22	346	346.5	346.1
211	12105	-51.1	-63.1	23	0.04	249	23	346.4	346.5	346.4
209	12167	-51.9	-64.9	20	0.03	249	23	346	346.2	346.1
200	12450	-54.5	-63.5	32	0.04	250	25	346.3	346.5	346.3
175	13291	-62.1	-66.8	53	0.03	255	38	347.3	347.4	347.3
166	13616	-64.1	-71.1	38	0.02	256	43	349.2	349.3	349.2
154	14072	-67.7	-71.9	55	0.02	259	50	350.6	350.7	350.6
150	14230	-68.7	-74.7	42	0.01	260	53	351.6	351.6	351.6
146	14392	-68.7	-76.7	31	0.01	258	49	354.3	354.3	354.3
126	15263	-74.3	-80.3	39	0.01	245	30	359.4	359.4	359.4
122	15452	-71.1	-81.1	22	0	247	27	368.6	368.6	368.6
106	16277	-74.7	-86.7	14	0	256	11	376.8	376.8	376.8
104	16389	-71.7	-86.7	9	0	257	9	384.6	384.6	384.6
100	16620	-72.5	-89.5	6	0	260	5	387.4	387.4	387.4
87	17431	-76.9	-92.9	6	0	5	12	394.3	394.3	394.3
73.5	18399	-78.3	-94.3	6	0	90	10	410.8	410.8	410.8
70	18680	-76.1	-93.1	5	0	115	10	421.3	421.3	421.3
69.1	18755	-75.3	-93.3	5	0	115	10	424.5	424.5	424.5
62.2	19363	-76.3	-95.3	4	0	119	9	435.3	435.3	435.3
60.8	19495	-73.1	-93.1	3	0	119	8	445.2	445.2	445.2
58.4	19734	-68.5	-92.5	2	0	120	8	460.8	460.8	460.8

PRES [hPa]	HGHT [m]	TEMP [C]	DWPT [C]	RELH [%]	MIXR [g/kg]	DRCT [deg]	SKNT [knot]	THTA [K]	THTE [K]	THTV [K]
51.6	20486	-62.7	-92.7	1	0	124	6	490.9	490.9	490.9
50	20680	-63.3	-93.3	1	0	125	6	493.9	493.9	493.9
49.3	20767	-63.9	-93.9	1	0	124	7	494.5	494.5	494.5
38.3	22320	-62.9	-92.9	1	0	99	22	534	534	534
34.6	22955	-57.7	-89.7	1	0	89	28	563.3	563.4	563.3
31.7	23505	-60.5	-91.5	1	0	80	33	570.1	570.1	570.1
30	23850	-58.5	-89.5	1	0	75	36	584.6	584.6	584.6
25.9	24791	-50.9	-84.9	1	0.01	73	30	631.2	631.3	631.2
20	26480	-49.9	-83.9	1	0.02	70	20	682.7	682.9	682.7
13.1	29265	-46.7	-81.7	1	0.04			781.4	781.9	781.5

Station information and sounding indices

Station number	76679
Observation time	130517/0000
Station latitude	19.43
Station longitude	-99.13
Station elevation	2231
Lifted index	-0.64
LIFT computed using virtual temperature	-0.93
Convective Available Potential Energy	104.38
CAPE using virtual temperature	126.1
Convective Inhibition	-45.16
CINS using virtual temperature	-37.15
Equilibrum Level	359.46
Equilibrum Level using virtual temperature	359.27
Level of Free Convection	586.28
LFCT using virtual temperature	587.56
Bulk Richardson Number	53.07
Bulk Richardson Number using CAPV	64.12
Temp [K] of the Lifted Condensation Level	276.03
Pres [hPa] of the Lifted Condensation Level	606.98
Mean mixed layer potential temperature	318.38
Mean mixed layer mixing ratio	7.84
1000 hPa to 500 hPa thickness	5898
Precipitable water [mm] for entire sounding	23.02

May 22th

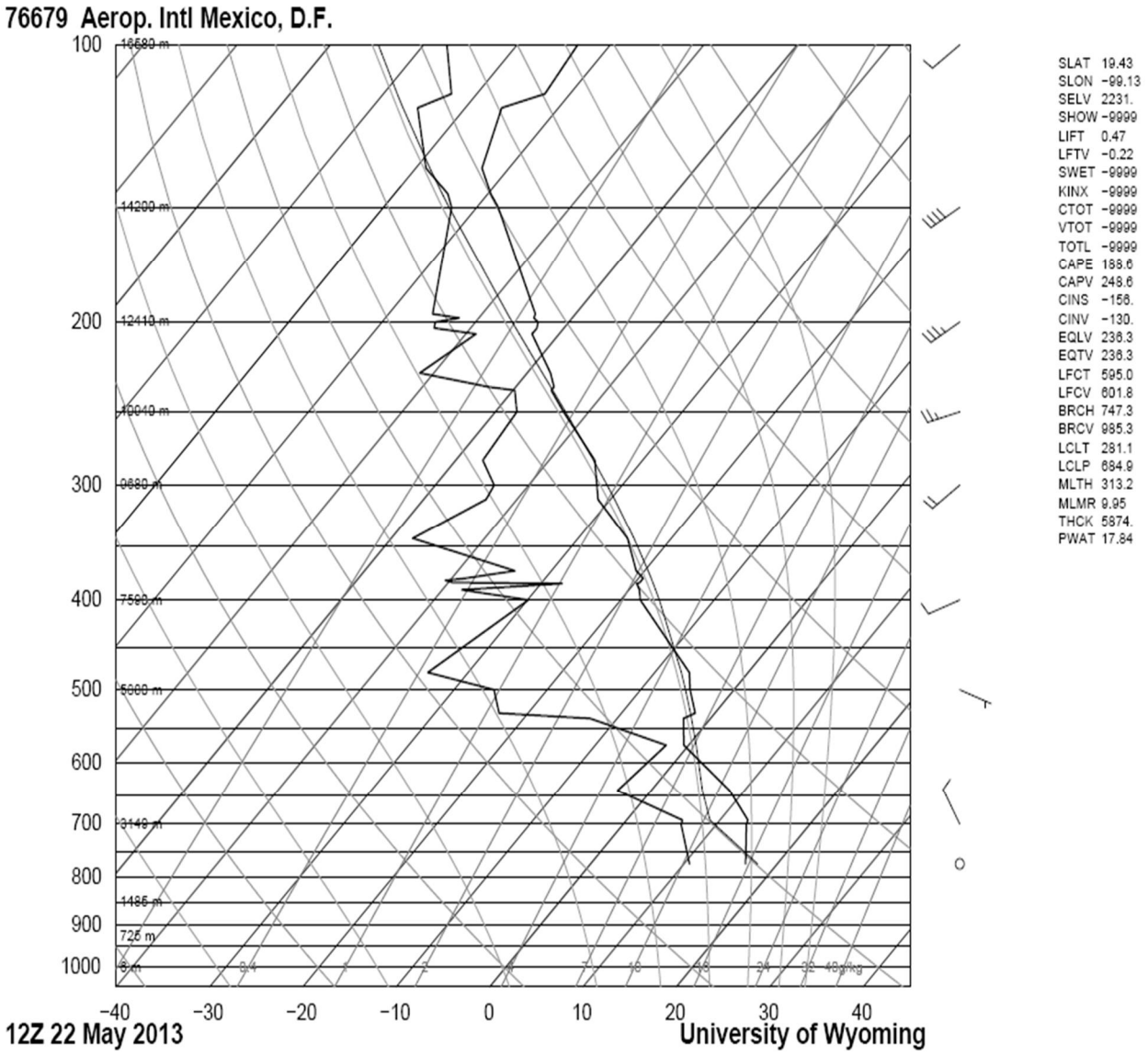

76679 Aerop. Intl Mexico, D.F. Observations at 12Z 22 May 2013

PRES [hPa]	HGHT [m]	TEMP [C]	DWPT [C]	RELH [%]	MIXR [g/kg]	DRCT [deg]	SKNT [knot]	THTA [K]	THTE [K]	THTV [K]
1000	6									
925	725									
850	1485									

PRES [hPa]	HGHT [m]	TEMP [C]	DWPT [C]	RELH [%]	MIXR [g/kg]	DRCT [deg]	SKNT [knot]	THTA [K]	THTE [K]	THTV [K]
773	2231	16.6	10.6	68	10.49	0	0	311.9	344.4	313.8
700	3149	13.2	6.2	63	8.57	330	10	317.1	344.4	318.7
693	3234	13	6	62	8.53	334	10	317.8	345.1	319.4
643	3859	8.4	-3.6	43	4.58	5	9	319.4	334.6	320.3
574	4784	-0.5	-2.4	87	5.62	53	8	319.5	337.9	320.6
537	5315	-2.9	-12.9	46	2.65	80	8	322.8	331.9	323.3
530	5419	-2.1	-23.1	18	1.13	86	8	325	329.1	325.2
500	5880	-4.7	-25.7	18	0.95	110	7	327.2	330.8	327.4
479	6216	-6.3	-34.3	9	0.44	137	8	329.3	331	329.4
400	7590	-17.9	-29.9	34	0.8	250	12	331.6	334.7	331.8
390	7779	-18.9	-37.9	17	0.38	249	13	332.7	334.2	332.8
384	7894	-19.7	-27.7	49	1.03	248	13	333.2	337	333.4
383	7913	-19.5	-39.5	15	0.33	248	13	333.7	335	333.7
381	7952	-19.5	-40.5	14	0.29	247	13	334.2	335.4	334.2
379	7991	-19.5	-38.5	17	0.36	247	13	334.7	336.1	334.8
372	8129	-20.9	-33.9	30	0.59	246	14	334.6	336.9	334.7
343	8724	-24.7	-47.7	10	0.15	242	15	337.3	337.9	337.3
311	9426	-31.3	-43.3	30	0.27	237	17	337.6	338.8	337.7
300	9680	-32.7	-43.7	33	0.27	235	18	339.2	340.3	339.2
282	10114	-35.1	-47.1	28	0.2	242	21	341.8	342.6	341.8
250	10940	-42.7	-47.7	58	0.21	255	26	342.4	343.3	342.5
237	11298	-45.9	-49.8	65	0.17	251	29	342.9	343.6	342.9
235	11355	-45.9	-52.9	45	0.12	251	29	343.7	344.2	343.7
227	11585	-47.5	-61.5	18	0.04	249	31	344.7	344.9	344.7
206	12219	-52.9	-58.9	48	0.07	242	36	345.9	346.2	345.9
203	12314	-52.9	-63.9	25	0.03	241	36	347.4	347.5	347.4
200	12410	-53.3	-64.3	25	0.03	240	37	348.2	348.4	348.2
198	12475	-54.1	-62.1	37	0.05	240	37	347.9	348.1	347.9
196	12540	-54.3	-65.3	25	0.03	240	37	348.6	348.8	348.6
150	14200	-67.7	-72.7	49	0.01	240	41	353.3	353.3	353.3
145	14403	-69.7	-74.3	51	0.01	243	38	353.2	353.3	353.2
136	14783	-72.9	-78.9	40	0.01	248	32	354.1	354.1	354.1
117	15660	-76.1	-85.1	23	0	260	17	363.8	363.8	363.8
113	15863	-72.7	-82.7	21	0	254	15	373.7	373.8	373.7
100	16580	-73.5	-87.5	10	0	235	9	385.5	385.5	385.5
80.2	17851	-78.7	-91.7	11	0	220	4	399.9	399.9	399.9
70.8	18564	-76.3	-93.3	5	0	11	13	419.5	419.5	419.5
70	18630	-74.3	-92.3	5	0	25	14	425.1	425.1	425.1
67.9	18809	-71.1	-91.1	4	0	31	14	435.7	435.7	435.7
63	19255	-70.3	-97.3	1	0	47	15	446.9	446.9	446.9
57	19860	-64.5	-94.5	1	0	68	16	473	473	473

PRES [hPa]	HGHT [m]	TEMP [C]	DWPT [C]	RELH [%]	MIXR [g/kg]	DRCT [deg]	SKNT [knot]	THTA [K]	THTE [K]	THTV [K]
52.8	20328	-66.1	-95.1	1	0	84	17	479.8	479.8	479.8
50	20660	-64.9	-94.9	1	0	95	18	490.1	490.1	490.1
42.3	21691	-59.1	-90.1	1	0	90	22	528.4	528.5	528.4
35.1	22858	-58.5	-89.5	1	0	85	27	558.9	559	558.9
31.5	23535	-59.3	-90.3	1	0	81	30	574.3	574.4	574.3
30	23840	-58.9	-89.9	1	0	80	31	583.5	583.5	583.5
23.1	25523	-47.1	-82.1	1	0.02	70	25	663.4	663.6	663.4
20.3	26381	-44.9	-79.9	1	0.03	66	21	695	695.4	695
20	26480	-45.5	-80.5	1	0.03	65	21	696.1	696.5	696.1
15.9	27991	-50.7	-84.7	1	0.02			726.3	726.5	726.3
13	29309	-48.5	-82.5	1	0.03			776.9	777.3	776.9
11.1	30366	-40.9	-77.9	1	0.08			840.3	841.4	840.3

Station information and sounding indices

Station number	76679
Observation time	130522/1200
Station latitude	19.43
Station longitude	-99.13
Station elevation	2231
Lifted index	0.47
LIFT computed using virtual temperature	-0.22
Convective Available Potential Energy	188.61
CAPE using virtual temperature	248.67
Convective Inhibition	-156.63
CINS using virtual temperature	-130.88
Equilibrum Level	236.36
Equilibrum Level using virtual temperature	236.38
Level of Free Convection	595.03
LFCT using virtual temperature	601.83
Bulk Richardson Number	747.33
Bulk Richardson Number using CAPV	985.33
Temp [K] of the Lifted Condensation Level	281.15
Pres [hPa] of the Lifted Condensation Level	684.99
Mean mixed layer potential temperature	313.28
Mean mixed layer mixing ratio	9.95
1000 hPa to 500 hPa thickness	5874
Precipitable water [mm] for entire sounding	17.84

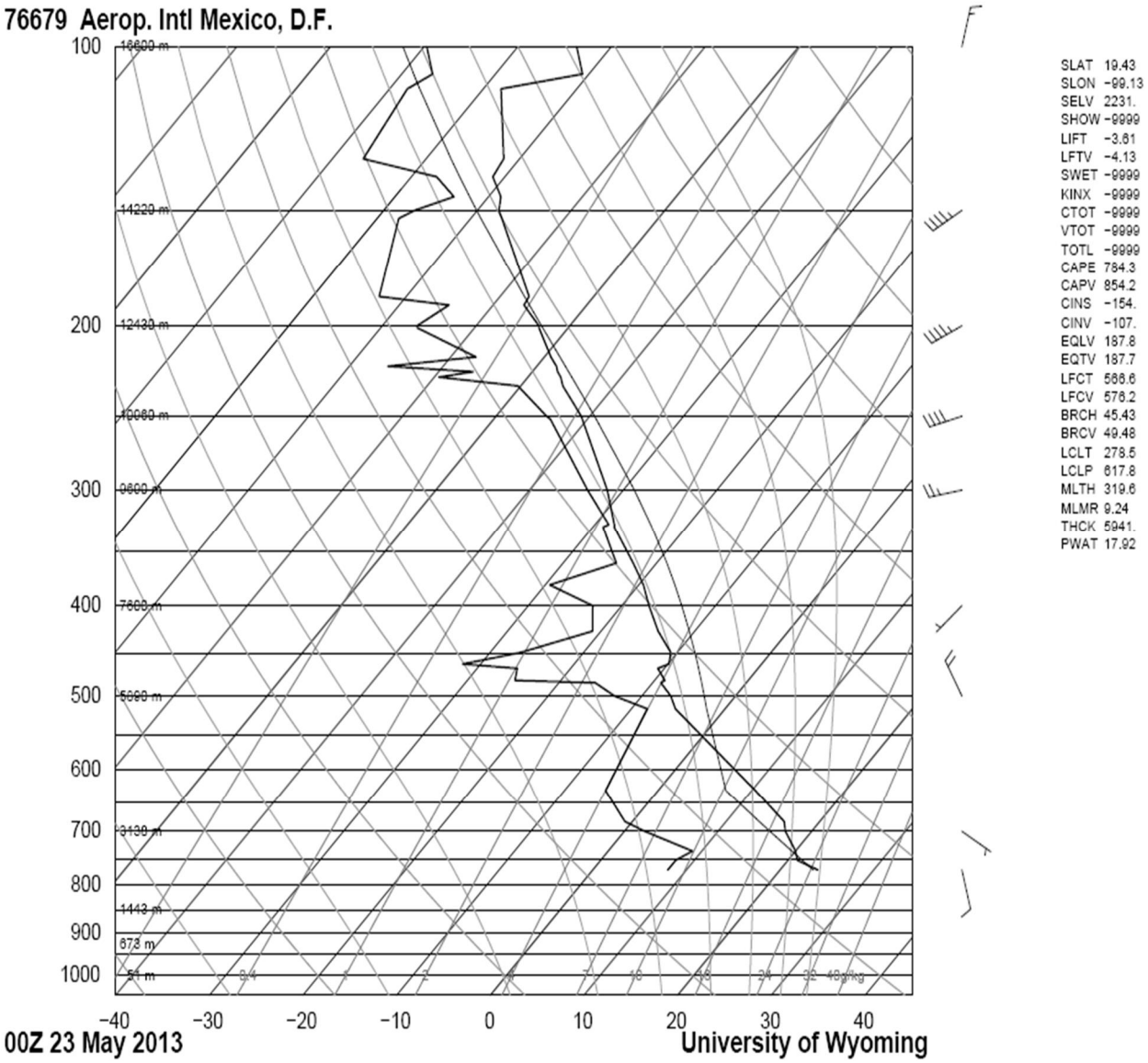

76679 Aerop. Intl Mexico, D.F. Observations at 00Z 23 May 2013

PRES [hPa]	HGHT [m]	TEMP [C]	DWPT [C]	RELH [%]	MIXR [g/kg]	DRCT [deg]	SKNT [knot]	THTA [K]	THTE [K]	THTV [K]
1000	-51									
925	673									
850	1443									
770	2231	24	8	36	8.81	165	10	320.2	348.7	321.9
752	2458	21	8	43	9.03	154	9	319.1	348.1	320.8
735	2676	20	9	49	9.9	143	8	320.1	351.9	322
700	3138	17.2	2.2	37	6.45	120	5	321.5	342.7	322.8

PRES [hPa]	HGHT [m]	TEMP [C]	DWPT [C]	RELH [%]	MIXR [g/kg]	DRCT [deg]	SKNT [knot]	THTA [K]	THTE [K]	THTV [K]
683	3348	16.2	-0.8	31	5.31	109	6	322.6	340.3	323.7
632	4001	10.4	-5.6	32	4.01	74	9	323.3	336.8	324.1
516	5643	-5.3	-8.3	79	3.98	344	17	323.6	337	324.4
500	5890	-6.9	-12.9	62	2.85	330	18	324.6	334.4	325.1
484	6143	-9.1	-16.1	57	2.26	315	16	324.9	332.8	325.3
481	6191	-8.9	-24.9	26	1.06	313	16	325.7	329.6	325.9
467	6419	-10.7	-25.7	28	1.02	299	14	326.2	330	326.4
462	6502	-9.9	-31.9	15	0.58	295	13	328.2	330.4	328.4
449	6722	-10.7	-26.7	26	0.96	282	11	329.9	333.5	330.1
426	7124	-13.9	-20.9	55	1.71	258	8	330.8	337	331.2
400	7600	-17.1	-23.1	60	1.5	230	4	332.7	338.2	333
380	7982	-19.5	-29.5	41	0.88	235	8	334.4	337.8	334.6
360	8381	-22.5	-24.3	85	1.5	241	12	335.6	341.2	335.9
329	9033	-27.7	-28.9	89	1.07	250	19	337.2	341.3	337.4
327	9077	-27.9	-28.5	95	1.12	251	19	337.5	341.8	337.8
300	9690	-31.7	-33.8	82	0.74	260	26	340.6	343.5	340.7
252	10906	-40.5	-43.9	70	0.31	255	38	344.9	346.2	345
250	10960	-40.9	-44.6	67	0.29	255	39	345.1	346.3	345.2
232	11461	-45.5	-50.3	58	0.16	252	40	345.6	346.3	345.6
227	11606	-46.5	-59.5	21	0.06	251	41	346.2	346.5	346.2
224	11693	-47.3	-56.3	35	0.08	250	41	346.3	346.7	346.3
221	11782	-47.9	-65.9	11	0.02	249	41	346.7	346.8	346.7
216	11932	-49.3	-57.3	39	0.08	248	42	346.8	347.2	346.8
201	12398	-53.1	-66.1	19	0.03	245	43	348	348.1	348
200	12430	-53.3	-66.3	19	0.03	245	43	348.2	348.3	348.2
190	12758	-56.7	-64.7	36	0.03	244	43	347.9	348	347.9
186	12892	-56.9	-72.9	12	0.01	244	43	349.7	349.7	349.7
153	14101	-66.7	-77.7	20	0.01	240	44	353	353	353
150	14220	-67.7	-76.7	27	0.01	240	44	353.3	353.3	353.3
145	14424	-68.7	-73.7	48	0.01	243	42	355	355	355
138	14718	-71.3	-77.3	41	0.01	247	38	355.4	355.5	355.4
132	14981	-71.7	-86.7	9	0	251	35	359.3	359.3	359.3
111	15988	-78.1	-88.1	19	0	265	23	365.5	365.5	365.5
107	16202	-70.7	-86.7	8	0	304	19	383.4	383.4	383.4
100	16600	-73.7	-89.7	7	0	15	13	385.1	385.1	385.1
79.7	17909	-78.5	-94.5	6	0	85	6	401	401	401
74.4	18305	-73.9	-92.9	4	0	96	13	418.6	418.6	418.6
70	18660	-74.7	-94.7	3	0	105	19	424.2	424.3	424.2
68.2	18811	-75.7	-96.7	3	0	101	19	425.3	425.3	425.3
55.2	20057	-68.5	-97.5	1	0	70	17	468.2	468.2	468.2
51.5	20478	-63.3	-93.3	1	0	59	16	489.7	489.8	489.7

PRES [hPa]	HGHT [m]	TEMP [C]	DWPT [C]	RELH [%]	MIXR [g/kg]	DRCT [deg]	SKNT [knot]	THTA [K]	THTE [K]	THTV [K]
50	20660	-63.1	-93.1	1	0	55	16	494.4	494.4	494.4
44.2	21425	-60.5	-91.5	1	0	69	18	518.4	518.4	518.4
40.8	21923	-61.5	-91.5	1	0	79	20	527.9	527.9	527.9
34.8	22919	-57.9	-89.9	1	0	98	22	561.9	561.9	561.9
32.9	23273	-58.5	-89.5	1	0	104	23	569.4	569.4	569.4
30	23860	-54.5	-86.5	1	0.01	115	25	595.5	595.5	595.5
29.7	23924	-53.9	-86.9	1	0.01	114	25	598.8	598.9	598.8
24	25295	-53.5	-86.5	1	0.01	85	28	637.6	637.7	637.6
23.1	25540	-54.3	-87.3	1	0.01	80	28	642.2	642.3	642.2
20.7	26253	-48.1	-82.1	1	0.02	65	30	681.4	681.7	681.5
20	26480	-48.7	-82.7	1	0.02	60	30	686.3	686.6	686.4
17.1	27512	-47.5	-82.5	1	0.03			721.6	721.9	721.6
14.9	28415	-50.7	-84.7	1	0.02			739.9	740.1	739.9
13.6	29015	-46.5	-81.5	1	0.04			773.8	774.2	773.8

Station information and sounding indices

Station number	76679
Observation time	130523/0000
Station latitude	19.43
Station longitude	-99.13
Station elevation	2231
Lifted index	-3.61
LIFT computed using virtual temperature	-4.13
Convective Available Potential Energy	784.38
CAPE using virtual temperature	854.29
Convective Inhibition	-154.76
CINS using virtual temperature	-107.76
Equilibrum Level	187.83
Equilibrum Level using virtual temperature	187.79
Level of Free Convection	566.67
LFCT using virtual temperature	576.2
Bulk Richardson Number	45.43
Bulk Richardson Number using CAPV	49.48
Temp [K] of the Lifted Condensation Level	278.59
Pres [hPa] of the Lifted Condensation Level	617.81
Mean mixed layer potential temperature	319.69
Mean mixed layer mixing ratio	9.24
1000 hPa to 500 hPa thickness	5941
Precipitable water [mm] for entire sounding	17.92

May 28th

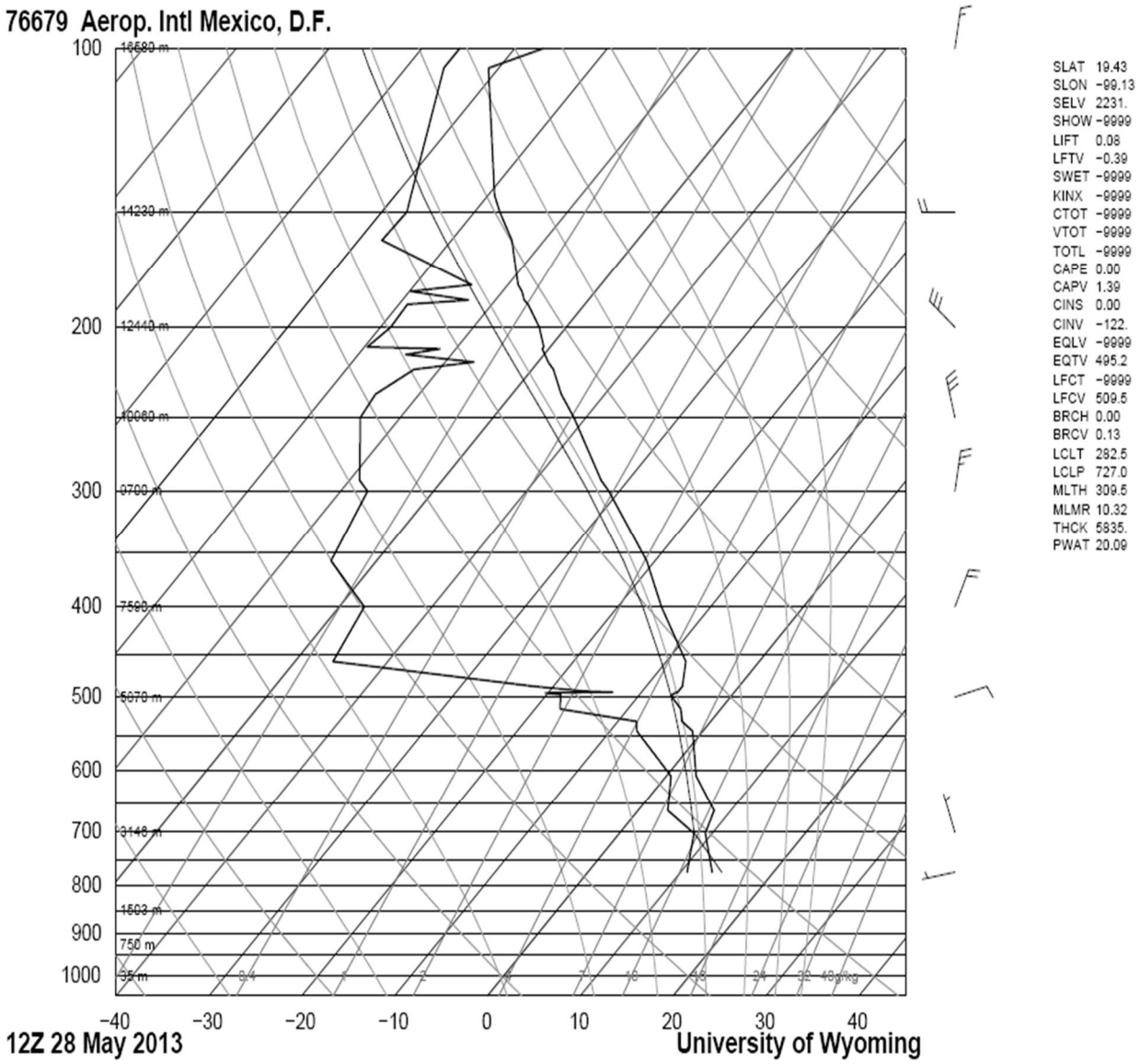

76679 Aerop. Intl Mexico, D.F. Observations at 12Z 28 May 2013

PRES [hPa]	HGHT [m]	TEMP [C]	DWPT [C]	RELH [%]	MIXR [g/kg]	DRCT [deg]	SKNT [knot]	THTA [K]	THTE [K]	THTV [K]
1000	35									
925	750									
850	1503									

PRES [hPa]	HGHT [m]	TEMP [C]	DWPT [C]	RELH [%]	MIXR [g/kg]	DRCT [deg]	SKNT [knot]	THTA [K]	THTE [K]	THTV [K]
773	2231	13.4	10.7	84	10.56	260	3	308.4	340.8	310.4
701	3133	9.2	8	92	9.69	339	6	312.5	342.7	314.3
700	3146	9.2	7.8	91	9.57	340	6	312.6	342.5	314.4
663	3597	8.2	3.2	71	7.32	355	6	316.4	339.8	317.8
608	4307	3.2	0.5	82	6.57	20	7	318.6	339.8	319.8
544	5203	-1.1	-7.1	64	4.15	51	8	323.7	337.7	324.6
531	5396	-3.1	-8	69	3.96	58	8	323.6	337	324.4
515	5638	-4.3	-17.3	36	1.92	67	9	325	331.8	325.4
500	5870	-6.3	-18.3	38	1.82	75	9	325.3	331.7	325.6
497	5917	-6.5	-18.5	38	1.8	74	9	325.6	332	326
495	5949	-6.3	-20.3	32	1.55	73	9	326.2	331.8	326.5
494	5964	-6.1	-13.1	58	2.84	72	10	326.7	336.5	327.2
493	5980	-6.1	-16.1	45	2.22	72	10	326.9	334.7	327.3
487	6076	-6.1	-22.1	27	1.34	69	10	328	332.9	328.3
458	6554	-7.9	-45.9	3	0.14	55	13	331.6	332.1	331.6
400	7590	-15.3	-47.3	5	0.13	25	19	335	335.6	335
357	8440	-20.9	-54.9	3	0.06	19	21	338.6	338.8	338.6
300	9700	-31.1	-57.1	6	0.06	10	24	341.4	341.7	341.4
292	9890	-32.9	-58.9	6	0.05	6	25	341.5	341.7	341.5
250	10960	-41.3	-64.3	7	0.03	345	29	344.5	344.7	344.5
236	11350	-44.7	-64.7	9	0.03	336	30	345.1	345.2	345.1
222	11757	-47.7	-62.7	16	0.04	326	31	346.6	346.8	346.6
218	11878	-48.9	-56.9	39	0.08	324	31	346.5	346.9	346.6
214	11999	-49.9	-64.9	15	0.03	321	31	346.8	347	346.8
211	12092	-50.7	-61.7	26	0.04	318	31	347	347.2	347
210	12123	-50.7	-69.7	9	0.02	318	31	347.4	347.5	347.4
200	12440	-52.9	-68.9	13	0.02	310	32	348.8	348.9	348.8
189	12802	-56.1	-69.1	18	0.02	302	30	349.4	349.5	349.4
187	12869	-56.9	-62.9	46	0.04	301	30	349.1	349.3	349.1
183	13005	-57.9	-69.9	20	0.02	298	29	349.7	349.8	349.7
180	13109	-58.9	-63.9	52	0.04	295	28	349.7	349.9	349.7
161	13800	-63.5	-77.5	13	0.01	280	24	353.3	353.3	353.3
150	14230	-67.3	-77.3	23	0.01	270	22	354	354	354
144	14475	-69.3	-78.3	26	0.01	273	20	354.6	354.7	354.6
105	16303	-81.1	-85.9	45	0	295	5	365.7	365.7	365.7
100	16580	-76.9	-85.9	23	0	10	15	378.9	378.9	378.9
89.4	17231	-74.5	-87.5	12	0	27	18	396	396	396
75	18251	-77.3	-90.3	11	0	54	23	410.5	410.5	410.5
70.5	18609	-76.1	-92.1	7	0	64	25	420.4	420.4	420.4
70	18650	-75.5	-91.5	7	0	65	25	422.5	422.6	422.5
65.1	19078	-68.7	-89.7	3	0	73	27	446.2	446.2	446.2

PRES [hPa]	HGHT [m]	TEMP [C]	DWPT [C]	RELH [%]	MIXR [g/kg]	DRCT [deg]	SKNT [knot]	THTA [K]	THTE [K]	THTV [K]
57.5	19825	-66.7	-92.7	2	0	85	29	466.9	466.9	466.9
56.3	19952	-67.3	-94.3	1	0	88	30	468.3	468.3	468.3
50	20670	-66.3	-95.3	1	0	100	32	486.8	486.8	486.8
47	21044	-66.7	-95.7	1	0	101	30	494.6	494.6	494.6
37.4	22456	-57.3	-89.3	1	0	103	23	552	552	552
34.6	22947	-58.3	-89.3	1	0	104	21	561.8	561.8	561.8
30	23850	-55.3	-87.3	1	0.01	105	17	593.3	593.4	593.3
28.2	24245	-53.1	-86.1	1	0.01	100	20	610	610	610
21.6	25953	-53.7	-86.7	1	0.01	81	35	656.5	656.6	656.5
20	26450	-50.1	-84.1	1	0.02	75	39	682.1	682.2	682.1
16.9	27559	-46.1	-81.1	1	0.03			728.5	728.9	728.5
14	28815	-44.5	-80.5	1	0.04			774.2	774.7	774.2
13.8	28911	-44.7	-79.7	1	0.05			776.7	777.3	776.7

Station information and sounding indices

Station number	76679
Observation time	130528/1200
Station latitude	19.43
Station longitude	-99.13
Station elevation	2231
Lifted index	0.08
LIFT computed using virtual temperature	-0.39
Convective Available Potential Energy	0
CAPE using virtual temperature	1.39
Convective Inhibition	0
CINS using virtual temperature	-122.13
Equilibrum Level using virtual temperature	495.29
LFCT using virtual temperature	509.52
Bulk Richardson Number	0
Bulk Richardson Number using CAPV	0.13
Temp [K] of the Lifted Condensation Level	282.58
Pres [hPa] of the Lifted Condensation Level	727.07
Mean mixed layer potential temperature	309.56
Mean mixed layer mixing ratio	10.32
1000 hPa to 500 hPa thickness	5835
Precipitable water [mm] for entire sounding	20.09

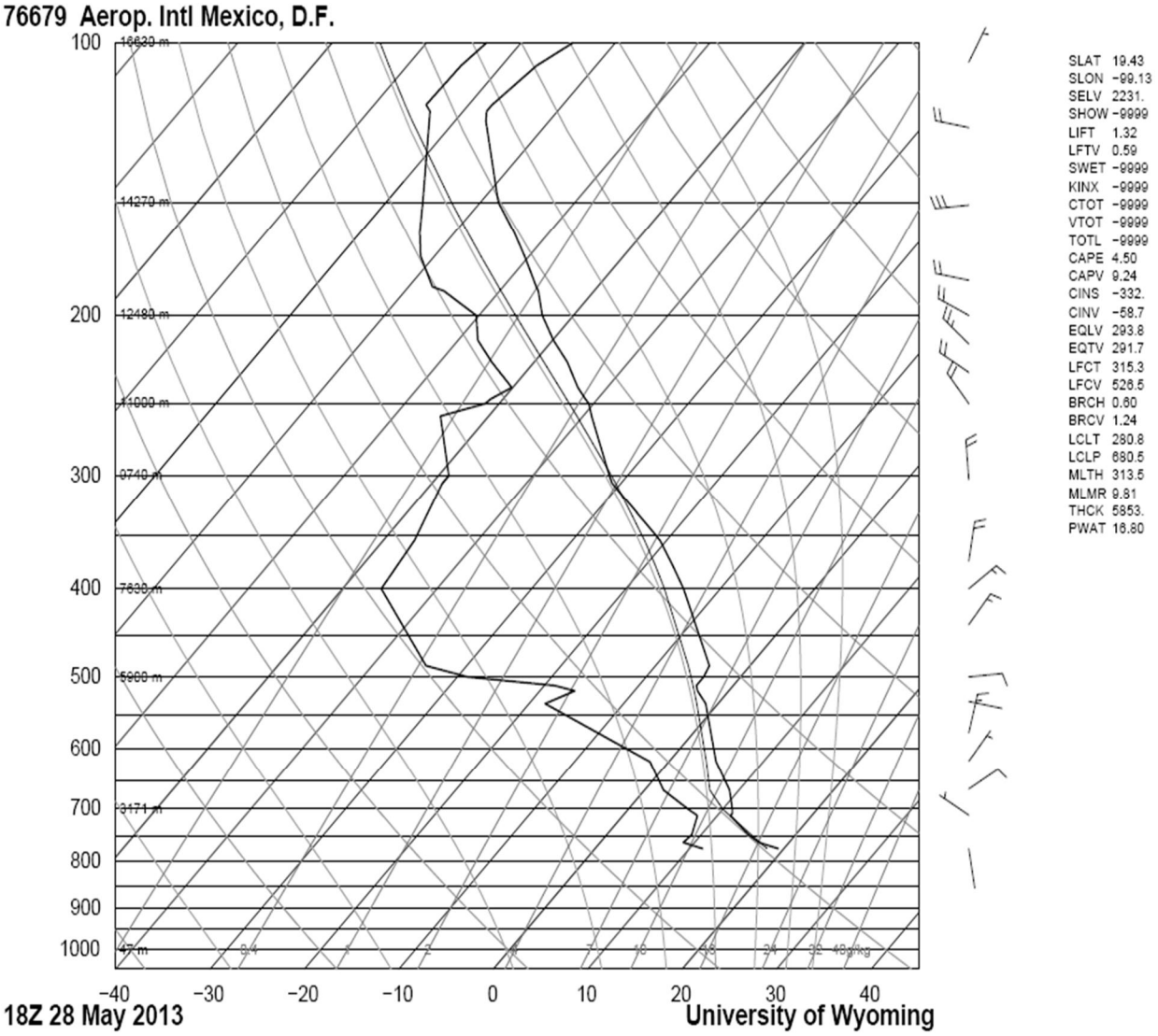

76679 Aerop. Intl Mexico, D.F. Observations at 18Z 28 May 2013

PRES [hPa]	HGHT [m]	TEMP [C]	DWPT [C]	RELH [%]	MIXR [g/kg]	DRCT [deg]	SKNT [knot]	THTA [K]	THTE [K]	THTV [K]
1000	47									
774	2231	19.4	11.4	60	11.06	170	2	314.8	349.5	316.9
763	2367	17	9	59	9.54	55	2	313.5	343.4	315.3
762	2379	16.8	8.8	59	9.41	46	2	313.4	342.9	315.1
747	2566	15	9	67	9.74	274	1	313.2	343.7	315
746	2579	14.9	9	68	9.73	265	1	313.2	343.6	315
729	2794	13.2	8.4	73	9.6	115	1	313.4	343.5	315.2

PRES [hPa]	HGHT [m]	TEMP [C]	DWPT [C]	RELH [%]	MIXR [g/kg]	DRCT [deg]	SKNT [knot]	THTA [K]	THTE [K]	THTV [K]
712	3014	11.4	7.9	79	9.48	310	4	313.6	343.2	315.3
711	3027	11.4	7.8	78	9.41	300	4	313.7	343.2	315.4
708	3066	11.4	7.4	76	9.21	323	4	314.1	343	315.8
702	3145	11.1	6.6	74	8.77	10	3	314.5	342.1	316.1
700	3171	11	6.3	73	8.63	5	3	314.6	341.9	316.3
694	3243	10.6	5.5	71	8.25	350	2	315	341.1	316.6
667	3573	9	2	62	6.67	55	10	316.8	338.2	318
665	3598	8.8	1.8	61	6.62	60	11	316.9	338.1	318.1
662	3636	8.6	1.6	61	6.53	57	11	317	338	318.2
635	3978	6.3	-0.7	61	5.76	30	8	318.2	336.9	319.3
620	4175	5	-2	61	5.36	39	7	318.9	336.4	319.9
619	4188	4.9	-2.2	60	5.3	40	7	318.9	336.3	319.9
602	4412	3.7	-5.3	52	4.32	10	15	320.1	334.4	320.9
592	4548	3	-7.1	47	3.81	35	13	320.8	333.6	321.5
576	4769	1.9	-10.1	41	3.09	15	13	321.9	332.4	322.6
535	5364	-1.3	-18.3	26	1.7	94	3	325	331.1	325.4
532	5409	-1.6	-17.9	28	1.76	100	2	325.1	331.4	325.5
518	5621	-3.3	-16.3	36	2.08	68	3	325.6	333	326.1
511	5728	-3.9	-18.9	30	1.69	52	3	326.2	332.2	326.5
510	5744	-3.9	-19.8	28	1.57	50	3	326.4	332	326.7
504	5837	-3.9	-25.2	17	0.98	90	9	327.5	331.1	327.7
500	5900	-3.9	-28.9	12	0.71	85	8	328.2	330.9	328.4
490	6059	-4.2	-32.7	9	0.5	70	14	329.8	331.7	329.9
486	6124	-4.3	-34.3	8	0.43	68	14	330.4	332.1	330.5
438	6928	-9.4	-40.5	6	0.26	40	13	333.9	334.9	333.9
400	7630	-13.9	-45.9	5	0.16	55	13	336.8	337.5	336.9
385	7918	-16	-46.1	6	0.16	35	13	337.8	338.4	337.8
376	8096	-17.3	-46.3	6	0.16	16	17	338.4	339	338.4
373	8156	-17.8	-46.4	6	0.16	10	19	338.5	339.2	338.6
354	8545	-20.7	-46.7	8	0.16	6	19	339.6	340.3	339.7
306	9600	-30.9	-48.9	15	0.15	356	18	339.8	340.4	339.8
303	9670	-31.4	-48.9	16	0.15	355	18	340	340.7	340.1
300	9740	-31.9	-48.9	17	0.15	345	16	340.3	340.9	340.3
298	9786	-32.2	-49.2	17	0.15	340	15	340.5	341.1	340.5
258	10786	-39.1	-55.1	17	0.08	324	19	344.7	345.1	344.7
250	11000	-40.5	-51.5	30	0.13	320	20	345.7	346.3	345.7
249	11027	-40.8	-51.4	31	0.13	315	19	345.7	346.3	345.8
247	11082	-41.3	-51.3	33	0.14	313	19	345.7	346.3	345.8
240	11277	-43.1	-50.1	46	0.16	308	20	345.9	346.6	345.9
231	11533	-45.1	-52.7	42	0.13	300	21	346.6	347.1	346.6
225	11709	-46.5	-54.5	40	0.1	304	22	347.1	347.6	347.1

PRES [hPa]	HGHT [m]	TEMP [C]	DWPT [C]	RELH [%]	MIXR [g/kg]	DRCT [deg]	SKNT [knot]	THTA [K]	THTE [K]	THTV [K]
215	12009	-49.3	-57.3	39	0.08	310	23	347.3	347.6	347.3
213	12071	-49.9	-57.9	38	0.07	308	23	347.3	347.6	347.3
200	12480	-53.3	-60.3	42	0.06	295	22	348.2	348.5	348.2
188	12875	-55.9	-65.9	27	0.03	285	21	350.2	350.4	350.2
186	12943	-56.5	-67.5	24	0.02	283	21	350.3	350.4	350.3
183	13045	-57.3	-68.3	23	0.02	280	21	350.6	350.7	350.6
172	13434	-60.5	-71.5	22	0.01	275	24	351.6	351.7	351.6
162	13804	-63.7	-73.7	24	0.01	270	26	352.3	352.4	352.3
151	14230	-67.7	-75.9	30	0.01	265	29	352.6	352.6	352.6

Station information and sounding indices

Station number	76679
Observation time	130528/1800
Station latitude	19.43
Station longitude	-99.13
Station elevation	2231
Lifted index	1.32
LIFT computed using virtual temperature	0.59
Convective Available Potential Energy	4.5
CAPE using virtual temperature	9.24
Convective Inhibition	-332.83
CINS using virtual temperature	-58.72
Equilibrum Level	293.8
Equilibrum Level using virtual temperature	291.71
Level of Free Convection	315.37
LFCT using virtual temperature	526.56
Bulk Richardson Number	0.6
Bulk Richardson Number using CAPV	1.24
Temp [K] of the Lifted Condensation Level	280.86
Pres [hPa] of the Lifted Condensation Level	680.55
Mean mixed layer potential temperature	313.51
Mean mixed layer mixing ratio	9.81
1000 hPa to 500 hPa thickness	5853
Precipitable water [mm] for entire sounding	16.8